

**NASA CONTRACTOR  
REPORT**

**NASA CR-2765**



**NASA CR-2**

0061373



**LOAN COPY: RETURN TO  
AFWL TECHNICAL LIBRARY  
KIRTLAND AFB, N. M.**

**ENVIRONMENTAL DYNAMICS  
AT ORBITAL ALTITUDES**

*Gerald R. Karr*

*Prepared by*

**THE UNIVERSITY OF ALABAMA IN HUNTSVILLE**

Huntsville, Ala. 35807

*for George C. Marshall Space Flight Center*



**NATIONAL AERONAUTICS AND SPACE ADMINISTRATION • WASHINGTON, D. C. • DECEMBER 1976**



TECHNICAL RE

0061373

1. REPORT NO. NASA CR-2765	2. GOVERNMENT ACCESSION NO.	3. REPORT NUMBER	
4. TITLE AND SUBTITLE Environmental Dynamics at Orbital Altitudes		5. REPORT DATE December 1976	6. PERFORMING ORGANIZATION CODE
		8. PERFORMING ORGANIZATION REPORT # M-193	
7. AUTHOR(S) Gerald R. Karr	9. PERFORMING ORGANIZATION NAME AND ADDRESS School of Graduate Studies and Research The University of Alabama in Huntsville Huntsville, Alabama 35807		10. WORK UNIT NO.
11. CONTRACT OR GRANT NO. NAS8-28248			
13. TYPE OF REPORT & PERIOD COVERED Contractor			
12. SPONSORING AGENCY NAME AND ADDRESS National Aeronautics and Space Administration Washington, D. C. 20546		14. SPONSORING AGENCY CODE	
		15. SUPPLEMENTARY NOTES This work was performed under the technical direction of the Aerospace Environment Division, Space Sciences Laboratory, Marshall Space Flight Center.	
16. ABSTRACT <p>The work reported involved the improvement of aerodynamic theory for free molecular and transition flow regimes. The improved theory has been applied to interpretation of the dynamic response of objects traveling through the atmosphere.</p> <p>Satellite drag analysis includes analysis methods, atmospheric super rotation effects, and satellite lift effects on orbital dynamics. Transition flow regimes were studied with falling sphere data and errors resulting in inferred atmospheric parameters from falling sphere techniques. Improved drag coefficients reveal considerable error in previous falling sphere data. The drag coefficient has been studied for the entire spectrum of Knudsen Number and speed ratio, with particular emphasis on the theory of the very low-speed ratio regime.</p>			
17. KEY WORDS		18. DISTRIBUTION STATEMENT  STAR Category 46	
19. SECURITY CLASSIF. (of this report) Unclassified	20. SECURITY CLASSIF. (of this page) Unclassified	21. NO. OF PAGES 147	22. PRICE \$5.75

\* For sale by the National Technical Information Service, Springfield, Virginia 22161

11  
12  
13

## TABLE OF CONTENTS

	<u>Page</u>
INTRODUCTION	1
CHAPTER I. INFLUENCE OF SATELLITE AERODYNAMICS ON ATMOSPHERIC DENSITY DETERMINATION	4
CHAPTER II. SATELLITE AERODYNAMICS AND ATMOSPHERIC DENSITY DETERMINATION FROM SATELLITE DYNAMIC RESPONSE	11
CHAPTER III. AERODYNAMIC LIFT EFFECT ON SATELLITE ORBITS	31
CHAPTER IV. DUAL FALLING SPHERE DETERMINATION OF DENSITY AND TRANSITION FLOW PARAMETER	42
CHAPTER V. A SPHERE DRAG BRIDGING RELATIONSHIP IN THE LOW MACH NUMBER TRANSITION REGIME	50
CHAPTER VI. IMPROVEMENTS IN FALLING SPHERE DATA ANALYSIS IN THE 80 TO 120 KM REGION	64
CHAPTER VII. FREE MOLECULE DRAG AT SPEED RATIO LESS THAN UNITY	86
CHAPTER VIII. RECOMMENDATIONS FOR FUTURE WORK	91
A. Proposal to Develop Zero-g Brownian Motion Experiments	92
B. An Experiment Using the Molecular Beam Apparatus Proposed for Space Shuttle	100
APPENDIX	105

## INTRODUCTION

Work supported under Contract Number NAS8-28248 began in January 1972 and has continued with varying degrees of effort to the present time. The work has involved the application of improved aerodynamic theory towards the goal of obtaining more accurate knowledge of the upper atmosphere. Advancements have been made both in the area of aerodynamic theory and the interpretation of the dynamic response of objects traveling through the atmosphere.

The work began as a study of ways of improving models of the upper atmosphere as deduced from observation of satellite decay. In the development of atmospheric models, it was found that the decay of the orbit of a satellite due to drag had been modeled as simply a sphere with a drag coefficient of 2.2 traveling through a rotating atmosphere. The assumption of a sphere of  $C_D = 2.2$  was of course recognized to be only an approximation and of particular use in the analysis of the drag decay of foreign or some domestic satellites for which limited knowledge existed concerning the shape or other physical parameters. One of the goals of this work was to investigate the magnitude of error made in the assumption of a sphere of  $C_D = 2.2$  and to propose more accurate data reduction techniques.

Chapter 1 describes the major influence revealed in this study concerning the influence of real satellite aerodynamics on the determination of upper atmospheric density. Chapter 2 presents a method of analysis of satellite drag data which includes the effect of satellite lift and the variation in aerodynamic properties around the orbit.

The method was applied to the data from OVI 15 satellite. One of the interesting results obtained from analysis of satellite orbit decay has been the super rotation of the atmosphere deduced by King-Hele. In Chapter 3, a study is presented which shows that satellite lift effects may be responsible for the observed orbit precession rather than a super rotation of the upper atmosphere.

Emphasis of this work gradually came to the lower altitude regime and the 80 to 120 km region in particular. This region of the atmosphere is of great importance since it serves as a major boundary between the lower atmosphere which is constant in molecular weight and the upper atmosphere which reaches out many thousands of km having considerable variation in molecular composition. This important region of the atmosphere has received little experimental attention due to the difficulty and expense of performing measurements at these altitudes. The falling sphere method is found to be the primary source of information for this region. As with satellite drag measurements, it was found that simple assumptions concerning the aerodynamics of objects were often employed in the falling sphere analysis. The influence of the errors made due to the simplifying assumptions were evaluated and an improved method of analysis was proposed and applied as reported in Chapter 4.

The work on falling sphere data analysis also revealed that most of the 80-120 km results were based on values of drag coefficient in the transition regime that were extrapolated from wind tunnel results that were far outside the transition regime. In the work reported here, more recent wind tunnel data reported in the literature were obtained and more accurate drag coefficient relationships were developed based on these data. This work is reported in Chapter 5.

The improved drag coefficient relationships revealed a considerable error in previous falling sphere drag interpretation. These data were reanalyzed using the more accurate relationships. The result of this work is given in Chapter 6.

In this work the drag coefficient has been studied for the entire spectrum of Knudsen Number and speed ratio. One region which was of particular interest is in the very low speed ratio region. This region of the aerodynamic spectrum has received little experimental attention except for highly viscous flows due to the experimental difficulty of obtaining drag data in a low-density, slow-flow situation. The theoretical work in this region is discussed in Chapter 7.

The recommendations for future work are presented in the form of two proposals given in Chapter 8. Both proposals would involve additional analytic work and subsequent experiments using the shuttle space craft.

The computer programs generated during the period of performance of the contract are given in the appendix.

## CHAPTER I

### INFLUENCE OF SATELLITE AERODYNAMICS ON ATMOSPHERIC DENSITY DETERMINATION

A preprint of a paper by G. R. Karr and R. E. Smith from Preprint Volume of the International Conference on Aerospace and Aeronautical Meteorology was published by AMS, Boston, Mass. Presentation was given May 22-26, 1972.

## INFLUENCE OF SATELLITE AERODYNAMICS ON ATMOSPHERIC DENSITY DETERMINATION\*

Gerald R. Karr

Coordinated Science Laboratory  
University of Illinois  
Urbana, Illinois

and

Robert E. Smith

National Aeronautics and Space Administration  
Marshall Space Flight Center  
Huntsville, Alabama

### 1. INTRODUCTION

Drag-deduced densities of the upper atmosphere have been a primary source of data in the development of atmospheric models and to the study of the upper atmosphere. In the past, the determination of atmospheric density has been through the observation of satellite orbital decay over a long period of time which necessarily required knowledge of only the average drag properties of the satellite. However, as tracking techniques become more accurate and the use of sensitive accelerometers increases, the assumption of average drag properties is no longer valid and a more accurate treatment of satellite aerodynamics must be made.

The purpose of the following discussion will be to focus on three principle satellite aerodynamic factors which influence the interpretation of satellite dynamic response; these are, (1) the influence of satellite orientation and shape on the drag coefficient, (2) the effect of changes in the gas flow properties with altitude, and (3) the influence of upper atmospheric winds on the interpretation of data.

The three topics to be treated are effects causing the greatest source of error in current data reduction. Other factors such as aerodynamic lift, changing atmospheric composition, and changing satellite surface properties will not be treated here but such factors could be of importance for particular satellite systems having large aerodynamic lift forces and widely varying gas and surface properties. The following will then be limited to a discussion of aerodynamic drag effects only and the assumption of constant satellite surface properties. The atmospheric gas will be considered of single species having the average properties associated with a particular altitude.

The three factors to be discussed are of importance in the interpretation of past data as well as the application to future more accurate measurements. For this reason, an estimate will be made of the possible correction to present density models based on the results of the present study. As a basis for calculation and comparison only, the Jacchia (1971) model is employed in the analysis. Other current models could be used for the same purposes with similar results.

### 2. SATELLITE AERODYNAMICS

The aerodynamic flow regime experienced by the majority of satellites is free molecular. That is, the mean free path between collisions of molecules in the upper atmosphere is greater than the dimensions of the majority of Earth satellites. This assumption is certainly true for altitudes greater than 200 km where the near free path is on the order of kilometers. Although departures from free molecular flow will occur in regions of high density, the assumption of free molecular flow may be considered reasonably accurate to an altitude of 100 km where the mean free path is of the order of meters. For convenience, free molecular flow is assumed through out the altitude range being considered in this discussion.

In the free molecular flow of space, by definition, collisions of molecules with the satellite surface predominate. For this reason, the study of satellite aerodynamics requires an understanding of the interaction of gas molecules with solid surfaces. The drag properties of a satellite are influenced primarily by the exchange of momentum with the surface during the molecular impact.

The description of the molecular impact to be employed in this discussion is the generalized gas surface interaction (GSI) model which has direct application to the problem of satellite drag, see Karr (1969). This model is represented in Figure 1 showing a general non-specular type of reflection. The reflected molecules produce a momentum vector in the direction  $\theta_r$  with an average velocity of  $U_r$ . The reflected properties are assumed to depend upon the incident flow properties such that

\* This work was supported in part by the Joint Services Electronics Program (U.S. Army, U.S. Navy, and U.S. Air Force) under Contract DAAB-07-67-C-0199; and in part by the National Aeronautics and Space Administration and the American Society for Engineering Education through the 1971 ASEE-NASA Summer Faculty Fellowship Program at Marshall Space Flight Center.

$$\theta_j = \frac{\pi}{2} P_j + (1-P_j)\delta$$

$$U_j = \sqrt{1-\alpha_j} U$$

where  $\alpha_j$  and  $P_j$  are parameters of the interaction.

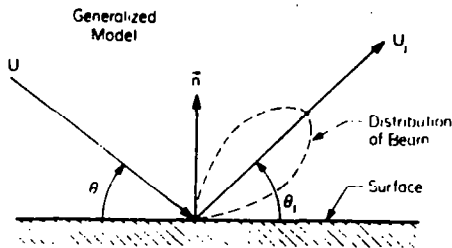


Fig. 1. Description of the gas surface interaction.

Using the model of the interaction described, the force components in the direction of drag can be expressed locally at the surface. The total force is obtained by integrating over the entire surface exposed to the flow. If the satellite velocity is much higher than the random kinetic motion of the gas molecules, the gas molecules can be considered stationary as the satellite sweeps out molecules in its path. The assumption of such conditions (the hypervelocity assumption) allows one to determine the drag coefficient based upon the area projected to the flow.

Under the assumption of hypervelocity flow and the generalized gas surface interaction the following results are obtained for four shapes of interest. The drag coefficient is defined as

$$C_D = \text{Drag} / \frac{1}{2} \rho V^2 \bar{A}$$

where  $\bar{A}$  is a reference area taken to be a constant, independent of angle of attack.

#### Flat plate with angle of attack $\beta$

$\bar{A}$  = Area of plate

$$C_D = 2 \sin^2 \beta - 2\sqrt{1-\alpha_j} \sin \beta \cos \frac{\pi}{2} P_j + (2-P_j)\beta$$

#### Cylinder with axis perpendicular to flow

$\bar{A}$  = DL, D = diameter, L = length

$$C_D = 2 + 2\sqrt{1-\alpha_j} \left[ \frac{\cos \frac{\pi}{2} P_j}{(1-P_j)(3-P_j)} \right]$$

where the bracketed term is equal to  $\frac{\pi}{4}$  when  $P_j = 1.0$ . A value of  $P_j = 3$  is not meaningfully applied to this shape.

#### Cone with axis parallel to flow

$\bar{A}$  = Area of base of cone =  $\pi r^2$

$$C_D = 2 - 2\sqrt{1-\alpha_j} \cos \left[ \frac{\pi}{2} P_j + (2-P_j)\delta \right]$$

where  $\delta$  is the cone half angle.

#### Sphere

$$\bar{A} = \pi r^2$$

$$C_D = 2 + \sqrt{1-\alpha_j} \left[ \frac{4(1-\cos \frac{\pi}{2} P_j)}{P_j(4-P_j)} \right]$$

where the bracketed term is equal to zero for  $P_j = 0$ . A value of  $P_j = 4$  is not applicable.

The above results clearly illustrate the influence of the GSI and the shape on the drag properties. The results for a sphere are shown plotted in Figure 2. A range of  $C_D$  from a minimum of 2.0 to a maximum of 4.0 is seen depending upon the values of gas surface interaction parameters,  $\alpha_j$  and  $P_j$ . The results for the cone shape reveals that depending upon the cone half angle,  $C_D$  values less than one are possible. Thus, it is seen that satellite shape and satellite surface properties are strong influences on the drag properties.

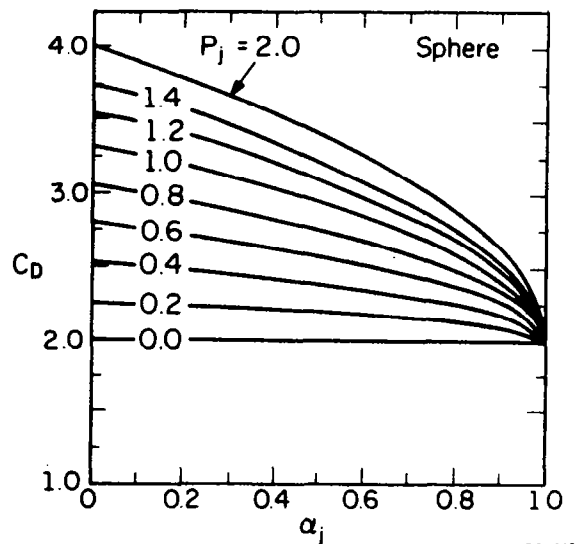


Fig. 2. Drag coefficient of sphere as a function of gas surface interaction parameters.

### 3. THE EFFECT OF SATELLITE ORIENTATION

Satellites rarely present the same shape to the flow during an orbit. For this reason, the effect of satellite orientation, which is important in determining the instantaneous drag properties of a satellite, is also important in determining the average drag properties. In order to illustrate the effect of angle of attack, consider first a cylinder with spherical end caps with an angle of attack  $\alpha$ . For the special case of specular reflection ( $P_j = 0$ ) and

hypervelocity flow, the following analytic results are obtained.

Cylinder with spherical ends;  $P_j = 0$ , hypervelocity flow and angle of attack  $\alpha$ .

$$C_D = 2 \left[ 1 + \frac{4}{\pi} \frac{L}{D} \sin \alpha \right] + \sqrt{1 - \alpha_j} \frac{4}{\pi} \frac{L}{D} \sin \alpha \left[ \frac{8}{3} \sin^2 \alpha - 2.0 \right]$$

where  $\bar{A} = \pi r^2$  and  $L/D$  is the length to diameter ratio of the cylinder.

These results reveal that  $C_D$ , for the cylinder with spherical ends, changes considerably depending upon the angle of attack and the shape (length to diameter ratio). As expected, the  $C_D$  value is that of a sphere when  $\alpha$  is zero and is progressively influenced by the cylinder as the angle of attack is increased to a value of  $\frac{\pi}{2}$ . Since  $\pi r^2$  is used as the reference area at all angles of attack,  $C_D$  will reach high values for large values of  $L/D$ .

For more complex shapes such as the cone, results must be obtained numerically. Figure 3 shows such results for a  $35^\circ$  half angle cone. The plot is a three axis presentation of the surface  $C_D(P_j, \beta)$  where  $P_j$  varies from zero at the front to a value of  $\frac{1}{2}$  at the rear. The angle of attack is varied from zero on the right to  $180^\circ$  on the left. The value of  $\alpha_j$  was taken to be zero in constructing this plot. The function has a maximum value of 4.00 and a minimum value of 0.399. These results illustrate further the strong dependence of aerodynamic drag on the shape, orientation, and GSI.

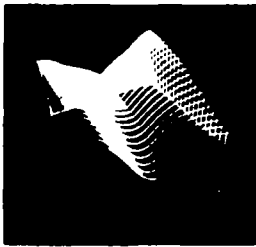


Fig. 3. Computer generated plot of surface  $C_D(P_j, \beta)$  for a  $35^\circ$  half angle cone with flat base where  $P_j$  varies from zero to two from front to back and  $\beta$  varies from zero to  $180^\circ$  from right to left. The values of  $C_D$  vary from 0.399 to 4.00.

Just as the instantaneous values of  $C_D$  are influenced by angle of attack, the average value of  $C_D$  over an orbit also depends upon the attitude history the satellite experiences over the orbit. In order to illustrate this factor, consider the determination of the average drag coefficient over an orbit of the satellite. The time average of  $C_D$  is given by

$$\bar{C}_D = \frac{1}{T} \int_0^T C_D dt.$$

For a circular orbit the satellite will travel at a constant rate and, for this case,

$$\bar{C}_D = \frac{1}{2\pi} \int_0^{2\pi} C_D d\alpha.$$

Consider now a spin-stabilized cone shaped satellite with a flat base. The orientation of the satellite spin axis with respect to the orbit is given by the angle  $\lambda$  as shown in Figure 4. The angle  $\theta_s$  serves to oriente the

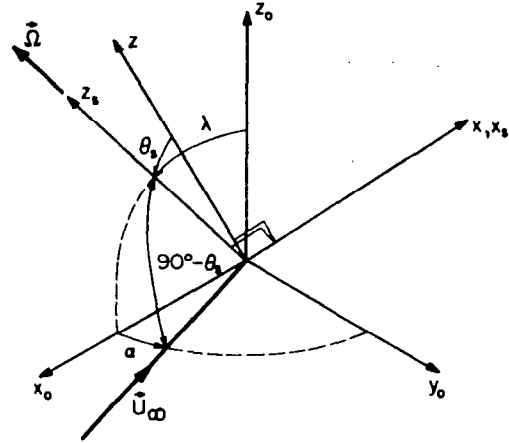


Fig. 4. Coordinated system describing orientation of spin stabilized satellite with respect to orbit plane.

spin axis with respect to the velocity vector  $\bar{U}_\infty$ . For a circular orbit, the velocity vector will rotate about the spin stabilized satellite at a constant rate. Since the instantaneous value of  $C_D$  for each point in the orbit can be determined, the average  $C_D$  over the orbit can also be determined by numerical quadrature. The results of such a study are presented in Figure 5 for five cone half angles and for  $\lambda$  from 0 to  $90^\circ$ . The base area of the cone was chosen as the reference area in each case and the same GSI parameters used for each plot.

The results given in Figure 5 illustrate the importance of taking the satellite orientation history into account in selecting an average drag coefficient. Since the satellite orbit and the satellite spin axis will tend to drift in space, the average drag coefficient should not be expected to remain constant. The amount of variation is seen to increase as the amount of non-symmetry of the satellite is increased. Only spherically symmetric shapes will experience no variation.

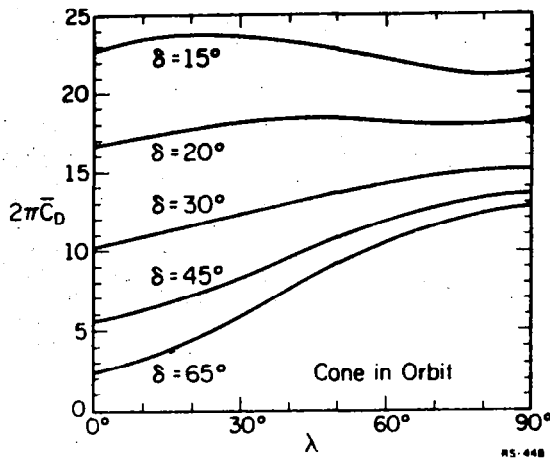


Fig. 5. Average drag coefficient for spin stabilized cone shaped satellites as a function of spin axis orientation with respect to orbit.

#### 4. EFFECT OF ALTITUDE ON DRAG COEFFICIENT (THE SPEED RATIO EFFECT)

The assumption of hypervelocity flow used in obtaining the results of the preceding sections will now be examined. A discussion of this assumption is facilitated by introducing a flow parameter termed the speed ratio,  $S$ , defined as the ratio of the satellite velocity to the random velocity of the gas molecules in thermal equilibrium. The speed ratio is given by

$$S = U_{\infty} / \sqrt{2RT/M}$$

where  $R$  the universal gas constant,  $M$  the average molecular weight and  $T$  is the temperature of the gas. Hypervelocity flow, the assumed flow in the preceding work, is approached as the speed ratio approaches infinity.

Two factors influence the value of the speed ratio as the altitude of the satellite orbit is changed. First, considering circular orbits only, the velocity of the satellite decreases as altitude increases. Second, the temperature of the atmosphere and therefore the thermal velocity of the molecules increases with increasing altitude. These two factors combine to cause a considerable decrease in speed ratio as altitude increases. This effect is illustrated in Figure 6 which shows the value of the circular speed ratio as a function of altitude for four exospheric temperatures. This plot was constructed using values of temperature and mean molecular weight from Jacchia (1971).

In order to investigate the influence of speed ratio on the drag coefficient, consider a cylinder with spherical ends. Utilizing data from Karr and Yen (1972), Sentman (1961), and Fan and Andrews (1969), the value of  $C_D$  for three speed ratios were obtained giving the following results for the zero angle of attack

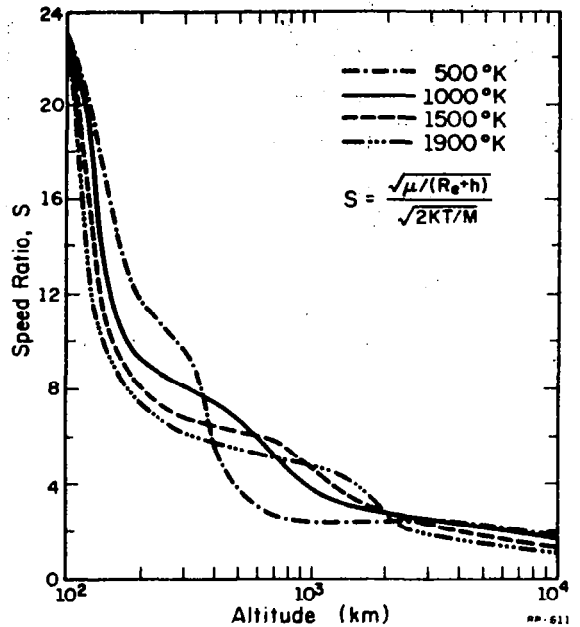


Fig. 6. Circular speed ratio as a function of altitude for four exospheric temperatures based on Jacchia 1971 model.

case. These three values were used to obtain a

$S$	$C_D$
$\infty$	2.0
8	$2.106 + 0.450(2L/\pi D)$
4	$2.249 + 0.885(2L/\pi D)$

second order polynomial approximation to the variation in  $C_D$  with  $S$ . The results are

$$\frac{C_D}{C_{D_{S=\infty}}} = 1 + (0.350 + 1.166 L/D)/S + (0.592 - .1528 L/D)/S^2.$$

This function is plotted in Figure 7 for three values of  $L/D$ . Two factors of importance are illustrated in these results. First, long slender object at low angles of attack are strongly influenced by speed ratio effects. Even at relatively high values of speed ratio, there is strong sensitivity to the length to diameter ratio for long slender objects. Second, for a given satellite shape, considerable change in the value of  $C_D$  is seen to occur over the range of interest from  $S=4$  to  $S=20$ .

Combining the results of the polynomial fit of  $C_D$  values for a sphere with the change of  $S$  with respect to altitude, the change in  $C_D$  for a sphere over the altitude range from 100 to 1000 km is obtained and presented in Figure 8. These results, for the same four exospheric

## 5. EFFECT OF ATMOSPHERIC WINDS ON DRAG STUDIES

Recent analytic and experimental studies point to high velocity atmospheric winds in the upper atmosphere. Velocities of as much as 400 m/sec have been reported. Since satellite velocities are of the order 7 km/sec, atmospheric winds are expected to be an influence on the satellite motion. In order to investigate such influence, consider a simple model of the upper atmospheric wind structure which includes the rotation of the atmosphere at the rotation rate of the Earth. In addition to the rotation, consider an east-west wind which varies in both magnitude and direction. Results of Challinor (1969), suggest that the east-west component could be assumed to approximate a sinusoid variation with a longitude angle,  $\alpha$ , measured from a reference point of zero wind. The velocity of a satellite with respect to the atmospheric gas in circular orbit is then given by

$$U_{\infty} = \sqrt{\frac{\mu}{r}} - r\Omega_e - v_{\max} \sin\alpha$$

where  $v_{\max}$  is the peak wind velocity,  $r$  is the distance from the center of the earth and  $\Omega_e$  is the angular velocity of the earth. At some longitudes, the wind is seen to subtract from the atmospheric velocity while adding at other longitudes.

The instantaneous drag acting on a satellite at any point in the orbit is given by

$$D = \frac{1}{2} \rho U_{\infty}^2 C_D \bar{A}$$

The average drag over one revolution is found by integrating over the time in the circular orbit

$$\begin{aligned} \bar{D} &= \frac{1}{2\pi} \int \frac{1}{2} \rho U_{\infty}^2 C_D \bar{A} d\alpha \\ &= \frac{1}{2} \rho C_D \bar{A} \left[ \sqrt{\frac{\mu}{r}} - r\Omega_e \right]^2 + \frac{1}{2} v_{\max}^2 \end{aligned}$$

the average drag is found to be increased by a factor,  $F_{\text{wind}}$ , where

$$F_{\text{wind}} = \frac{\frac{1}{2} v_{\max}^2}{\left[ \sqrt{\frac{\mu}{r}} - r\Omega_e \right]^2}$$

The increase in drag due to winds for a circular orbit is found to be small enough to be neglected. The increase is less than 1% for typical values of velocities.

Consider now a more severe case when a satellite in an elliptic orbit has its perigee at the peaks of wind velocity. Such a situation is likely since, often times, observations of elliptic satellite orbits are made to determine atmospheric properties in the region of perigee. Much of the knowledge of latitude and longitude variations in the atmosphere have developed from such observations.

Consider the perigee passage at  $\alpha = 90^\circ$ , where the wind velocity subtracts, with the

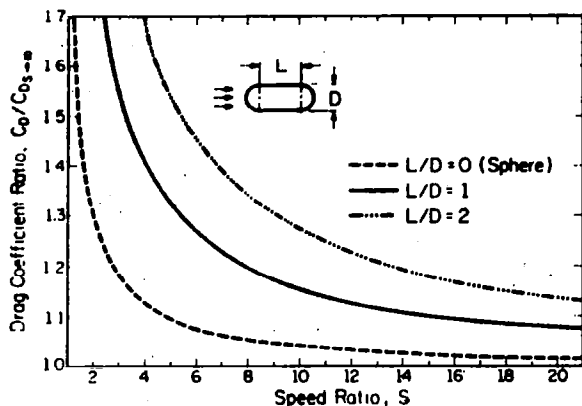


Fig. 7. Change in drag coefficient as a function of speed ratio for three values of L/D.

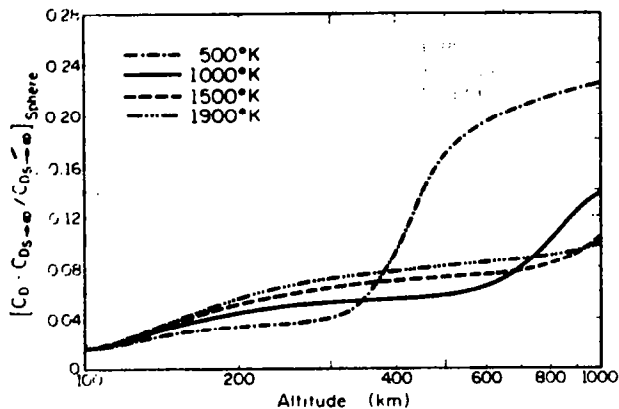


Fig. 8. Change in drag coefficient as a function of altitude for four exospheric temperatures.

temperatures as in Figure 6, show that a sphere will experience a change in  $C_D$  of from 2 to 10% depending upon the atmospheric temperature. Even greater changes would be expected for non-spherical satellites such as the cylinder with spherical ends.

Of importance is the fact that the noted change in  $C_D$  with altitude is found to be systematic with altitude. For this reason then, it is to be expected that present drag deduced density values will have these systematic errors incorporated into the results. This factor could account for some of the discrepancies in densities at high altitude in comparison to densities at lower altitudes. Similar results and conclusions were found by Izakov (1965) using an analytic expression for  $C_D$  of a sphere as a function of  $S$ .

perigee passage at  $270^\circ$ , where the wind velocity adds. For similar orbits and constant density, the ratio of drag at perigee for these two cases could be taken to be

$$\frac{D_{90^\circ}}{D_{270^\circ}} \sim \left[ \frac{\sqrt{\frac{\mu}{r_p}} \sqrt{1+e} - r_p \Omega_e - v_{\max}}{\sqrt{\frac{\mu}{r_p}} \sqrt{1+e} - r_p \Omega_e + v_{\max}} \right]^2$$

$$\approx 1 - \frac{4 v_{\max}}{\sqrt{\frac{\mu}{r_p}} \sqrt{1+e} - r_p \Omega_e}$$

where  $r_p$  is the orbit radius at perigee and  $e$  is the eccentricity of the orbit. In the altitude range from 100 to 1000 km,  $r_p \Omega_e$  is approximately .5 km/sec, and  $\sqrt{\mu/r_p}$  is approximately 7.5 km/sec. For  $e$  values less than 0.2, percentage differences in drag of the order of three percent are obtained for  $v_{\max}$  values of 200 to 400 m/sec. The wind effect is found to be much larger for this case than for the circular orbit case. Due to the lag in solar heating of the atmosphere, the  $\alpha = 90^\circ$  point would occur after sunset while the  $270^\circ$  point would be after sunrise. The results obtained reveal that a difference in drag of a maximum of 3% at about 200 km is explainable by wind effects. If these wind effects were not taken into consideration, the difference in drag would be misinterpreted as being caused by a corresponding difference in atmospheric density. Therefore, wind effects could explain some of the day-night variation in density deduced from satellite drag.

## 6. CONCLUSIONS AND DISCUSSION OF RESULTS

The preceding discussion has emphasized the variability of satellite drag coefficients. In particular, the effect of the gas surface interaction is seen to dominate. Unfortunately, values of  $P_j$  and  $\alpha$  have yet to be determined accurately enough to be used in satellite drag studies. This factor leads to considerable uncertainty in the specification of satellite drag coefficients which could cause errors of as much as 50% in the values of  $C_D = 2.2$  used in past data reductions.

In view of the influence on drag coefficients of non-spherically symmetric shapes and the speed ratio, values of  $C_D$  of around 2.2 are likely too low for most satellite shapes. This observation is based on the fact that for a sphere the minimum  $C_D$  for  $S \rightarrow \infty$  is 2.0. Speed ratio effects cause the minimum value to be increased to values of 2.1 or higher. In order for the sphere to have the minimum  $C_D$ , the gas surface interaction would have to be specular or the accommodation coefficient would have to be unity corresponding to reflection at near zero velocity. Such limiting interactions appear unlikely, meaning that  $C_D$  values higher than 2.2 are likely.

Although an absolute value for  $C_D$  may be lacking presently, the results obtained for

changes of  $C_D$  due to shape, orientation, and altitude reveal that systematic variation of  $C_D$  around an absolute value would occur under most circumstances. These variations should be included in the analysis of future satellite data where information on satellite orientation may be available.

The effects of atmospheric winds were illustrated assuming a simple model of the wind structure. These results illustrate still another source of error in drag deduced density values. Future planned work will consider a more sophisticated model of the wind structure. This study is expected to lead to improved knowledge of the upper atmospheric density and wind structure.

## 7. REFERENCES

- Challinor, R. A., 1969, Neutral-air Winds in the Ionospheric F-region for an Asymmetric Global Pressure System, *J. Atmos. Sci.*, 17, pp. 1097-1106.
- Fan, Chien and Andrews, C. Donalds, 1969, Application of the Nocilla Wall Reflection Model to Calculate Aerodynamic Coefficients for Orbital Vehicles with Complex Geometry, Lockheed Missiles and Space Company, HBEC-4401-1, Huntsville, Alabama.
- Izakov, M. N., 1965, Some Problems of Investigating the Structure of the Upper Atmosphere and Constructing its Model, *Space Res.*, V, pp. 1191-1213.
- Jacchia, L. G., 1971, Revised Static Models of the Thermosphere and Exosphere with Empirical Temperature Profiles, SAO Special Report 332, Smithsonian Institution, Cambridge, Mass.
- Karr, Gerald R., 1969, A Study of Effects of the Gas-Surface Interaction on Spinning Convex Bodies with Application to Satellite Experiments, Coordinated Science Laboratory Report R-435, University of Illinois, Urbana, Illinois (Ph.D. thesis).
- Karr, G. R. and Yen, S-M, 1972, Aerodynamic Properties of Spinning Convex Bodies in a Free Molecule Flow, *Rarefied Gas Dynamics*, Seventh Symposium, Academic Press, (in press), 8 pages.
- Sentman, Lee H., 1969, Free Molecule Flow Theory and its Application to the Determination of Aerodynamic Forces, Lockheed Missiles and Space Tech. Report, LMSC-448514, Sunnyvale, California.

**CHAPTER II**

**SATELLITE AERODYNAMICS AND ATMOSPHERIC DENSITY DETERMINATION FROM  
SATELLITE DYNAMIC RESPONSE**

SATELLITE AERODYNAMICS AND ATMOSPHERIC DENSITY DETERMINATION FROM  
SATELLITE DYNAMIC RESPONSE

by

Gerald R. Karr

ABSTRACT

A method for determining satellite aerodynamic properties and upper atmospheric density from observed satellite dynamic response has been successfully developed and tested.

The aerodynamic drag and lift properties of a satellite are first expressed as a function of two parameters associated with gas-surface interaction at the satellite surface. The dynamic response of the satellite as it passes through the atmosphere is then expressed as a function of the two gas-surface interaction parameters, the atmospheric density, the satellite velocity, and the satellite orientation to the high speed flow. By proper correlation of the observed dynamic response with the changing angle of attack of the satellite, it is found that the two unknown gas-surface interaction parameters can be determined. Once the gas-surface interaction parameters are known, the aerodynamic properties of the satellite at all angles of attack are also determined. The atmospheric density may then be accurately calculated once the true aerodynamic properties are known.

Employing accelerometer data from the OV1-15 satellite, analysis was successfully made of the aerodynamic properties of that satellite and a determination was made of the absolute value of atmospheric density near the orbit perigee. These results constitute the first successful application of the proposed method of analysis. These results also serve to illustrate the potential of the technique in the analysis and prediction of satellite orbit decay in the atmosphere and the accurate determination of upper atmospheric density from satellite dynamic response.

## 1. Introduction

The problem of satellite orbit decay prediction and the problem of upper atmospheric density determination have encountered a common source of unknown error which can be traced to a lack of knowledge of satellite aerodynamics. The basic equation employed in both orbit decay and density determination is the familiar drag equation:

$$\text{Drag} = 1/2 \rho U^2 C_D \bar{A}$$

where  $\rho$  is the density,  $U$  is the velocity of the satellite with respect to the atmosphere,  $C_D$  is the drag coefficient, and  $\bar{A}$  is a suitable reference area. In most applications of this equation to satellites the value of  $C_D$  is considered to have a constant value. Generally, however, the assumption of constant drag coefficient is not valid and the use of such an assumption can lead to considerable error (see Karr, 1972). The uncertainty in satellite aerodynamics has prevented the assignment of even an approximate value of drag coefficient with a known range of uncertainty. A value of  $C_D$  of 2.0 or 2.2 is often used in satellite drag studies and in the determination of atmospheric density. These values of  $C_D$  are likely too small and, combined with the fact that  $C_D$  is not constant, have resulted in an overestimation of upper atmospheric densities (see Karr and Smith 1972).

A more accurate treatment of satellite aerodynamics has obvious benefit to the determination of upper atmospheric density and the prediction of satellite orbit decay. Satellites traveling in the earth's upper atmosphere experience the aerodynamic flow regime termed the free molecular flow regime. In this flow regime, the collision of atmospheric gas molecules with the satellite surface dominate the flow and collisions of gas molecules with other gas molecules may be ignored. Satellite aerodynamic properties are then the result of the interaction of high speed gas molecules with the solid satellite surface. Unfortunately, very little is known about the gas surface interaction at satellite velocities and this lack of information is the basic source of uncertainty in satellite aerodynamic properties.

In the interest of developing a more accurate treatment of satellite aerodynamics for application to orbit decay prediction and density determination, a model of the gas surface interaction has been developed which utilizes two parameters to describe the interaction (see Karr, 1969 and Karr and Yen, 1970). The advantage in this treatment of satellite

aerodynamics is that no a priori assumptions of the aerodynamic properties need be made. The gas surface interaction parameters are considered as unknowns to be determined from the observed dynamic response of the satellite as it travels through the atmosphere. The determination of the gas surface interaction parameters serves as the key to the subsequent determination of both the aerodynamic properties and the atmospheric density.

To test the proposed method of analysis, accelerometer data from the OVI-15 satellite is used. The accelerometer data provide an accurate, instantaneous measure of the level of aerodynamic force and the attitude of the satellite with respect to the flow. As is pointed out in the paper, accurate satellite attitude information is essential to the analysis. The OVI-15 satellite, although less than ideal in shape for an aerodynamic study, provided a good basis for the test of the proposed method of analysis. The results serve to illustrate the potential that this method of analysis has to future determinations of aerodynamic and atmospheric properties.

## 2. Satellite aerodynamics and the gas surface interaction.

Consider a local satellite surface element in which the high speed flow of molecules is incident at an angle of  $\theta$  as shown in Figure 1. Associated with the incident flow is the incident momentum which gives rise to the incident force  $\vec{F}_i$ . This force is colinear with the satellite velocity,  $U$ , with respect to the atmosphere. Assume for now that the speed ratio is infinite where the speed ratio is defined as the satellite velocity divided by the thermal velocity of the gas molecules. The thermal velocity of the gas molecules is taken to be equal to  $\sqrt{R T/M}$  where  $R$  is the gas constant,  $T$  is the temperature,  $M$  is the mean molecular weight.

The molecules reflected from the surface cause a net reaction force  $\vec{F}_r$  which is colinear with the mass-motion velocity vector  $\vec{U}_j$  of the molecules leaving the surface. The direction of  $U_j$  is given by the angle  $\theta_j$ .

Modeling of the interaction is performed by providing relationships between the incident and reflected quantities. The relationships are given by

$$U_j = \sqrt{1 - \alpha_j} U$$

$$\theta_j = \frac{\pi}{2} P_j + (1 - P_j) \theta$$

where  $\alpha_j$  and  $P_j$  are the parameters of the interaction. The subscript  $j$  is used if more than one set of interaction coefficients is to be considered in the analysis. ~~Until~~ more is learned of the interaction, these linear relationships provide a useful first approximation to the interaction that occurs at satellite velocities. The parameters  $\alpha_j$  and  $P_j$  are capable of describing a much wider range of possible interactions than other models. The development of this model and the capabilities are described in detail in Karr 1969 and Karr and Yen, 1970.

The model described above is particularly useful in the determination of forces acting on the satellite surface. The total vector force acting on the element of surface shown in Figure 1 is given by

$$d\vec{F} = -(\vec{U} - \sigma_j \vec{U}_j) \rho \vec{U} \cdot \vec{n} dA$$

where  $\sigma_j$  is employed if more than one gas surface interaction is employed in the analysis. In order to conserve mass at the surface, the sum of the  $\sigma_j$  values must be unity.

The magnitude and direction of  $U_j$  is determined by the parameters  $\alpha_j$  and  $P_j$ . The vector force acting on the local element of surface is then expressed as a function of  $\alpha_j$ ,  $P_j$ ,  $U$ ,  $\rho$ , and  $\theta$ . For a given satellite shape (assumed to be convex) the total aerodynamic forces and torque acting on the satellite are found by integration of  $d\vec{F}$  and  $\vec{R} \times d\vec{F}$  over the surface exposed to the flow. In general, the results will be of the form

$$\text{Drag} = 1/2 \rho U^2 C_D (\alpha_j, P_j, \beta) \bar{A}$$

$$\text{Lift}_{1,2} = 1/2 \rho U^2 C_{L1,2} (\alpha_j, P_j, \beta) \bar{A}$$

$$\text{Torque}_{1,2,3} = 1/2 \rho U^2 C_{T1,2,3} (\alpha_j, P_j, \beta) \bar{A} \bar{L}$$

where  $\theta$  is an angle of orientation and the subscripts on  $C_L$  and  $C_T$  are to indicate that there are two components of lift and three components of torque. The six aerodynamic properties are found to be a strong function of the gas surface interaction parameters. For non-spherical objects, the angle of orientation,  $\beta$ , also has a strong influence on the drag, lift and torque properties (see Karr and Yen, 1970).

### 3. Aerodynamics of the OVI-15 satellite.

The approximated shape of the OVI-15 satellite is a cylinder with spherical ends as shown in Figure 2. The satellite spin axis was normal to the longitudinal axis of the cylinder with a spin rate of about 10 rpm. Near the center of the satellite a three axis accelerometer detected the forces acting on the satellite. Since the data to be used in the subsequent analysis has been filtered and averaged over a number of spin cycles, the aerodynamic properties averaged over a spin cycle are developed.

The total instantaneous vector force acting on the satellite is given by

$$\vec{F} = 1/2 \rho U^2 \bar{A} (C_D D + C_{L1} L_1 + C_{L2} L_2)$$

where  $D$ ,  $L_1$ , and  $L_2$  are mutually orthogonal unit vectors in the drag and lift directions. The  $L_1$  and  $L_2$  directions are defined with respect to the instantaneous orientation such that  $L_1$  is perpendicular to the cylinder axis and the velocity vector. The direction of  $L_2$  is perpendicular to both  $L_1$  and  $D$ . Due to symmetry the lift force in the  $L_1$  direction is zero.

From Karr, 1969,  $C_D$  and  $C_{L2}$  are obtained for the infinite speed ratio case, given by

$$\begin{aligned} C_D &= 2 + 4 \sqrt{1 - \alpha_j} \left(1 - \cos \frac{\pi}{2} \frac{D}{r}\right) P_j (4 - P_j) \\ &\quad + 2 A_R \cos \theta_s \\ &\quad + A_R \sqrt{1 - \alpha_j} \int_{\pi}^{2\pi} [\cos \theta_s \sin \xi C_j - \cos^3 \theta_s \\ &\quad \sin^3 \xi (C_j + S_j)] d\xi \\ C_{L2} &= -\sqrt{1 - \alpha_j} A_R \cos^2 \theta_s \sin \theta_s \int_{\pi}^{2\pi} \sin^3 \xi (C_j + S_j) d\xi \\ C_{L1} &= 0 \end{aligned}$$

where the first two terms in  $C_D$  are due to the spherical ends and the remaining terms are due to the cylindrical section. The angle  $\xi$  is a cylindrical surface-integration angle. The quantity  $A_R$  is the area ratio of the cylinder to the sphere given by

$$A_R = \bar{A}_{cyl} / \bar{A}_{sph} = 2rL / \pi r^2 = 4L / \pi D$$

The quantities  $C_j$  and  $S_j$  contain the parameter  $P_j$  where

$$C_j = \frac{\cos(\pi/2 P_j + (1 - P_j) \theta)}{\cos \theta}$$

$$S_j = \frac{\sin(\pi/2 P_j + (1 - P_j) \theta)}{\sin \theta}$$

$$\theta = \sin^{-1}(-\cos \theta_s \sin \xi)$$

The angle  $\theta_s$  is an angle of instantaneous orientation defined as the angle between the velocity vector and the longitudinal axis of the cylinder.

Since the OVI-15 spin axis is perpendicular to the axis of the cylinder, the angle  $\theta_s$  is a function of the angle the spin axis makes with the velocity vector,  $\gamma$ , and a spin angle,  $\lambda$ , which changes from 0 to  $2\pi$  every spin cycle (see Figure 3).

For certain values of  $P_j$  the surface integrals over the angle  $\xi$  are easily performed. For  $P_j = 0$ , which corresponds to specular type reflection,

$$C_j \Big|_{P_j=0} = S_j \Big|_{P_j=0} = 1$$

For  $P_j = 1$  which corresponds to diffusive type reflection,

$$C_j \Big|_{P_j=1} = 0 \quad ; \quad S_j \Big|_{P_j=1} = -1/\cos \theta_s \sin \xi$$

For  $P_j = 2$  which corresponds to perfect backscatter type reflections

$$C_j \Big|_{P_j=2} = -1 \quad ; \quad S_j \Big|_{P_j=2} = 1$$

The values of  $C_D$  and  $C_{L2}$  at the three values of  $P_j = 0, 1, 2$ , were used to obtain an polynomial approximation for  $C_D$  and  $C_L$  as a function of  $P_j$ .

Since the accelerometers were body fixed, the output of the accelerometers were a function of both drag and lift forces given by

$$F/\frac{1}{2} \rho U^2 \bar{A} = \left[ -C_D \sin \gamma \cos \lambda + C_L \frac{1 - \sin^2 \gamma \cos^2 \lambda}{\cos \theta_s} \right] i$$

$$+ \left[ - C_D \sin \gamma \sin \lambda - C_L \frac{\sin^2 \gamma \cos \lambda \sin \lambda}{\cos \theta_s} \right] j$$

$$+ \left[ - C_D \cos \gamma - C_L \frac{\sin \gamma \cos \gamma \cos \beta}{\cos \theta_s} \right] k$$

where i, j, and k are unit vectors in the directions of the three axis of the accelerometers with i along the axis of the cylinder, k is in the direction of the nominal spin axis and j is orthogonal. Since the data being used in this analysis has been averaged over spin cycles, the component of force as expressed above were integrated over the angle  $\lambda$ . The results after averaging over one spin cycle were

$$\bar{F}_y = \sin \gamma \frac{1}{2} \rho U^2 \pi r^2 C_F (\alpha_j, P_j, \gamma)$$

$$\bar{F}_z = \cos \gamma \frac{1}{2} \rho U^2 \pi r^2 C_F (\alpha_j, P_j, \gamma)$$

where  $C_F$  is the integrated force coefficient.\* These results show that  $\bar{F}_y$  and  $\bar{F}_z$  measure the identical forces except for the factor  $\sin \gamma$  and  $\cos \gamma$ . This property was used by Fess and Young to obtain the angle  $\gamma$  which the spin axis makes with the velocity vector.

$$\gamma = \cos^{-1} \left[ \bar{F}_z / \sqrt{\bar{F}_y^2 + \bar{F}_z^2} \right]$$

The force coefficient  $C_F$  was found by fitting a 3<sup>rd</sup> order polynomial to the values of  $C_F$  and  $C_{L2}$  at the three values of  $P_j = 0, 1, \text{ and } 2$ .

$$C_F = A + \sqrt{1 - \alpha_j} (G + H P_j + Q P_j^2 + P P_j^3)$$

where

$$A = -2 - 4 A_R E(\gamma, \frac{\pi}{2}) / \pi$$

$$G = -4 A_R E(\gamma, \frac{\pi}{2}) / 3 \pi$$

$$H = 4 F - 2G - 2A$$

$$Q = -4 F + 5G/4 + 11 A/4$$

$$P = F - G/4 - 3 A/4$$

$$F = -4/3 - \pi A_R / 2$$

where  $E(\gamma, \frac{\pi}{2})$  is a complete elliptic integral of the second kind resulting from the average over one spin cycle.

\* The accelerometer in the x direction did not function so only  $\bar{F}_y$  and  $\bar{F}_z$  are treated in the analysis.

#### 4. Method of analysis.

The objective of the analysis is to find the best values of  $\alpha_j$ ,  $P_j$  and density which explains the observed accelerometer output of the OVI-15. Although  $\alpha_j$ ,  $P_j$ , and  $\rho$  are considered as unknowns in the analysis, certain assumptions on the characteristic variation of  $\rho$  are made to facilitate the analysis. The assumption made is that the density variation is symmetric with respect to the perigee of the orbit. The absolute value of density is still treated as an unknown quantity.

##### 4.1 Least squares fit.

Assuming symmetrical density variation about perigee, differences in forces measured at points equal distance from perigee must be due to changes in the aerodynamic force coefficient,  $C_F$ . Since the density is equal at these two points, we can write

$$\frac{1}{2} U_1^2 \rho_1 (T - \Delta t_i) = \frac{1}{2} U_2^2 \rho_2 (T + \Delta t_i)$$

where the subscript 1 indicates approach to perigee, subscript 2 indicates recession from perigee and  $T$  is the perigee passage time. The aerodynamic properties and forces measured at these two points must then satisfy the following relationship

$$\frac{\overline{F}_{i1}}{C_F(\alpha_j, P_j, \gamma_{i1})} = \frac{\overline{F}_{i2}}{C_F(\alpha_j, P_j, \gamma_{i2})}$$

where  $\gamma_{i1}$  and  $\gamma_{i2}$  are the angles of orientation at  $T - \Delta t_i$  and  $T + \Delta t_i$  respectively, and  $\overline{F} = \sqrt{\overline{F}_z^2 + \overline{F}_y^2}$ . In the analysis, the quantity  $DEL_i$  is found from the preceding relation, defined as,

$$DEL_i = \overline{F}_{i1} C_{F_{i2}} - \overline{F}_{i2} C_{F_{i1}}$$

where  $i$  is used to indicate a comparison made at  $T \pm \Delta t_i$ . A solution in the least squares sense is obtained by finding the values of  $\alpha_j$  and  $P_j$  which provide a minimum to the sum-of- $DEL_i$ -squared for a number of observations near perigee

$$SUM = \sum_{i=1}^n (DEL_i)^2$$

The best values of  $\alpha_j$  and  $P_j$  are those which satisfy

$$\frac{\partial(SUM)}{\partial(\sqrt{1-\alpha_j})} = 0 ; \quad \frac{\partial(SUM)}{\partial P_j} = 0$$

in the region of  $0 \leq P_j \leq 2$ , and  $0 \leq \sqrt{1-\alpha_j} \leq 2$ .

## 4.2 Perigee passage time.

The analysis requires first that the aerodynamic properties be different at the comparison points used in the analysis. If the  $C_F$  were not different, then the last equations would be satisfied for all values of  $\alpha_j$  and  $P_j$ . Although the OVI-15 satellite was designed to maintain a  $\gamma = 90^\circ$  throughout the orbit, considerable uncontrolled drift in the spin axis was found to occur. This malfunction was desirable for purposes of this analysis since the angle  $\gamma$  changed considerably during a given orbit. This factor resulted in a changing value of  $C_F$  over the orbit which provided a good sampling of  $C_F$  and  $\bar{F}$  values for a wide range of angles of orientation. The analysis also requires that the perigee passage time be accurately known since the comparisons are made at equal points on each side of this time. Since the report of Fess and Young did not provide a perigee passage time, it was necessary to calculate that time from the accelerometer output. Since the aerodynamic properties are changing during a perigee pass due to the changing angle of orientation, the peak in the  $\bar{F}$  curve is shifted in time from the peak in dynamic pressure. The derivative of  $\bar{F}$  during a perigee pass is

$$\bar{F}' = S C_F' + S' C_F$$

where  $S$  is the dynamic pressure. At the perigee passage time, the dynamic pressure is maximum and  $S' = 0$ . Therefore, at the perigee passage time

$$\bar{F}'(T) = \frac{F(T)}{C_F(T)} C_F'(T)$$

This equation was employed to find the true value of  $T$  for each data set employed. The quantities  $C_F$  and  $C_F'$  are a function of  $\alpha_j$  and  $P_j$  in addition to the angle  $\gamma$ . The analysis was able to take into consideration the expected shift in  $\bar{F}$  output which was found to vary from 3 to 15 seconds depending upon  $\alpha_j$ ,  $P_j$  and the rate of change in the angle  $\gamma$ .

## 4.3 Speed ratio effect.

As discussed by Karr 1972 and Karr and Smith 1972, changes in speed ratio with altitude result in a systematic increase of  $C_D$  with altitude. The amount of increase was found to be a function of the satellite shape and orientation. This factor was taken into consideration in the analysis of data of the OVI-15 by approximating the expected change in aerodynamics properties with respect to speed ratio. Using information from Karr and Smith 1972 and taking into account the average over a spin cycle, the following speed ratio correction factor was obtained.

$$\begin{aligned} \text{COF} = & 1 + .682/S + .56148/S^2 \\ & + .4 \sin^2 \gamma (1.66/S - .1528/S^2) \end{aligned}$$

The correction factor is a function of the angle of orientation which must be taken into account in the determination of  $\alpha_j$  and  $P_j$ . For the altitudes of interest for the OVI-15, speed ratios of about 10 are obtained which result in an increase in the aerodynamic force coefficient of about 5%. The determination of density is then strongly influenced by the speed ratio effect.

## 5. Results.

### 5.1 Data used in the analysis.

An example of the data employed in the analysis is shown in Figure 4. Data from orbits number 890, 893 and 896 were employed in the least squares fit to  $\alpha_j$  and  $P_j$ . These orbits had significant changes in  $\gamma$  during perigee passage and experienced approximately the same atmospheric conditions. These nearly polar orbits occurred in mid-September 1969 with perigees at 150 km, perigee latitude at 10°S latitude with a local perigee time at about 1930. Since the sun declination was near +3°, the variation in density with latitude near perigee is approximately zero according to the Jacchia 1971 model of the atmosphere.

The choice of orbits used in the analysis contributed to the reduction of errors resulting from any nonsymmetry of density variation. Further reduction in this type error was made by using only data within  $\pm 10^\circ$  of perigee. In addition, since data from three orbits was used, the errors due to wave motion or other short duration density disturbances would contribute only to the random error.

The values of accelerometer output  $\bar{F}$ , angle of orientation  $\gamma$ , and time in seconds from the beginning of data transmission are given in Table I. The units on  $\bar{F}$  is in counts in which 5.3 counts equals  $10^{-6}g$  of acceleration. The angle  $\gamma$  is given in degrees. The data is seen to cover an angle of attack range of about 28 degrees. All the data falls within 150 seconds of perigee which for these orbits means that the data is taken within  $\pm 10^\circ$  of perigee. Since the true perigee is always within  $\pm 20$  seconds of the peak  $\bar{F}$ , corrected perigee times will not change the range of data significantly.

### 5.2 Gas Surface interaction parameters.

Using the data given in Table I and taking into account the perigee passage time correction and the speed ratio correction, the results of the sum-of-the-squares-of- $DEL_i$  are given in Figure 5. These results show a unique minimum of the sum-of-the-squares-of- $DEL_i$  at  $P_j = .44$  and  $\sqrt{1 - \alpha_j} = .6$ . These values for  $\alpha_j$  and  $P_j$  mean that the reflection is between a specular and diffusive type reflection in direction and has moderate accommodation of energy.

### 5.3 Aerodynamic properties.

Using  $\alpha_j = .64$  and  $P_j = .44$ , the aerodynamic force properties of the OVI-15 satellite may be found using the equations already derived. The results are shown in Figure 6 which gives  $C_F$  as a function of angle of orientation. The level of  $C_F$  is dependent directly on the reference area,  $\bar{A}$ , chosen to represent the satellite. The plot is given for two acceptable areas (1) the maximum cross sectional area seen by the flow,  $\pi r^2 + 2rL$  and (2) the minimum cross sectional area seen by the flow,  $\pi r^2$ . These results are for the infinite speed ratio case and must be modified according to speed ratio influence.

At angles of 0, 90 and 180°, the quantity  $C_F$  is equal to the drag coefficient. At all other angles,  $C_F$  is influenced by both drag and lift coefficients. These results show that the drag coefficient is higher than the value of 2.2 normally assumed in drag analysis. The speed ratio correction will cause these values to be increased by about 5% to 10% for the altitudes at which the data was taken.

The atmospheric density values may be obtained since the values of  $C_F$  throughout the orbit have been calculated. Assuming an orbit of  $e = .113$  and perigee at 150 km, the value of  $U$  at the data points are obtained and density values are given by

$$P(I, J) = 2amF(I, J)/U^2(I, J)\bar{A}C_F(I, J) COF$$

where  $COF$  is the speed ratio correction factor dependent upon the angle  $\gamma(I, J)$ ,  $a$  is the conversion factor needed to convert accelerometer counts into accelerometer values ( $a = 10^6 g/5.3$  counts), and  $m$  is the satellite mass = 214 kg. The speed ratio correction requires an estimate of the speed ratio. For the date, time, and region of the atmosphere for which the data corresponds, an estimate was made of the exospheric temperature from information provided by Smith, 1972. In this region of the atmosphere the exospheric temperature remains essentially constant and was taken to be 1100°. Using the Jacchia 1971 model atmosphere, a value of  $T/M$  versus altitude were fitted to a polynomial over the altitude range of interest from 140 km to 220 km. The speed ratio is then given at each data point by

$$S = U/\sqrt{2RT/M}$$

where  $R$  is the universal gas constant. Values of density calculated in this manner are about 5 to 15% less than those predicted by the Jacchia 1971 model. A more complete discussion of these results will be made at a later date.

### 6. Discussion of results.

The results of this analysis are important for a number of reasons. First, the analysis illustrates a new method for the analysis of satellite.

dynamic response. Second, the results obtained for  $\alpha_j$  and  $P_j$  are the most accurate of measurements of the gas surface interaction parameters at satellite velocity. Third, the values of  $C_F$  obtained in the analysis are the most accurate of measurements of satellite aerodynamic properties. Finally, the results obtained for density are the most accurate of measurements of absolute values of upper atmospheric density.

Past drag analysis have required that critical assumptions be made on  $C_D$  or  $\rho$  or some of the gas surface interaction parameters. The analysis presented here on the other hand has employed very few assumptions in comparison. The assumption of symmetrical density variation about perigee is most subject to error. However, the possible error introduced by nonsymmetry is expected to be much less than the errors committed in past drag studies. The method presented here is far superior in terms of error than previous methods.

Improvement of the errors in the present analysis could be made by a more accurate treatment of aerodynamics and more accurate measurement of accelerations and angles of orientation. The accuracy of angle measurements was about  $\pm 1^\circ$  while the force measurements were accurate to  $\pm 5\%$  for the data used. The aerodynamic description of the OVI-15 could be improved by employing a more accurate expression for the variation in  $C_F$  with  $P_j$ . The polynomial approximation employed in the analysis could be improved or the exact expressions could be employed at the expense of computer time.

The results obtained for  $C_F$  as a function of angle of attack for the OVI-15 is of special interest because of the many drag analysis which have been performed on the satellite. For example, Champion, Marcos, and McIsaac, 1970; Marcos and Champion, 1972; Marcos, Champion, and Schweinfurth, 1971; have analyzed the accelerometer data of the OVI-15 to reveal a number of properties of the upper atmosphere. In these analyses, accelerometer data was used only when the satellite was broadside into the flow. This instantaneous attitude would correspond exactly to the  $0^\circ$  or  $180^\circ$  spin axis orientation of the OVI-15. At this attitude  $C_D$  is equal to  $C_F$  as given in Figure 5 and would have a value of 2.5396 for the case of infinite speed ratio and  $\alpha_j = .64$  and  $P_j = .44$ . This value of  $C_D$  is 15.4% greater than the value of 2.2 which was employed in these analysis. Additional correction would have to be made if speed ratio effects were taken into account. These corrections would result in substantial decrease in densities reported using a  $C_D$  of 2.2.

OVI-15 orbital data has been analyzed by Ching 1971 and King-Hele and Walker 1969. The King-Hele and Walker analysis employed a constant  $C_D$  of 2.2 independent of the satellite orientation. The reference area used by King-Hele and Walker was midway between the maximum of  $2.578 \pi r^2$  and the minimum of  $\pi r^2$  shown in Figure 5. On the basis of the reference area employed by King-Hele and Walker, a  $C_D$  value of between 4.543 and 3.889 would correspond to the values of  $\alpha_j$  and  $P_j$  found in the analysis.

The orbital decay analysis reported by Ching 1971 includes a factor to represent the changing aerodynamic drag properties of the OVI-15. The factor is based on the changing cross sectional area seen by the flow. The drag coefficient is considered constant while the reference area used in the analysis is changed by as much as 25%. A 25% correction factor is too large in view of the results of Figure 5 which show that the maximum change in  $C_D \bar{A}$  would be 16%.

In addition, the effect these results have on past analysis of OVI-15 data in particular, the results indicate that the assumption of  $C_D$  used in most drag studies have been too low. The value of  $C_D = 2.0$  or  $2.2$  which has been used for most past drag analysis is lower than could be expected for most shapes with  $\alpha_j = .64$  and  $P_j = .44$ . A sphere for example would have a  $C_{D_{sph}} = 2.352$  which is 7% higher than the  $2.2$  value often used. It should be noted, however, that the results obtained here are for one satellite surface and one atmospheric composition. It is expected that other surfaces and other compositions should change the values of  $\alpha_j$  and  $P_j$  and result in a change in aerodynamic properties. More data must be collected before a firm value of  $\alpha_j$  and  $P_j$  can be assigned to a given gas and surface combination. Future work should be directed towards this goal.

## REFERENCES

- Champion, K. S. W., F. A. Marcos, and J. P. McIsaac, 1970: Atmospheric Density Measurements by Research Satellite OVI-15. Space Research X, North-Holland Publishing Co., Amsterdam, 450-458.
- Ching, B. K., 1971: Atmospheric Density and Rotation Below 195 km From a High Resolution Drag Analysis of the Satellite OVI-15 (1968-059A), Journal of Geophysical Research, Vol. 76, No. 1, 197-201.
- Fess, W. A. and K. R. Young, 1969: OVI-15 (SPADES) Low G Accelerometer Data Processing. The Aerospace Corporation Report No. TOR-0066(5306)-7.
- Jacchia, L. G., 1971: Revised Static Models of the Thermosphere and Exosphere with Empirical Temperature Profiles. Smithsonian Astrophysical Observatory, Special Report 332.
- Karr, G. R., 1969: A Study of Effects of the Gas-Surface Interaction on Spinning Convex Bodies with Application to Satellite Experiments. Ph.D. Thesis, Coordinated Science Laboratory Report R-435, University of Illinois, Urbana, Illinois.
- Karr, G. R., 1972: Satellite Aerodynamics as a Function of Atmospheric Properties. Paper presented at AIAA 5th Fluid and Plasma Dynamics Conference, Boston, Mass., AIAA Paper No. 72-659, 10 pages.
- Karr, G. R. and R. E. Smith, 1972: Influence of Satellite Aerodynamics on Atmospheric Density Determination. Paper presented at International Conference on Aerospace and Aeronautical Meteorology, Washington, D. C., 6 pages.
- Karr, G. R. and S. M. Yen, 1970: Aerodynamic Properties of Spinning Convex Satellites, Seventh Rarefied Gas Dynamic Symposium, (in press).
- Marcos, F. A. and K. S. W. Champion, 1972: Gravity Waves Observed in High Latitude Neutral Density Profiles. Space Research XII, Akademie-Verlag, Berlin, 941-946.
- Marcos, F. A., K. S. W. Champion, and R. A. Schweinfurth, 1971: More Accelerometer and Orbital Drag Results from SPADES (OVI-15) and Cannon Ball I (OVI-16) Satellites. Space Research XI, Akademie-Verlag, Berlin, 941-946.

TABLE I

Orbit Number = 890

Time of Peak  $\bar{F} = 672$ 

I	F(i, 1)	GAMA(i, 1)	F(i, 2)	GAMA(i, 2)	TIME(i, 1)	TIME(i, 2)
1	317.5	137.75	320.0	134.8	647	697
2	307.0	139.50	306.0	133.25	622	722
3	291.5	141.75	291.0	132.25	597	747
4	270.0	142.50	268.0	130.0	572	772
5	251.0	144.0	244.0	129.0	547	797
6	225.0	145.75	214.0	127.5	522	822

Orbit Number = 893

Time of Peak  $\bar{F} = 681$ 

I	F(i, 1)	GAMA(i, 1)	F(i, 2)	GAMA(i, 2)	TIME(i, 1)	TIME(i, 2)
1	292.0	141.75	292.0	137.25	650	712
2	282.0	142.75	283.5	135.0	625	737
3	264.0	144.50	263.0	132.75	600	762
4	243.0	146.20	239.5	132.0	575	787
5	218.0	147.50	215.0	130.0	550	812
6	199.0	148.20	190.5	128.0	525	837

Orbit Number = 896

Time of Peak  $\bar{F} = 675$ 

I	F(i, 1)	GAMA(i, 1)	F(i, 2)	GAMA(i, 2)	TIME(i, 1)	Time(i, 2)
1	306.0	133.5	302.5	129.5	650	700
2	302.0	135.0	291.0	127.7	625	725
3	289.0	136.25	275.0	126.75	600	750
4	270.5	137.5	256.0	125.0	575	775
5	250.0	138.0	231.0	123.0	550	800
6	226.5	141.0	200.5	120.5	525	825

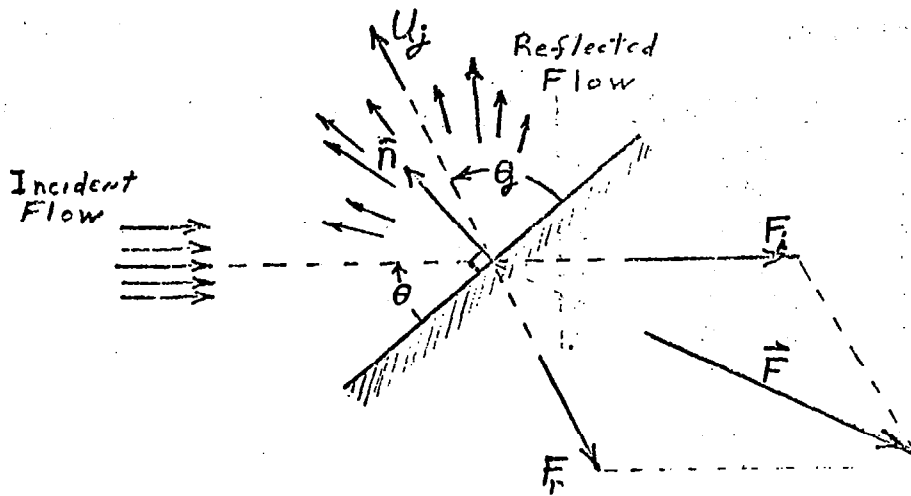


Figure 1. The gas surface interaction and the forces of the interaction.

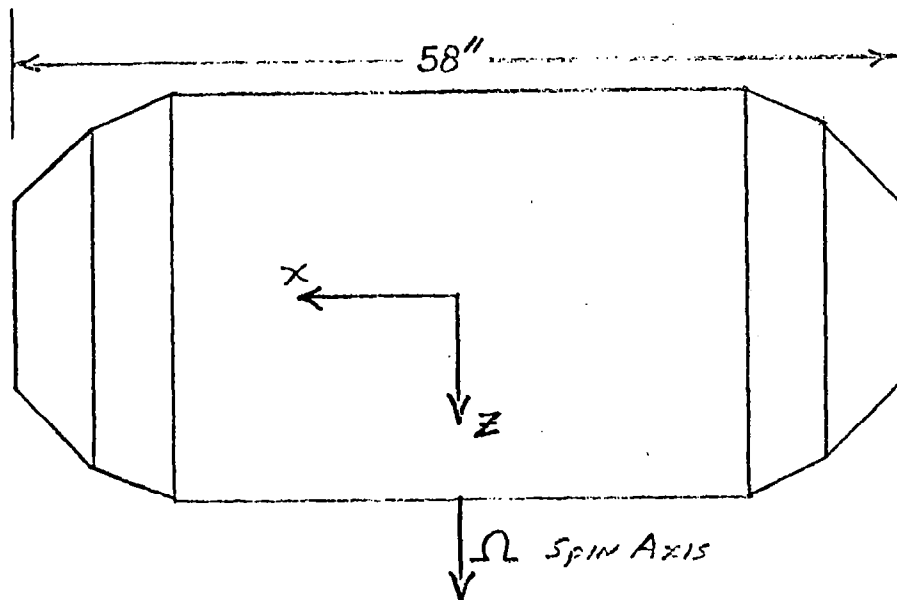


Figure 2. Configuration of the OVI-15 satellite.

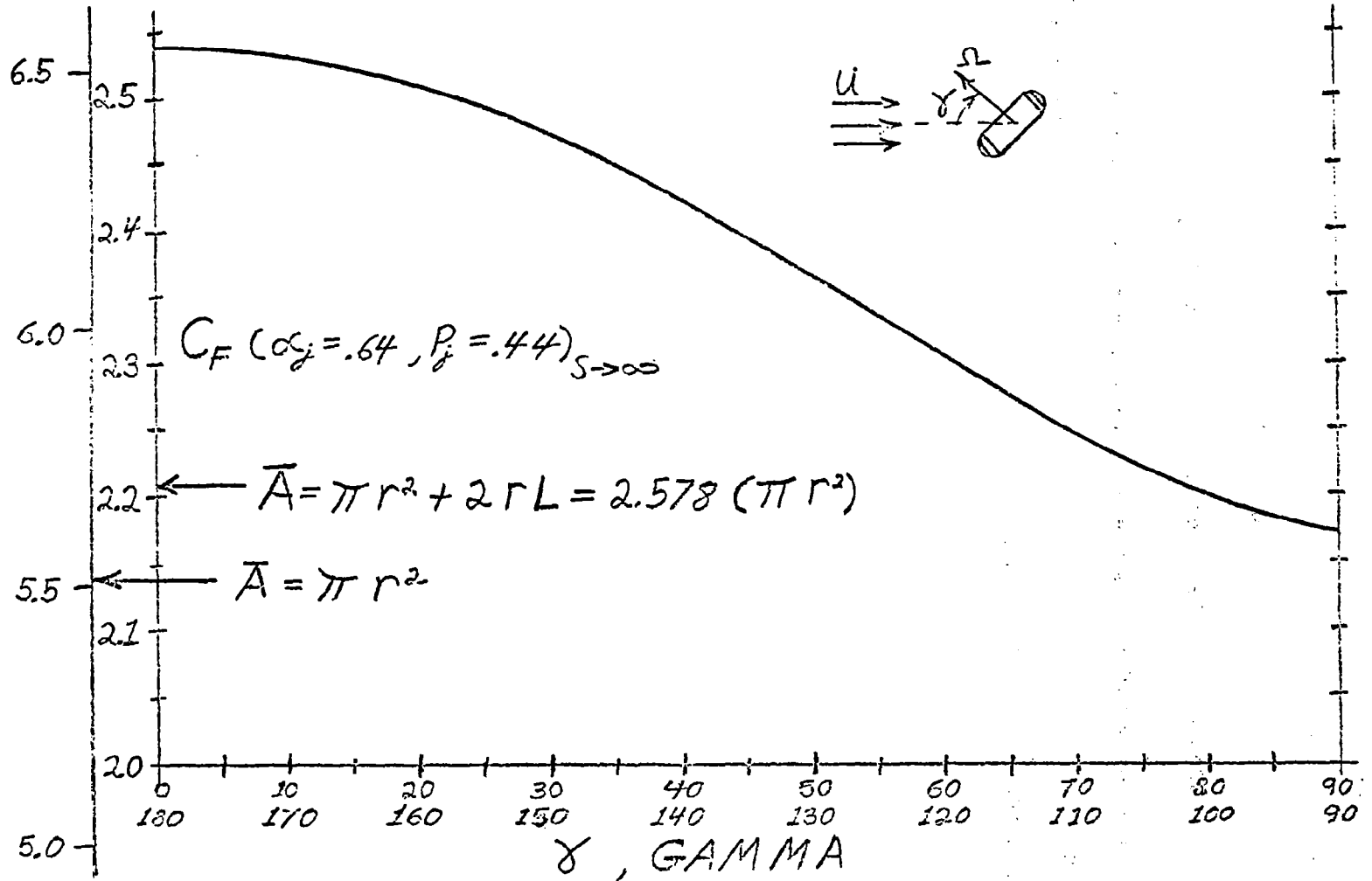


Figure 6. Force coefficient as a function of spin axis orientation of the OVI-15.

## CHAPTER III

### AERODYNAMIC LIFT EFFECT ON SATELLITE ORBITS

A paper submitted to the AIAA 13th Aerospace Sciences by  
G. R. Karr, J. G. Cleland and L. L. DeVries. Presentation was made  
during meeting held at Pasadena, California, January 20-22, 1975.

# AERODYNAMIC LIFT EFFECT ON SATELLITE ORBITS<sup>†</sup>

Dr. G. R. Karr\* and J. G. Cleland\*\*  
University of Alabama in Huntsville  
Huntsville, Alabama 35807

and  
Dr. L. L. DeVries\*\*\*  
NASA-Marshall Space Flight Center  
Huntsville, Alabama

## Abstract

Numerical quadrature is employed to obtain orbit perturbation results from the general perturbation equations. Both aerodynamic lift and drag forces are included in the analysis of the satellite orbit. An exponential atmosphere with and without atmospheric rotation is used. A comparison is made of the perturbations which are caused by atmospheric rotation with those caused by satellite aerodynamic effects. Results indicate that aerodynamic lift effects on the semi-major axis and orbit inclination can be of the same order as the effects of atmosphere rotation depending upon the orientation of the lift vector. The results reveal the importance of including aerodynamic lift effects in orbit perturbation analysis.

## I. Introduction

The perturbations of a satellite orbit caused by the interaction of the satellite with the earth's atmosphere has been a topic of considerable interest since orbital flight was proposed. The forces acting on a satellite during its passage through the atmosphere at speeds of near 8000 m/sec are predominantly the drag force which we will define to be that force which acts parallel to the velocity vector,  $\vec{V}$ , of the satellite with respect to the atmosphere. For a satellite having a drag coefficient  $C_D$  and a reference area  $\bar{A}$ , the aerodynamic drag force,  $\vec{F}_D$ , is given by

$$\vec{F}_D = \frac{1}{2} \rho V^2 C_D \bar{A} \frac{\vec{V}}{|\vec{V}|} \quad (1)$$

where  $\rho$  is the density of the atmosphere. Another aerodynamic force which may act on the satellite is the aerodynamic lift force which we define as the force perpendicular to velocity vector of the satellite with respect to the atmosphere. Aerodynamic lift forces arise when a nonspherical satellite travels through the atmosphere at an attitude such that atmospheric molecules are deflected by the satellite in a

nonsymmetric pattern with respect to the velocity vector. Consider, for example, a cylinder or cone with an axis of symmetry along the direction of the unit vector  $\bar{a}$ . If such an object were to travel through the atmosphere with  $\bar{a}$  in the same direction as  $\vec{V}$ , then only drag forces would result. However, if  $\bar{a}$  were at an angle  $\theta_s$  with respect to  $\vec{V}$ , then a lift force will arise given by

$$\vec{F}_L = \frac{1}{2} \rho V^2 C_L \bar{A} \frac{(\vec{V} \times \bar{a}) \times \vec{V}}{V^2 \sin \theta_s} \quad (2)$$

where  $C_L$  is the lift coefficient of the object and  $\bar{A}$  is assumed the same as the  $\bar{A}$  used in the drag equation (Eq. 1).

The drag and lift forces given in equations (1) and (2) are both defined using the velocity with respect to the atmosphere as distinguished from the inertial velocity of the satellite  $v$ . The inertial velocity is defined here as the velocity given by the orbital elements of the osculating orbit at the satellite.

$$v = \sqrt{\frac{\mu}{a} \frac{(1 + e \cos E)}{(1 - e \cos E)}} \quad (3)$$

where  $a$  and  $e$  are the osculating elements of the orbit and  $E$  is the eccentric anomaly. Since the atmosphere at orbital altitudes may have motions with respect to inertial space, the inertial velocity  $\vec{v}$  is not necessarily the same as the velocity of the satellite with respect to the atmosphere  $\vec{V}$ . This difference is due to the motion of the atmosphere,  $\vec{v}_A$ , at the satellite. The velocity  $\vec{V}$  is then modified by the atmospheric motion to give

$$\vec{V} = \vec{v} - \vec{v}_A \quad (4)$$

Orbital perturbations under the action of pure drag (i.e.,  $\vec{F}_L = 0$ ), with and without atmospheric motions with respect to inertial reference, have received considerable attention for the purposes of (1) predicting the orbit of a satellite into the future (see, for example, Ref. 1) and (2) deducing atmospheric properties from observed perturbations (see, for example, Ref. 2). The influence of nonzero lift ( $\vec{F}_L \neq 0$ ) has received little attention due to a number of factors which have been cited to reduce lift effects to negligible values. For example, random tumbling of a nonspherical satellite is often cited as a reason for neglecting lift since the lift vector would be randomly oriented and tend to average to zero

<sup>†</sup>This research was supported in part by the National Aeronautics and Space Administration, Marshall Space Flight Center, Huntsville, Alabama, through Contract NAS8-28248.

\*Assistant Research Professor, Mechanical Engineering Department, Associate Member AIAA.

\*\*Master's Degree Candidate, Mechanical Engineering Department.

\*\*\*Space Science Laboratory, NASA-MSFC, Member AIAA.

under such conditions. Second, lift forces are thought to be negligible for satellites based on the argument that the satellite is a poor reflector of molecules since the gas surface interaction is assumed to be inelastic. However, the assumption of inelastic reflection is not verified and the possibility still exists of significant lift coefficients. While many of the earlier satellites were nearly spherically symmetric and randomly tumbling (uncontrolled altitudes), many recent satellites are now spherical and may have large wing-like configurations (such as Skylab) and generally require altitude control by either active or passive means. Such satellites may then experience lift forces of greater magnitudes than experienced by past satellites.

Another reason that lift forces have received little attention is the possibility that orbital perturbations that have been caused by lift forces may have been wrongly attributed to other effects, such as atmospheric motions. Atmospheric motions that are not colinear with the inertial velocity can give rise to pure drag forces with components perpendicular to the inertial velocity vector. One of the major motions of the upper atmosphere often included in drag studies is that movement which is correlated with the rotation of the earth. The atmosphere is assumed to rotate in inertial space with about the same angular velocity of the earth. A pure drag satellite in an inclined orbit would then experience components of the drag force which are perpendicular to the orbital plane. These forces cause the orbit plane to rotate in space. The observation of rates of change of the orbital plane of selected satellites has been used as evidence of the rate of rotation of the upper atmosphere under the assumption of pure drag only (see Ref. 3). We will show that aerodynamic lift forces can give rise to orbital plane changes of magnitudes comparable to those caused by rotation of the upper atmosphere. This is not meant to imply that there is no atmospheric rotation because there is strong evidence to suggest a co-rotating atmosphere for the earth. We will show, however, that lift forces of seemingly small magnitude can at least produce orbital plane changes that are of the same magnitude as those assumed to be caused by atmospheric rotation. On this basis we feel that lift effects should be examined carefully in the reduction of orbit perturbation data for the purpose of deducing upper atmospheric motions.

The purpose of this paper is to examine the essential characteristics of orbit perturbations that result when a satellite has lifting properties. Comparisons will be made with pure drag cases where appropriate and comparison will also be made with the effect of the atmosphere rotating at the earth's rotation rate. The basic aerodynamic relations will be presented and employed in the general perturbation equations. Lift forces will be divided into two classes: (1) lift forces in the orbit plane and (2) lift forces perpendicular to the orbit plane. Numerical integration of the perturbation equations was made using an exponential atmosphere for purposes of illustration of the aerodynamic lift effects. Special emphasis is given to the dependence of lift effects on high eccentricities in order to expand on previous work valid at low

eccentricities. High eccentricity orbits also have the effect of concentrating all the aerodynamic effects at the perigee region since the atmospheric density drops off exponentially away from perigee.

## II. Aerodynamic Lift

In the free molecule environment at orbital altitudes, aerodynamic lift and drag forces are a direct function of the interaction of the atmospheric gas molecules with the exposed surfaces of the satellite. The characteristics of the gas surface interaction for collision of upper atmospheric molecules with satellite materials at velocities of the order of 8000 m/sec is not well understood. The gas surface interaction is described in a general manner using a model developed by Kari<sup>(4)</sup> in which the force acting on an element of surface exposed to the flow is divided into two components. With reference to Figure 1,

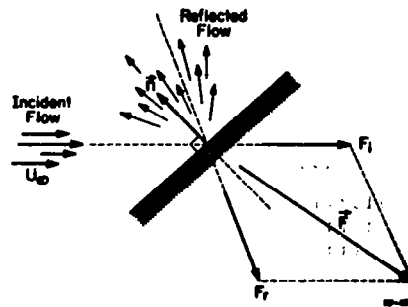


FIGURE 1. Illustration of Forces Acting Due to Gas Surface Interaction

the force acting on the surface will have components  $F_i$  which is the force associated with the momentum carried by the incoming molecules and  $F_r$  which is the reaction force associated with molecules leaving the surface. The group velocity of molecules leaving the surface,  $U_j$ , is assumed to be some fraction of the group velocity of the incoming molecules,  $U$ , due to possible inelastic collisions with the surface. The relationship between  $U_j$  and  $U$  is given by

$$U_j = \sqrt{1 - \alpha_j} U \quad (5)$$

where the proportionality term is expressed as  $\sqrt{1 - \alpha_j}$  in order that the parameter  $\alpha_j$  resemble what is customarily termed the thermal accommodation coefficient. A second parameter is introduced to provide the direction of the reflected force. The angle of reflection law chosen is a linear relationship between the angle of incidence,  $\theta$ , and angle of reflection,  $\theta_j$ , given by

$$\theta_j = \frac{1}{2} P_j + (1 - P_j) \theta \quad (6)$$

where  $P_j$  is the adjustable parameter with  $P_j = 0$

giving specular reflection ( $\theta_j = \theta$ ) and  $P_j = 1$  giving diffusive reflection ( $\theta_j = \pi/2$ , independent of  $\theta$ ). The mass flux impinging on an element of surface is given by

$$\dot{m} = -\rho \vec{U} \cdot \hat{n} dA \quad (7)$$

where  $\hat{n}$  is the unit outward normal of the surface. The exchange of momentum that takes place at the surface gives the net force acting on the surface

$$\vec{F} = -(\vec{U} - \vec{U}_j) \rho \vec{U} \cdot \hat{n} dA \quad (8)$$

The total drag and lift forces acting on an object are obtained by integrating equation 8 over the exposed surface of the satellite. Detailed results for spheres, cylinders, cones, and flat plates are given in reference 4 and 5.

The above equations show that forces perpendicular to the velocity vector can only arise through the  $\vec{U}_j$  term in equation 8. Since the magnitude and direction of  $\vec{U}_j$  are functions of  $\alpha_j$  and  $P_j$ , the lift force acting on any object is directly related to the gas surface interaction parameters. This observation provides added motivation for the study of lift-induced orbit perturbations, since measurements of such perturbations could yield information on the gas-surface interaction.

For purpose of illustration of lift-induced orbit perturbations, flat plate drag and lift properties will be used, given by

$$C_D = 2 \sin^2 \theta_s - 2\sqrt{1-\alpha_j} \sin \theta_s \cos \left[ \frac{\pi}{2} P_j + (2-P_j) \theta_s \right] \quad (9)$$

$$C_L = -2\sqrt{1-\alpha_j} \sin \theta_s \sin \left[ \frac{\pi}{2} P_j + (2-P_j) \theta_s \right] \quad (10)$$

where  $\theta_s$  is the angle of attack of the flat plate. For  $\theta_s = 0$  the plate is edge-on into the flow while for  $\theta_s = \pi/2$ , the plate has the outward surface normal into the flow. Equation 10 shows that the factor  $\sqrt{1-\alpha_j}$  plays an important role in determining the lift magnitude. If the molecules have an inelastic collision with the surface, the velocity of reflection may be extremely low, the value of  $\alpha_j$  would be near unity, and the lift very small. The perfectly elastic or perfect specular reflection ( $P_j = 0$ ,  $\alpha_j = 0$ ) would provide the highest possible values of lift.

Laboratory experiments at velocities corresponding to satellite velocities are not conclusive on the gas surface interaction to expect at orbital altitudes. Work by Hulpke<sup>6</sup> for example tends to show elastic collisions while other experimenters have found diffusive type reflection (Ref. 9) or both (Ref. 6). Due to

uncertainties in upper atmospheric density, accurate determinations of the gas surface interaction from drag studies alone is not feasible. Recent work by Reiter and Moe,<sup>7</sup> however, on the analysis of drag and torque acting on a paddlewheel satellite provides the best values of gas surface interaction parameters since atmospheric density is eliminated in the analysis. Reiter and Moe, employing a number of gas surface interaction models, concluded that the energy accommodation  $\alpha_j$  is in the range of .75 - .95. This would put  $\sqrt{1-\alpha_j}$  in the range of .5 to .22. The accommodation coefficients coming from their studies are high, indicating inelastic collisions. The value of  $\sqrt{1-\alpha_j}$  is seen to be significant even at high accommodation coefficient values (for example,  $\alpha_j = .99$  gives  $\sqrt{1-\alpha_j} = .1$ ) which implies that lift forces may also have significant values.

The ratio of lift forces to drag forces acting on an object is a nondimensional measure of the magnitude of lift effects. For the flat plate, this ratio is obtained from equations 8 and 9

$$\frac{F_L}{F_D} = \frac{\sqrt{1-\alpha_j} \sin \left[ \frac{\pi}{2} P_j + (2-P_j) \theta_s \right]}{1 - \sqrt{1-\alpha_j} \cos \left[ \frac{\pi}{2} P_j + (2-P_j) \theta_s \right]} \quad (11)$$

The lift to drag ratio given in the above equation is tabulated in Table I for four sets of gas surface interaction parameters. The values are tabulated as a function of angle of attack and show that (1) small angles of attack of a flat plate yield the highest L/D values, (2) specular reflection causes the highest L/D values ( $L/D = \tan \theta_s$ , for specular reflection) and (3) highly inelastic collisions ( $\alpha_j = .99$ ,  $P_j = 1$ ) cause lift forces which are almost 10% of the drag force. The values of  $\alpha_j = .75$ ,  $P_j = 1$  were chosen to simulate the gas surface interaction results obtained by Reiter and Moe. This set of parameters produced L/D values of near 0.5 and this value of L/D will be used to illustrate the orbital perturbation caused by lift forces. The intermediate case ( $\alpha_j = .5$ ,  $P_j = .5$ ) was chosen only to illustrate the effect of reflections other than specular and diffuse. The L/D values for the intermediate case are seen to be near unity at the small angles of attack.

A typical satellite would not have the high L/D values as experienced by the flat plate which is an ideal lifting body at orbital altitudes. For comparison, Table II gives the L/D values obtained from results given by Sentman (Ref. 10) for a typical satellite shape and typical gas surface interaction values. The shape is a cylinder with a conical end and having a total length of 4 times the diameter. The values of L/D are generally lower than the flat plate values because this object maintains a high drag profile at all angles of attack. The peak value of L/D of .044 is seen to occur at near 25° angle of attack. While this L/D is much smaller than flat plate values, the lift force will be nearly 5% of the drag force for this typical satellite shape.

Having now established the likely existence of aerodynamic lift forces of magnitudes from a few percent of the drag force and greater, the

orbital perturbations that are characteristic of these forces will be presented. In view of the fact that the aerodynamic drag force is the principle source of orbital perturbations, a lift force of even a few percent of the drag force is expected to be significant. In order to enhance the lift effects and to reduce computer time, an L/D value of .5 was chosen for most of the studies. The computer simulation employed a light satellite weight also for the purpose of enhancing the aerodynamic effects. For these reasons, the results obtained are not likely to simulate any known satellite but are presented only to illustrate the character of lift-induced orbit perturbations.

Table I

Flat Plate Lift to Drag Ratios

$\theta$	Specular $\alpha_j=0, P_j=0$	Diffuse $\alpha_j=.75, P_j=1$	Diffuse $\alpha_j=.99, P_j=1$	Inter. $\alpha_j=.5, P_j=.5$
0°		0.5	0.1	1.0
2°	28.636	0.491	0.100	0.997
5°	11.430	0.477	0.099	0.985
10°	5.671	0.453	0.097	0.947
15°	3.732	0.428	0.094	0.896
25°	2.145	0.374	0.087	0.772
35°	1.428	0.318	0.078	0.642
45°	1.000	0.261	0.066	0.514
55°	0.700	0.203	0.053	0.392
65°	0.466	0.145	0.039	0.276
85°	0.088	0.029	0.006	0.054

Table II

L/D for Typical Satellite Shape  
(from Sentman, Ref. 10)

Angle of Attack	L/D
0	0.0
10	0.037
15	0.041
25	0.044
35	0.033
45	0.023
55	0.013

### III. Orbit Perturbation Equations

The approach will be similar to that taken by others in that the expressions for perturbing force will be substituted into the general perturbation equations for the time derivatives of the osculating orbital elements  $a, e, i, \omega,$  and  $\Omega$ ; the semi-major axis, eccentricity, inclination, argument of perigee, and right ascension of the ascending node, respectively. Numerous good references provide details of the derivation of these equations with specific application to drag forces (see, for example, Ref. 11). The forms of the equations most useful for this work are given as

$$\frac{da}{dt} = \frac{2f}{(\mu a)^{1/2} (1-e^2)^{1/2}} T \quad (12)$$

$$\frac{de}{dt} = \left[ \frac{a(1-e^2)}{\mu} \right]^{1/2} \frac{1}{f} \left[ \frac{2(1-e^2) \cos E}{1-e \cos E} T + (1-e^2)^{1/2} \sin E N \right] \quad (13)$$

$$\frac{di}{dt} = \frac{r \cos(\theta + \omega)}{(\mu a)^{1/2} (1-e^2)^{1/2}} W \quad (14)$$

$$\frac{d\Omega}{dt} = \frac{r \sin(\theta + \omega)}{(\mu a)^{1/2} (1-e^2)^{1/2} \sin i} W \quad (15)$$

$$\frac{d\omega}{dt} = \frac{1}{ef} \left( \frac{a}{\mu} \right)^{1/2} \frac{2 \sin E}{1-e \cos E} T \quad (16)$$

$$- \frac{1}{ef} \left[ \frac{a(1-e^2)}{\mu} \right]^{1/2} (e + \cos E) N \quad (17)$$

$$- \frac{r \sin(\theta + \omega)}{(\mu a)^{1/2} (1-e^2)^{1/2} \tan i} W \quad (18)$$

where

$$f = \left[ (1-e^2) (1 + e \cos E) \right]^{1/2} (1-e \cos E)^{-1/2} \quad (19)$$

The angle  $\theta$ , the true anomaly, can be expressed in terms of  $E$ , the eccentric anomaly, by

$$\theta = \cos^{-1} \left( \frac{\cos E - e}{1 - e \cos E} \right) \quad (20)$$

and the radius,  $r$ , can also be expressed as a function of  $E$  by

$$r = a (1 - e \cos E) \quad (21)$$

The  $T$  component of force is tangent to the orbit path and positive in the direction of motion; the  $N$  component is positive in the direction of the

outward normal to the orbit path and is in the orbit plane; the W component is the force perpendicular to the orbit plane with positive being in the same direction as the orbit angular momentum vector. The aerodynamic force acting on the satellite will be expressed in components along N, T, and W.

Consider a flat plate in orbit with the orientation of the plate held constant with respect to the N, T, W coordinate system. The unit vector  $\hat{x}$  will be taken as the normal to the flat plate with components in the N, T, W directions given by

$$\begin{aligned} a_T &= \cos \theta_W \cos \theta_{NT} \\ a_N &= \cos \theta_W \sin \theta_{NT} \\ a_W &= \sin \theta_W \end{aligned} \quad (22)$$

Equations 1 and 2 give the lift and drag force as a function of the relative velocity  $\vec{V}$ . The relative velocity  $\vec{V}$  is first found with respect to the R, S, W coordinate system in which the R direction is radially outward from the geocenter and S is perpendicular to R and W with positive being in the direction of motion. An atmosphere rotating at the earth's rotation rate,  $\vec{\Omega}_e$ , is to be considered the only atmospheric motion for purposes of this study. The velocity field produced by the atmospheric rotation is given by

$$\begin{aligned} \vec{V}_A &= \vec{\Omega}_e \times \vec{r} \\ &= r \Omega_e [\cos i \hat{S} - \sin i \cos(\theta+w) \hat{W}] \end{aligned} \quad (23)$$

where  $\hat{S}$ ,  $\hat{W}$ , and  $r$  are unit vectors. The inertial velocity of the satellite is given by

$$\vec{V} = \dot{r} \hat{R} + r \dot{\theta} \hat{S} \quad (24)$$

The relative velocity  $\vec{V}$  is given by equation 4. Equations 4, 23, and 24 are substituted into equations 1 and 2 to obtain the components of lift and drag in the R, S, W coordinate system. The unit vector  $\hat{x}$  will have components  $a_R$ ,  $a_S$ , and  $a_W$  in the R, S, W system. The transformation from the N, T, W system to the R, S, W system is obtained from the following relationship between the unit vectors

$$\begin{aligned} \hat{N} &= \frac{1}{r} [(1 + e \cos \theta) \hat{R} - e \sin \theta \hat{S}] \\ \hat{T} &= \frac{1}{r} [e \sin \theta \hat{R} + (1 + e \cos \theta) \hat{S}] \end{aligned} \quad (25)$$

Using equations 25 and 22, we find

$$\begin{aligned} a_R &= \frac{1}{r} \left[ \cos \theta_W \sin \theta_{NT} (1 + e \cos \theta) \right. \\ &\quad \left. + \cos \theta_W \cos \theta_{NT} e \sin \theta \right] \\ a_S &= \frac{1}{r} \left[ \cos \theta_W \cos \theta_{NT} (1 + e \cos \theta) \right. \\ &\quad \left. - \cos \theta_W \sin \theta_{NT} e \sin \theta \right] \\ a_W &= \sin \theta_W \end{aligned} \quad (26)$$

The angle  $\theta_s$  called for in the drag and lift relationships can be obtained in terms of the orbit parameter and the angles  $\theta_W$  and  $\theta_{NT}$  from

$$\theta_s = \sin^{-1} \left( \frac{\vec{V} \cdot \hat{x}}{|\vec{V}|} \right) \quad (27)$$

where

$$\vec{V} = \dot{r} \hat{R} + (r \dot{\theta} - \Omega_e r \cos i) \hat{S} + [\Omega_e r \cos(\theta+w) \sin i \hat{W}] \quad (28)$$

It is convenient to write the velocity  $\vec{V}$  as a function of E and  $\dot{E}$ . To do this, the following relationships are employed

$$\begin{aligned} r &= a e \sin E \dot{E} \\ r \dot{\theta} &= a (1 - e^2)^{1/2} \dot{E} \\ &\quad 5/2 \\ r &= \frac{a}{\sqrt{\mu}} (1 - e \cos E)^2 \dot{E} \\ \dot{E} &= \frac{\sqrt{\mu}}{a^{3/2} (1 - e \cos E)} \end{aligned} \quad (29)$$

Substitution of these relationships into the force equations, and taking components in the  $\hat{R}$ ,  $\hat{S}$ ,  $\hat{T}$  directions, we obtain the following components of force R, S, and T.

$$\begin{aligned} R &= \rho V^2 \dot{E} \left\{ \frac{R_L \hat{a}_R}{n \sin \theta_s} (1 - e \cos E) \right. \\ &\quad \left. - \frac{2a}{V} \sin E (R_L \cot \theta_s + R_D) \right\} \end{aligned} \quad (30)$$

$$S = \rho v^2 \dot{E} \left\{ \frac{R_L \hat{a}_S}{n \sin \theta_s} (1 - e \cos E) - \left[ (1-e^2)^{1/2} \frac{\Omega_e \cos i}{n} (1-e \cos E)^2 \right] \left( \frac{a}{v} \right) (R_L \cot \theta_s + B_D) \right\} \quad (31)$$

$$W = \rho v^2 \dot{E} \left\{ \frac{R_L \hat{a}_W}{n \sin \theta_s} (1 - e \cos E) - \frac{\Omega_e a}{n v} (1 - e \cos E)^2 \cos(\theta + \omega) \sin i (R_L \cot \theta_s + B_D) \right\} \quad (32)$$

where  $B_D = \frac{C_D \bar{A}}{2m}$ ,  $R_L = \frac{C_L \bar{A}}{2m}$ ,  $m = \text{mass}$  of satellite and  $n = \sqrt{\mu / a^3}$ .

This concludes the development of the orbit perturbation relationships. Equations 30, 31, and 32 along with the transformation relations given in equation 25, provide the necessary relations to write the orbit perturbation equations in the form

$$\begin{aligned} \frac{da}{dE} &= f_a(C_L, C_D, \theta_W, \theta_{NT}, a, e, i, w, \Omega, E) \\ \frac{de}{dE} &= f_e(C_L, D_D, \theta_W, \theta_{NT}, a, e, i, w, \Omega, E) \\ \text{etc.} & \end{aligned} \quad (33)$$

The atmosphere density called for in the perturbation equations is given by

$$\rho(r) = \rho_p e^{-(h-h_p)/H} \quad (34)$$

where  $\rho_p$  is the density at perigee,  $h$  is the height of perigee,  $H$  is the scale height at perigee, and  $h_p$  is the height of the satellite given by  $h = r - R_E$  where  $R_E$  is the radius of the earth.

#### IV. Method of Calculations

The orbit perturbation equations were integrated numerically using  $E$  as the independent variable. A modified Runge-Kutta fourth order process due to Gill (1962) and discussed in ref. 13 was used. Double precision was used to maintain accuracy.

The step size on  $\Delta E$  was taken as small as 0.1 degree depending on the rate of variation of the orbital elements. The accuracy of the results is not expected to be good near the final stages of decay since the orbital elements are changing rapidly. Errors also build up at low eccentricities due to the high rate of change in  $\omega$  which invalidates the assumption of constant orbital angular momentum implied in equations 29.

The integration of the equations stepwise in  $E$  is a departure from previous work by Cook (Ref. 14) in which a series expansion was employed to facilitate the integration analytically from 0 to  $2\pi$ . We did not take this approach for two reasons: First, the results obtained by Cook are only valid at low eccentricities (less than .2) and expansions for high eccentricities were not found. Second, we were interested in the lift effects on orbit decay which are not apparent if one takes, as Cook did, equation 12 to imply that lift forces have no effect on decay of the semi-major axis. Equation 12 shows that the rate of change in  $a$  is, to first order, a function of only forces tangent to the orbital path. For a non-rotating atmosphere, drag forces only would produce tangential components and lift forces would not effect  $a$ . We find that in a non-rotating atmosphere,  $\Omega_e = 0$ , lift forces do affect the value of  $a$  over  $\frac{1}{2}$  that of drag alone. This is clearly a second order effect which we find is comparable to the effect of atmospheric rotation on  $a$  for  $L/D = .5$ . Results such as these are found by stepwise integration of the orbit equations and would be lost if integration from  $E = 0$  to  $2\pi$  were done assuming all parameters remain constant over the interval.

#### V. Results

The results are grouped into three classes of lift orientation: (A) Lift forces perpendicular to the orbit plane, (B) Lift forces in the orbit plane and in the same direction around the orbit, and (C) Lift forces in the orbit plane which change direction at perigee and apogee. The first and last type of lift orientation serves to approximate cases in which satellites maintain an orientation with respect to inertial space. The second type of lift orientation serves to approximate the earth oriented object.

##### A. Lift Perpendicular to the Orbit Plane

For a flat plate with angles of orientation with respect to the N, T, W coordinate system given by ( $\theta_W = \text{constant}$  other than zero,  $\theta_{NT} = 0$ ), lift forces will be produced in the W direction which is perpendicular to the orbit plane. The effect on the orbit of aerodynamic forces perpendicular to the orbit plane have been studied by Cook and Plimmer (Ref. 15) and Cook (Ref. 16) for the case of a satellite having pure drag with the perpendicular forces arising due to the rotation of the atmosphere. For comparison, we took the case of a non-rotating atmosphere with an aerodynamic lift force of  $L/D = .5$  and  $.1$  acting perpendicular to the orbit.

The orbit parameters most sensitive to forces perpendicular to the orbit plane is the orbital inclination  $i$  and right ascension of the ascending node  $\Omega$ . As pointed out in reference 15, the

perturbations in  $\Omega$  caused by aerodynamic forces perpendicular to the orbit are less than .1% of those caused by the oblateness of the earth. The inclination  $i$  is not affected by earth oblateness to such an extent and is therefore a sensitive indicator of aerodynamic forces perpendicular to the plane.

The characteristics of orbital inclination changes caused by aerodynamic lift were found to be not much different from those caused by atmospheric rotation acting on a pure drag satellite. One difference is, of course, that the magnitude of component of drag force in the W direction caused by atmospheric rotation is proportional to  $\sin i$  whereas aerodynamic lift forces are independent of  $i$ . Therefore, inclination changes of near zero inclination orbits must be caused by aerodynamic lift effects only, since atmospheric rotation can have no influence at zero inclination. For comparison purposes, the lift induced rate of change in inclination with no atmospheric rotation was normalized with respect to the inclination rate of change for a pure drag satellite at  $i = 45^\circ$  in an atmosphere rotating at the earth's rotation rate. These results are presented in Figure 2 for  $L/D = .5$  and  $L/D = .1$  with  $B_D = .2 \text{ m}^2/\text{Kg}$  and  $B_L = .1 \text{ m}^2/\text{Kg}$ .

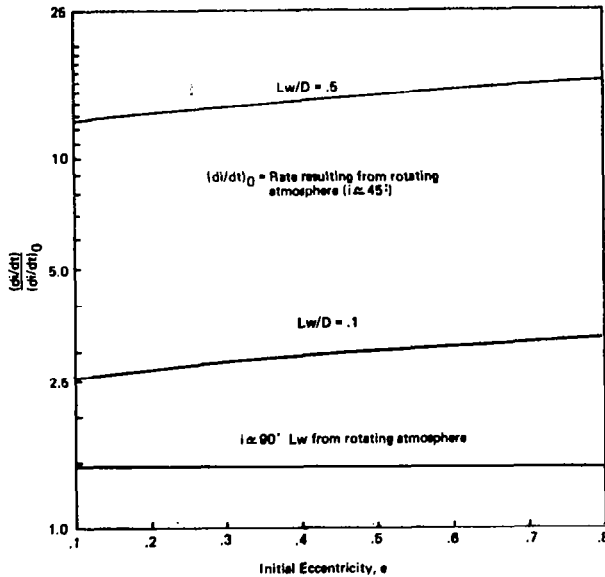


FIGURE 2. Out-of-Plane Effects On Orbital Inclination

The notation  $L_W$  is used to signify that the lift force is in the W direction. Figure 2 shows that the rate of change in inclination for  $L/D = .1$  is over twice that that would be caused by atmospheric rotation. The curve for  $L/D = .5$  shows that the effect is proportional to  $L/D$ . Figure 2 also shows a comparison of the atmospheric rotation at  $i = 90^\circ$  with respect to that at  $i = 45^\circ$ . The effect is proportional to the ratio of the sines of the angles as would be expected.

Figure 2 shows an increase in the rate ratio as a function of  $e$ . The reason for this increase is due to the decrease in  $di/dt$  for the atmospheric rotation effect as  $e$  is increased since the inertial velocity near perigee increases with

$e$ . The atmospheric rotation effect on  $i$  decreases since it is proportional to the ratio of  $V$  to  $v$  which decreases with eccentricity. The aerodynamic lift force is not affected by  $e$  since  $L/D$  is independent of velocity.

### B. In-Plane-Lift Forces Constant in Direction

Consider now a flat plate with angles of orientation such that  $\theta_N = 0$  and  $\theta_W = \text{constant}$  (other than zero). This orientation would produce a lift force that is in the N direction and constant in sign around the orbit. Two cases will be considered, (1)  $L/D = .5$  with the lift force directed always in the positive N direction and (2)  $L/D = .5$  with the lift force directed always in the negative N direction. As pointed out above, equation 12 shows that these lift forces do not cause a change in  $a$  to first order.

We investigated the change in  $a$  and  $e$  ( $\Delta a/\Delta t$  and  $\Delta e/\Delta t$ ) at a point near perigee, but always after perigee, using the numerical methods described. The results are given in figures 3, 4, and 5 in which the effect of lift and the effect of atmospheric rotation are both compared to the effects caused by pure drag only with no atmospheric rotation. The notation  $L_N$  is used to signify that the lift force is in the N direction.

Figure 3 shows that  $\Delta a/\Delta t$  is positive or negative depending upon the orientation of the lift vector. The magnitude of the effect is dependent on the eccentricity, being larger for smaller values of  $e$ . Also plotted in Figure 3 is the effect on  $\Delta a/\Delta t$  due to a rotating atmosphere ( $i = 45^\circ$ ). The magnitudes of the two effects are comparable and are seen to be of order 5% of the drag-nonrotating-atmosphere effect alone. The lift effects are second order effects as pointed out above while the atmospheric rotation effects are first and second order. The first order effect due to atmospheric rotation comes in because the force in the T direction is decreased by the wind for  $i$  between  $0$  and  $90^\circ$ . Figure 4 shows that the effect on  $e$  has much the same character as the effects on  $a$ .

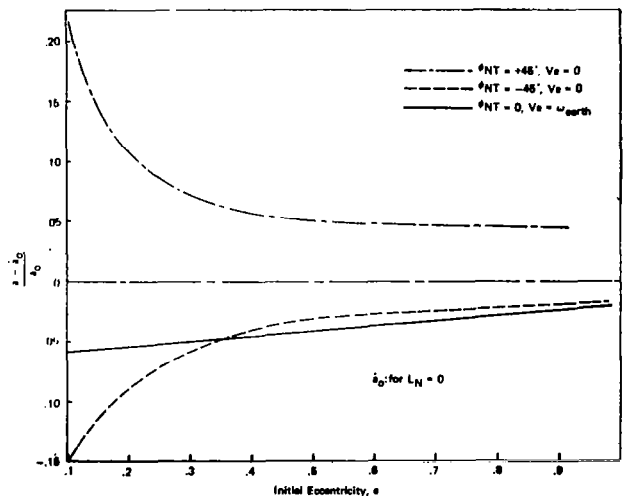


FIGURE 3. In-Plane-Lift Effects on Semi-Major Axis Decay Rates

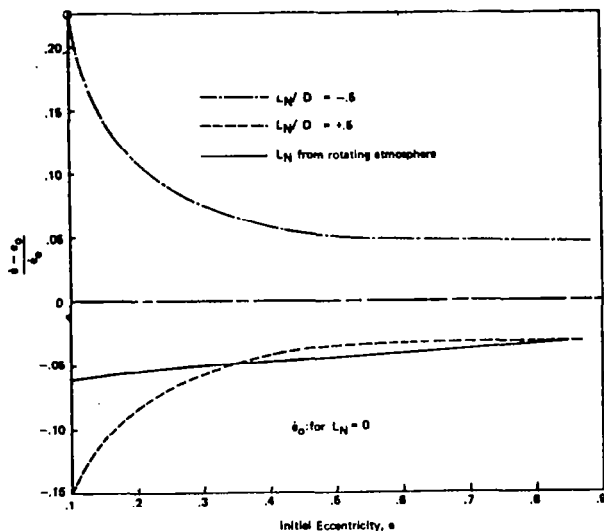


FIGURE 4. In-Plane-Lift Effects on Eccentricity Decay Rates

Figure 5 shows the dependence of  $\Delta a/\Delta t$  on perigee height for two eccentricity values  $e = .2$  and  $e = .8$ . Below a perigee altitude of 130 Km, the rotating atmosphere effect is seen to tend to reverse while the lift effects become larger and do not change sign as does the atmospheric rotation effect.

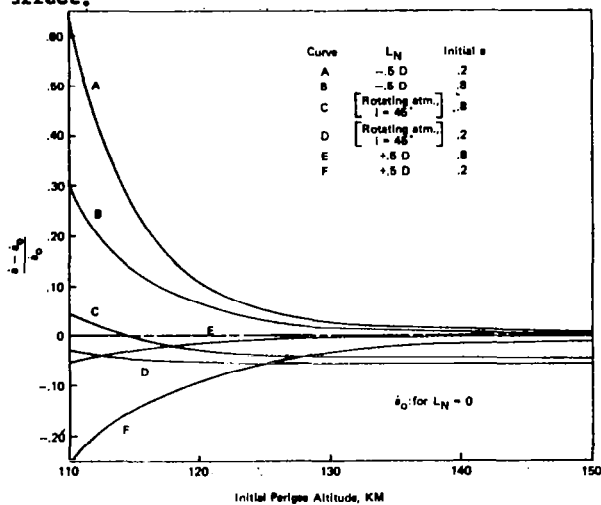


FIGURE 5. In-Plane-Lift Effects on Instantaneous Semi-Major Axis Decay Rates as a Function of Perigee Height

The effect of constant lift on the orbital lifetime is shown in Figure 6. The lifetime is computed from time of initial conditions until the altitude becomes circular. Although the computation technique was not desired to handle zero eccentricities, little error is involved since the orbit eccentricity usually would become zero from initially high values only very near final decay. The lifetimes are normalized with respect to the lifetime of a pure drag satellite having the same drag as the lifting satellite. The atmosphere was taken to have zero rotation in order to clearly show the effect of lift. The results show that in-plane lift effects tend to decrease the lifetime for high eccentricity orbits, independent of the direction of

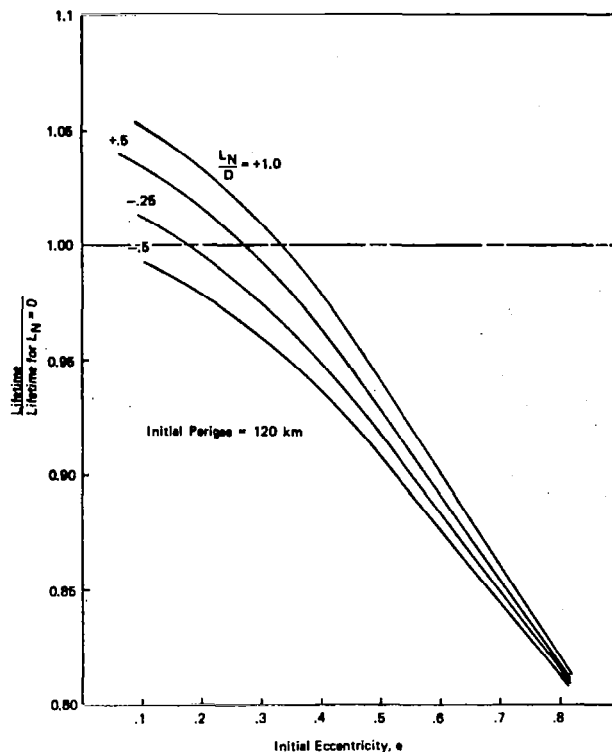


FIGURE 6. In-Plane-Lift Effects on Satellite Lifetimes

the lift vector  $N$  (assumed to be constant in sign around the orbit). At low eccentricities, the effect on lifetime is less but there is separation of the effect according to the sign and magnitude of the lift vector. The results at low eccentricities contain some error due to the rapid rotation of the orbit in space. For this reason, the magnitudes of the influence on lifetime may be in error at low eccentricities by an unknown amount. The curve is presented here in order to show the clear tendency of lift effects to reduce lifetime as eccentricity is increased.

With reference to equation 16, the effect of constant lift force around the orbit should have a significant effect on  $\dot{\omega}$  since the  $N$  component of force is multiplied by  $\cos E$ . This was also noted and evaluated by Cook (Ref. 14) for low eccentricities. Using the same aerodynamic values used by Cook, we evaluated  $\dot{\omega}$  for low and high eccentricities and compared the results as seen in Figure 7. The comparison with the Cook result is seen to be good at the lowest eccentricities used in our numerical work. In addition, our results show that  $\dot{\omega}$  for higher eccentricities continues to decrease with increasing  $e$ .

### C. In-Plane-Lift Forces Which Change in Sign at Perigee and Apogee

Consider a flat plate flown such that the angle of attack in the  $NF$  plane changes discontinuously in sign, but remains constant in magnitude, at perigee and apogee. This special case is of interest since it has the effect of approximating a spacecraft with attitude controlled with respect to inertial space. Two cases arise; (1) lift in positive

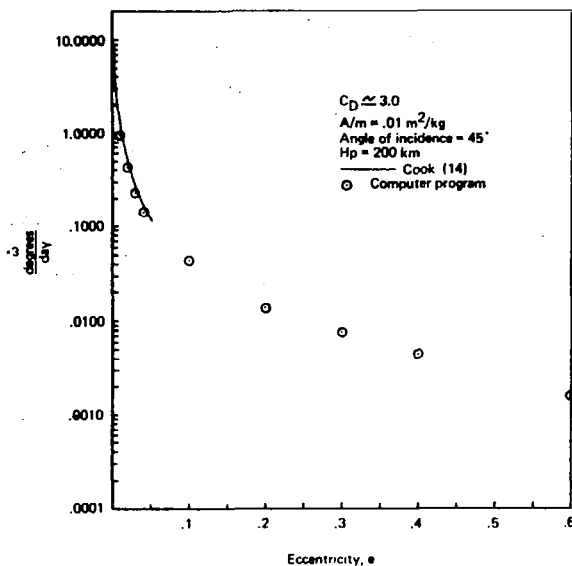


FIGURE 7. Argument of Perigee Rate of Change with Lift and Drag

direction of  $N$  before perigee and in negative direction after perigee and (2) lift in negative direction of  $N$  before perigee and in positive direction after perigee. These types of lift histories have the effect of making the  $N \sin E$  term in the equation for  $de/dt$  (Eq. 13) either always negative, case 1, or always positive, case 2. Case 1 is the same as that considered by Cook in reference 14. Instantaneous values of  $\Delta a/\Delta t$  and  $\Delta e/\Delta t$  at a point just past perigee for both positive and negative values of lift are given in figures 3 and 4. Values of  $\Delta e/T$  where  $T$  is the orbit period were computed and found to agree well with the results published by Cook and will not be presented here. Of special interest, however, was the effect of the discontinuous lift cases on orbit lifetime which was not considered by Cook.

The lifetime of the orbit was found to be strongly affected by the discontinuous lift cases. The results are given in Table III in which the lifetime is normalized to the lifetime of a satellite having drag of the same magnitude as the lifting satellite and with no atmospheric rotation. The lifetimes for case 1 lift histories were seen to be increased by 1.7 to 3.5 times over the drag only lifetimes. Only three lifetimes were computed due to the long computing times required as

Table III

Discontinuous Lift Effect on Lifetime ( $L/D=.5$ )

e	(Lifetime) / (Pure Drag Lifetime)	
	Case 1 N sin E is Neg.	Case 2 N sin E is Pos.
.1	1.7	.52
.2	3.2	.48
.3	3.5	.41

the eccentricity was increased. The case 2 lift history is seen to reduce the lifetime to about half compared to the drag-only case. Careful analysis of our results shows that the case 1 lift

history has the effect of reducing the perigee decay rate of the orbit, thereby reducing the drag effect, whereas the case 2 lift history causes the perigee height to decrease faster than the pure drag case. This effect is best understood by considering the relationship for perigee radius,  $r_p$ , given by

$$r_p = (1 - e) a \quad (35)$$

The time derivative of  $r_p$  is

$$\frac{dr_p}{dt} = (1-e) \frac{da}{dt} - a \frac{de}{dt} \quad (36)$$

The values of  $da/dt$  and  $de/dt$  are negative for pure drag and for both case 1 and case 2 lift histories. The action of case 1 and case 2 lift histories is to modify the decay of perigee height with respect to the pure drag case in the following manner:

$$\frac{dr_p}{dt} = (1 \pm X) \left( \frac{dr_p}{dt} \right)_o + (\text{higher order terms}) \quad (37)$$

where  $X$  is a number of magnitude .1. The plus sign is taken for case 1 and the negative sign is taken for case 2. The subscript  $o$  refers to the pure drag values of  $\dot{r}_p$ .

## VI. Conclusions

Satellite lift forces were shown to be of the order of a few percent of the drag force for an ordinary satellite and may range up to near unity for a satellite designed to have high lifting forces. Reference to figure 2 concerning the lift effects on the orbit inclination leads us to conclude that an  $L/D$  of only .01 would produce an orbital inclination rate of change of a magnitude nearly 25% of that attributed to atmospheric rotation. Clearly, then, an attitude stabilized satellite with a lift force consistently perpendicular to the orbit plane could produce large changes in the inclination which may be wrongly attributed to high velocity upper atmospheric winds.

The results obtained concerning the effect of different lift histories on the lifetime of the orbit are conclusive on three points: (1) constant lift directed either positive or negative along  $N$  about the orbit causes a reduction in lifetime at high eccentricities, (2) a discontinuous lift with change in sign at perigee and apogee, such as to have positive lift before perigee, causes increased lifetime over a drag-only satellite, (3) a discontinuous lift change of the other type, in which the lift is negative before perigee, causes a reduced lifetime of the satellite. These conclusions are apparent from the results given in figure 6 and those given in Table III.

Due to difficulties we had in the numerical procedure near final decay of the satellite, the numbers on lifetime may be in error. For this reason, we stress that the results merely provide the character of the orbital perturbations due to lift and may be in error in absolute value. We

found it difficult to put a realistic estimate of error on the results obtained. All work was carried out in double precision and the step size was decreased until no changes in previous results were found. We did find variations from the smooth curves of figures 3, 4, and 5 of the order of 1 to 5%. The results are considered accurate enough to indicate the controllability of satellite orbits by lift.

The results show the influence of satellite lift on the orbital elements and also open the possibility of utilizing satellite lift to non-propulsively control the satellite orbit plane and orbital lifetime. A flying spacecraft would have an advantage over the propulsive satellite if the aerodynamic shape could be incorporated into the design without increased weight. The weight of the propulsion system and its fuel could then be used as payload.

Future work should be done on the observation of lifting effects on existing satellite orbits in order to confirm the results obtained here. In addition, analytic work and further numerical studies need to be done on the influence of lift on the orbital elements.

#### References

1. P. R. Escobal, Methods of Orbit Determination, John Wiley and Sons, 1965.
2. Desmond King-Hele, Theory of Satellite Orbits in an Atmosphere, Butterworth and Co., 1964.
3. D. G. King-Hele and Diana W. Scott, "The Effect of Atmospheric Rotation on a Satellite Orbit, When Scale Height Varies With Height\*," Planet. Space Sci., Vol. 17, pp. 217 to 232, 1969.
4. Gerald Ray Karr, "A Study of Effects on the Gas-Surface Interaction on Spinning Convex Bodies With Application to Satellite Experiments," Univ. of Illinois, Urbana, Illinois, Report R-435, 1969.
5. G. R. Karr, "Satellite Aerodynamics as a Function of Atmospheric Properties," AIAA 5th Fluid and Plasma Dynamics Conference, No. 72-659, 1972.
6. Jack A. Alcalay and Eldon L. Knuth, "Experimental Study of Scattering in Particle-Surface Collisions With Particle Energies of the Order of 1 eV," Rarefied Gas Dynamics, Fifth Symposium, Vol. I, Academic Press, 1967.
7. Gordon S. Reiter and Kenneth Moe, "Surface-Particle-Interaction Measurements Using Paddle-wheel Satellites," Rarefied Gas Dynamics, Sixth Symposium, Vol. II, pp. 1543-1555, Academic Press, 1969.
8. E. Hulpke, "A Simple Model Which Correctly Predicts the Scattering of Heavy Particles From a Well Defined Surface at Translational Energies Between 2 and 20 eV," Rarefied Gas Dynamics, Proc. of the Ninth International Symposium, pp. E.5-1 to E.5-10, Vol. II, 1974.
9. K. Jakus and F. C. Hurlbut, "Gas Surface Scattering Studies Using Nozzle Beams and Time-of-Flight Techniques," Rarefied Gas Dynamics, Sixth Symposium, Vol. II, pp. 1171 - 1185, Academic Press, 1969.
10. Lee H. Sentman, "Free Molecule Flow Theory and its Application to the Determination of Aerodynamic Forces," Technical Report LMSC-448514, Lockheed Missiles and Space Company, Sunnyvale, California, 1961.
11. Philip M. Fitzpatrick, Principles of Celestial Mechanics, Academic Press, 1970.
12. S. Gill, (Proc. Cambridge Philos Soc., Vol. 47, pp. 96-108, 1951).
13. Orbital Flight Handbook, Space Flight Handbooks, Vol. 1, NASA SP33, Part 1, National Aeronautics and Space Administration, 1963.
14. G. E. Cook, "The Effect of Aerodynamic Lift on Satellite Orbits," Planet. Space Sci., Vol. 12, pp. 1009-1020, Pergamon Press, 1964.
15. G. E. Cook and R. N. A. Plimmer, Proc. Roy. Soc. A258, 516, 1960.
16. G. E. Cook, Proc. Roy. Soc. A261, 246, 1961.

CHAPTER IV

DUAL FALLING SPHERE DETERMINATION OF DENSITY AND  
TRANSITION FLOW PARAMETER

Paper submitted to AIAA 12th Aerospace Sciences Meeting by  
G. R. Karr. Presentation was made during meeting held in Washington,  
D. C., January 30-February 1, 1974.

Gerald R. Karr  
 Assistant Research Professor  
 The University of Alabama in Huntsville  
 Huntsville, Alabama 35807

### Abstract

A new approach to the analysis of falling sphere drag data is described in which the data from two trajectories through the same region of the atmosphere are analyzed simultaneously. The analysis provides important aerodynamic information which is used to obtain an improved value of atmospheric density. The technique is applied to a set of falling sphere data in which a sphere transition-flow parameter and atmospheric density results are obtained in the 80-120 km region from published data for falling spheres over Kwajalein. Another set of data for a falling sphere test over Wallops Island is also analyzed with comparable results.

### Introduction

The falling sphere technique has been the prime source of measurements of atmospheric density and temperature in the important altitude range of 80 to 120 km. In particular, the results from three falling sphere experimental groups provided the information used to supplement the 1962 U. S. Standard Atmosphere.<sup>1,2</sup> These groups were Peterson, Hansen, McWatters and Bonfanti,<sup>3</sup> of the University of Michigan; Faire and Champion<sup>4</sup> of the Air Force Cambridge Research Laboratories; and Pearson<sup>5</sup> of Australian Weapons Research Establishment. The results obtained by these groups are summarized in the 1966 supplements to the U. S. Standard Atmosphere.<sup>2</sup> The method of analysis in all these experiments was to first measure the acceleration,  $a$ , acting on the sphere from either trajectory analysis or accelerometer readings. The drag equation

$$\text{Drag} = \frac{1}{2} \rho V^2 C_D \bar{A} = ma \quad (1)$$

is then employed to deduce the density,  $\rho$ , where  $V$  is the velocity,  $C_D$  is the drag coefficient,  $\bar{A}$  is a reference area and  $m$  is the mass. The mass, acceleration, velocity, and area are all measured quantities, leaving only  $\rho$  and  $C_D$  as unknowns in equation (1). A table of  $C_D$  as a function of Reynolds number,  $Re$ , and Mach number,  $M$ , is usually employed to obtain a value of  $C_D$ . A density value is then determined by solving equation (1). Since  $C_D$  is a function of Reynolds number and Mach number which are density and temperature dependent,

\*This work was supported by the National Aeronautics and Space Administration under Contract NAS8-28248 through NASA/MSFC, Huntsville, Alabama.

the analysis of the drag data usually involves a number of iterations until there is convergence to a final density value.

The work reported here is the result of an examination of the falling sphere technique for the purpose of proposing possible improvements, particularly in the area of aerodynamics. As with all drag deduced density experiments, the values employed for the drag coefficient in the data reduction is a major source of error. The possibility of error due to drag coefficient is largest in the 80 to 120 km region, due to the passage of the sphere through various aerodynamic regimes. A typical falling sphere trajectory will be in a free molecule flow regime at high altitude and will pass through transition flow into continuum flow at low altitudes during descent. In addition, the speed of the falling sphere may pass from subsonic to supersonic and back to subsonic during a typical trajectory.

A considerable improvement in knowledge of sphere drag coefficients has been made recently through a comprehensive experimental program at ARO which was sponsored by AFCRL for specific application to the falling sphere program. The ARO work reported by Bailey and Hiatt<sup>6</sup> covers a velocity range from 0.1 to 6.0 in Mach number and a Reynolds number range from 20 to 100,000. While this data is extremely useful, there is still a lack of accurate information for the near-free molecule drag coefficients which would correspond to Reynolds numbers below 100.

In the work reported here, two new methods of falling sphere data analysis are proposed which should find application in the low density, high altitude region of the atmosphere where accurate aerodynamic information is still lacking. The proposed methods involve the simultaneous analysis of the trajectory of two spheres travelling through the same region of the atmosphere with different velocity. As an illustration, the falling sphere data of Peterson,<sup>3</sup> et al. and Peterson and McWatters<sup>7</sup> is analyzed using one of the proposed techniques.

### Basic Theory of Dual Falling Sphere Experiments

Consider an experiment in which two sphere drag measurements are performed in the same region of the atmosphere but at different velocities.

$$D_1 = \frac{1}{2} \rho V_1^2 C_{D1} \bar{A}_1 \quad (2)$$

$$D_2 = \frac{1}{2} \rho V_2^2 C_{D2} \bar{A}_2 \quad (3)$$

Since the spheres are in the same region of the atmosphere, the values of density are the same for equation (2) and (3). Assume also that the dependence of  $C_D$  on  $\rho$ ,  $V$  and a third quantity  $B$ , which will be discussed later, is well understood. Then, in general

$$C_{D1}(\rho, B, V_1) \neq C_{D2}(\rho, B, V_2) \quad (4)$$

and equations (2) and (3) represent a set of two equations in the unknowns  $\rho$  and  $B$ . The values of  $\rho$  and  $B$  are found by solving equations (2) and (3) simultaneously.

$$\rho = \rho(D_1, D_2, V_1, V_2, \bar{A}_1, \bar{A}_2) \quad (5)$$

$$B = B(D_1, D_2, V_1, V_2, \bar{A}_1, \bar{A}_2) \quad (6)$$

In the process, not only is a value of density obtained but also the two drag coefficients are determined for the two cases.

The basic theory of dual falling sphere analysis depends on the fact that the drag coefficient is not independent of the velocity and can be written as the function of two other parameters at most. The dependence of the drag coefficient on density and the quantity  $B$  must be known in order to write equations (5) and (6). The quantity  $B$  will be seen to be the temperature for the first case discussed below and the transition flow parameter for the second case. If the drag coefficient were a function of more than two unknowns, for example

$$C_D = C_D(\rho, B_1, B_2, B_3, \dots, B_m) \quad (7)$$

then two possibilities exist. One could consider multiple falling sphere experiments designed so that  $m+1$  drag measurement would provide information necessary to invert the  $m+1$  drag equations, giving

$$\rho = \rho(D_1, D_2, \dots, D_{m+1}, V_1, V_2, \dots, V_{m+1}, \bar{A}_1, \bar{A}_2, \dots, \bar{A}_{m+1})$$

$$B_1 = B_1(D_1, D_2, \dots, D_{m+1}, V_1, \dots)$$

$$B_2 = B_2(D_1, D_2, \dots, D_{m+1}, V_1, \dots) \quad (8)$$

.

$$B_m = B_m(D_1, \dots, D_{m+1}, V_1, \dots)$$

The second possibility, and the one more practical to consider, would be to assume all but two of the quantities needed to determine the drag coefficient in equation (7). An error is of course made depending upon the accuracy of the assumptions but the total error is expected to be

less than in single falling sphere analysis where all the  $B_i$  quantities must be assumed. The approach taken in the following discussion is to reduce the unknowns in the drag coefficient to the density and one other quantity called  $B$  in the above. The potential of the dual falling sphere technique appears to be greatest in the high altitude region in which the flow is free molecule and the drag coefficient is very sensitive to the atmospheric temperature as discussed in the next section.

#### Temperature and Density Determination in Free Molecule Flow

In the free molecule flow regime the drag coefficients of a sphere is strongly dependent upon the speed ratio for speed ratios of order unity and less. The speed ratio is defined as the ratio of the sphere velocity to the thermal velocity of the gas given by

$$S = V/\sqrt{2 RT} \quad (9)$$

the free molecule sphere drag coefficient is obtained from free molecule theory to be

$$C_{D_{fm}} = 2 \left[ \left( 1 + \frac{1}{S^2} - \frac{1}{4S^4} \right) \operatorname{erf} S + \left( \frac{1}{S} + \frac{1}{2S^3} \right) \frac{e^{-S^2}}{\sqrt{\pi}} \right] (1 + K) \quad (10)$$

where  $K$  is a factor of order unity dependent on the gas surface interaction.

The drag coefficient is found to be independent of density in a free molecule flow. The nature of the dependence of  $C_D$  on  $S$  is better illustrated by the expansion of equation (10) for the cases of large and small values of  $S$ . The results are

$$C_{D_{fm}} = \frac{2}{\pi} \left[ \frac{8}{3} \frac{1}{S} + \frac{8}{15} S - \frac{8}{240} S^3 \right] (1+K) \quad (11)$$

$$S \leq 1.25$$

$$C_{D_{fm}} = 2 \left[ 1 + \frac{1}{S^2} - \frac{1}{4S^4} \right] (1 + K) \quad (12)$$

$$S \geq 1.25$$

Equation (11) shows that  $C_{D_{fm}}$  tends to infinity as  $S$  tends to zero while equation (12) shows that  $C_{D_{fm}}$  tends to  $2(1+K)$  as  $S$  tends to infinity. Values of  $S$  of order unity and less are seen to cause the greatest variation in  $C_{D_{fm}}$ .

Since falling sphere velocities at high altitudes typically correspond to speed ratios of unity or less, a dual falling sphere analysis may be feasible and fruitfully applied in this region. Consider two sphere drag measurements at free molecule conditions

$$m_1 a_1/A_1 = \frac{1}{2} \rho v_1^2 C_{Dfm} (S_1, K_1)$$

$$= \frac{1}{2} \rho v_1^2 C_{Dfm} (T, v_1, K_1) \quad (13)$$

$$m_2 a_2/A_2 = \frac{1}{2} \rho v_2^2 C_{Dfm} (S_2, K_2)$$

$$= \frac{1}{2} \rho v_2^2 C_{Dfm} (T, v_2, K_2) \quad (14)$$

where the speed ratio has been written as a function of temperature which must be the same for both measurements. Since free molecule drag coefficient is independent of density, the density can be eliminated in the above equations giving

$$\frac{m_1 a_1}{\frac{1}{2} v^2 C_{Dfm} (T, v_1, K_1) A_1}$$

$$= \frac{m_2 a_2}{\frac{1}{2} v^2 C_{Dfm} (T, v_2, K_2) A_2} \quad (15)$$

Equation (15) now contains the unknowns  $T$ ,  $K_1$ , and  $K_2$ . If the two spheres have the same surface properties and  $v_1$  is not much different from  $v_2$ , one would expect the gas surface interaction to be the same for both spheres. Therefore,

$$K_1 = K_2 = K \quad (16)$$

and the common factor  $(1+K)$  can be eliminated from equation (15), leaving a single equation in the unknown temperature  $T$ . Therefore, from equation (15)

$$T = T (m_1 a_1, m_2 a_2, v_1, v_2, A_1, A_2) \quad (17)$$

and either equation (13) or (14) may be used to obtain

$$\rho = \rho [m a, C_{Dfm} (T, v, K)] \quad (18)$$

Notice that the value of  $K$  becomes important in determining the value of density but is not required in determining temperature.

#### Discussion of Proposed Free Molecule Analysis

The above procedure would provide a more accurate measurement of temperature at high altitudes than that provided by single sphere experiments. In single falling sphere experiments, the temperature is deduced from the density values by integration of the hydrostatic equation beginning at the high altitudes. As discussed by Bartman, Chang, Jones and Liu,<sup>7</sup> this method of determining temperature is subject to large errors at the high altitudes. The dual sphere analysis,

however, is independent of the density determination and becomes more accurate at higher altitudes where free molecule conditions prevail.

A survey of published falling sphere data did not produce data of the type needed for an example analysis of the free molecule type. The proper data could be obtained by launching two spheres at near the same time but with different velocities. Another technique would be to track the sphere both during ascent and descent since the velocities would be different due to drag effects. Data of the latter type is available but only at lower altitudes where the flow is transition rather than free molecule. Analysis in the transition regime is considered in the following section.

#### Dual Falling Sphere Analysis in the Transition Regime

As a falling sphere passes into regions of greater density, the drag coefficient must change from a free molecule value (2 and greater) to a continuum value (1 and less). The flow regime between the limits of free molecule and continuum is termed the transition flow regime. Since no theoretical expression is available which can be accurately applied to the transition flow regime, empirical and semi-empirical relationships are commonly employed. One such relationship given by Matting<sup>3</sup> has application to drag coefficient determination in the near-free molecule side of the transition regime. The expression is given as

$$C_D = C_{Dc} + (C_{Dfm} - C_{Dc}) e^{-E/Kn} \quad (19)$$

where  $C_{Dc}$  is the continuum drag coefficient,  $Kn$  is the Knudsen number, and  $E$  is the parameter which must be determined from experiment. The above equation is semi-empirical based on a first collision analysis of near-free molecule flow.

For application to falling sphere analysis the quantity  $E/Kn$  can be expressed as a function of density since

$$Kn \propto \frac{1}{\rho r}$$

where  $r$  is the sphere radius. Therefore, write

$$E/Kn \equiv C_3 \rho r \quad (20)$$

where  $C_3$  will be termed the transition flow onset parameter. Since  $C_{Dfm}$  and  $C_{Dc}$  are functions of velocity, temperature, and the gas surface interaction, the functional dependence of the transition flow drag coefficient is written from equations (19) and (20)

$$C_D = C_D (\rho, C_3, T, v, K) \quad (21)$$

Since  $C_D$  contains four unknown parameters, two parameters must be assumed in order to perform dual fully sphere analysis in the transition (falling) regime. The value of temperature will be assumed

to be given by the usual methods of integration of the hydrostatic equation since Bartman,<sup>8</sup> et al. point out that the temperature deduced by the integration methods becomes more accurate at the lower altitudes. The second parameter to be assumed in the analysis is the gas surface interaction parameter, K. The value of K = 0 will be employed in the analysis for reasons discussed later. A gas surface interaction in which molecules are reflected in the specular direction corresponds to K = 0, independent of the degree of accommodation to the surface temperature. Therefore, C<sub>3</sub>, is chosen as the unknown parameter which will be determined in the analysis in addition to the density ρ. The value of C<sub>3</sub> is not well established due to a lack of experimental results in the near-free molecule regime. The analysis will then help establish the value of this important parameter for use in future experiments.

Having chosen the unknown parameters, the method of analysis is similar to the free molecule flow analysis. Consider two drag measurements in the transition regime at the same region of the atmosphere but at different velocities.

$$D_1 = \frac{1}{2} \rho V_1^2 \left[ C_{Dc1} + (C_{Dfm1} - C_{Dc1}) e^{-C_3 \rho r} \right] A$$

$$D_2 = \frac{1}{2} \rho V_2^2 \left[ C_{Dc2} + (C_{Dfm2} - C_{Dc2}) e^{-C_3 \rho r} \right] A \quad (22)$$

where the spheres are taken to be the same size so that A<sub>1</sub> = A<sub>2</sub> = A and r<sub>1</sub> = r<sub>2</sub> = r. The quantity exp(-C<sub>3</sub>ρr) can be eliminated in the above equation giving a single equation in the unknown density ρ.

$$\rho = \frac{(D_1/\frac{1}{2}V_1^2 A)(C_{Dfm2} - C_{Dc2}) - (D_2/\frac{1}{2}V_2^2 A)(C_{Dfm1} - C_{Dc1})}{C_{Dc1} C_{Dfm2} - C_{Dc2} C_{Dfm1}} \quad (23)$$

and C<sub>3</sub> is found from either of equations (22) once a value of ρ is determined from equation (23).

$$C_3 = -\frac{1}{\rho} \ln \left[ \frac{(D/\frac{1}{2}V^2 A) \frac{1}{\rho} - C_{Dc}}{C_{Dfm} - C_{Dc}} \right] \quad (24)$$

The transition flow analysis has been successfully applied to five sets of falling sphere measurements over Kwajalein made by the University of Michigan group in 1963 and 1964 as described in the next section.

#### Analysis of Kwajalein Falling Sphere Measurements

The University of Michigan falling sphere measurements consist of data taken both during ascent and during descent for one of the three spheres ejected from the rocket during the ascent phase. The spheres were made of Mylar inflated with isopentane having an inflated diameter of

0.66m and a mass of 50 grams. The velocity-altitude history of a typical flight is shown in Figure 1. In this particular flight there is an overlap of ascent and descent data in the region between 90 and 110 km. Data of the type shown in Figure 1 are suitable for analysis as a dual falling sphere experiment using the method outlined above.

Unfortunately, not all flights had regions of overlap. Of the 13 successful flights over Kwajalein, only six have any overlap. The sounding number and the region of overlap of the ascent and descent are the following:

Sounding 2;	100 to 102 km
Sounding 3;	99 to 102 km
Sounding 8;	104 to 109 km
Sounding 12;	99 to 104 km
Sounding 13;	96 to 107 km
Sounding 14;	at 102 km

The plots of these data are given in the reference by Peterson,<sup>3</sup> et al. The data used for the work reported here was obtained in the form of computer output of the University of Michigan analysis, a sample of which is also given in reference 3. The temperature data obtained in that analysis was used directly in this work after smoothing over the data in the region from 80 to 120 km using a third order least squares polynomial. The drag term required in equations (23) and (24) was obtained using the published values of C<sub>D</sub> and ρ in the following relationship

$$\frac{D}{\frac{1}{2} V^2 A} = (\rho C_D) \text{ published values} \quad (25)$$

Due to noise in the data, the application of equations (23) and (24) could not be made point by point. A smoothing of the data was then performed over the region of 80 to 120 km employing a second order least squares polynomial fit. This meant that the ascent and descent trajectories were smoothed over a distance of about 20 km.

The C<sub>Dfm</sub> values used were obtained from either equations (11) or (12) and C<sub>Dc</sub> values were obtained using a polynomial fit to the data given in Reference 6 for the highest Reynolds numbers. The mean molecular weight needed to determine speed ratio or Mach number was obtained from a polynomial fit to the mean molecular weight given in the 1962 U. S. Standard<sup>1</sup> for the region between 80 and 120 km.

#### Discussion of Results for 66 cm Spheres

Values of C<sub>3</sub> were calculated in the region of overlap for each of the soundings. Due to the smoothing operations only one value of C<sub>3</sub> could be obtained from each sounding. Soundings number 8, 13, and 14 were analyzed using all the data

points provided in the 80 to 120 km region. The results are

$$C_3(8) = 3.8200 \times 10^6 \text{ m}^2/\text{kg}$$

$$C_3(13) = 3.2352 \times 10^6 \text{ m}^2/\text{kg}$$

$$C_3(14) = 5.2345 \times 10^6 \text{ m}^2/\text{kg}$$

The data for soundings 2 and 3 were noisier than the rest and a value of  $C_3$  could only be obtained after eliminating a number of the most divergent points. The results were

$$C_3(2) = 5.852 \times 10^6 \text{ m}^2/\text{kg}$$

$$C_3(3) = 15.924 \times 10^6 \text{ m}^2/\text{kg}$$

The noisy data associated with these results is likely the cause for the values being higher than for the other three.

The data for sounding 12 was smooth yet a solution for  $C_3$  could not be obtained. It should be noted, however, that sounding 12 was also cause for concern by the Michigan group because of the anomalous behavior which they felt might be due to a small leak in the inflated sphere.

#### Results From 7 In. Sphere

Additional overlapping falling sphere data was obtained for an accelerometer instrumented 7 in. sphere experiment over Wallops Island flown in 1961. The data is published in NASA-CR-29 by Peterson and McWatters<sup>7</sup> consisting of results obtained from the first tests of the accelerometer system. The method of analysis was the same as used on the 66 cm data. The result obtained was

$$C_3(7 \text{ in}) = 1.5583 \times 10^6 \text{ m}^2/\text{kg}$$

This result is within a factor of two of that obtained for soundings 8, 13, and 14. The factor of two difference may be due to the different surface properties of the 7 in. as compared to the 66 cm. Also, the 7 in. sphere enters the transition regime at a lower altitude than does the 66 cm sphere due to its smaller size. The different molecular composition at lower altitudes may cause a change in  $C_3$ . These questions could be answered by analysis of more 7 in. trajectory data.

#### Atmospheric Density Calculations and Discussion of Results

After determining a value for  $C_3$ , the drag data taken in the original experiment may be reanalyzed to obtain new values of density employing equation (22). An iterative technique was employed using the unsmoothed temperature and drag values given in Reference 3. A comparison was made of the density values given in reference 3 with the density values obtained using

$C_3 = 4 \times 10^6 \text{ m}^2/\text{kg}$  which represents an average of the results for soundings 8, 13, and 14. A point by point comparison was made for each of the soundings 8, 13, and 14 and the average was obtained. The results are presented in Figure 2 which shows that the densities calculated using the methods described in this paper produce generally higher values than obtained in the original experiments.

Figure 3, obtained from reference 2, shows the mean values of density obtained in all 13 of the original experiments as compared to the 1962 U. S. Standard.<sup>1</sup> This figure shows that the original analysis resulted in a nearly 10% lower density value above 100 km than given in Reference 1. Application of the results of the current work shown in Figure 2 would cause the density to be nearly equal or somewhat greater than the U. S. Standard above 100 km. Both methods of analysis give a higher density in the 90 to 100 km region than that given in the U. S. Standard, but, neither analysis is correct in this region as discussed in the following:

In the 90 to 100 km region, the Knudsen number is of order .1 as is shown in Figure 2. Transition flow is considered to be within the limits of 10 to .1 which means that in the 90 to 100 km region the flow is near continuum rather than near free molecule. For this reason, equation (19), which is derived on the basis of near free molecule theory, is likely not valid in this lower region. The results could be improved by employing a more valid relationship. The method of analysis would remain the same however.

The results obtained in the 90 to 100 km region in the original analysis, reference 3, are also not correct due to inaccurate values of  $C_p$ . The recent work on  $C_p$  reported in reference 6 shows that the values of  $C_p$  used in the original analysis were about 10% higher than those measured in the wind tunnel. Therefore, somewhat higher values of density would be obtained in the 90 to 100 km region but not to the degree indicated by the results shown in figure 2.

Above 100 km, an average 10% higher density is found using the  $C_p$  values calculated from the transition flow analysis. This difference can partly be explained by the difference in the treatment of the gas surface interaction. In the current analysis, a value of  $K = 0$  was used while in reference 2 the treatment of the gas surface interaction resulted in an additive term of the form  $2\sqrt{\pi}/3S_w$  was used where  $S_w$  is the speed ratio molecules would have if they obtain the temperature of the sphere wall,  $T_w = 300^\circ\text{K}$ . Values of  $K$  which would compare more to the assumption made in reference 3 were attempted but the results for  $C_3$  obtained for higher values of  $K$  were not as consistent as the ones obtained with  $K = 0$ . In some cases, no solution for  $C_3$  could be found for  $K$  greater than zero. These results tend to

indicate that  $K = 0$  is a proper choice but more conclusive evidence is needed in order to fix this important parameter.

### Conclusions

The method of analysis reported here has demonstrated potential for application in high altitude falling sphere experiments. The values of  $C_3$  obtained represent one of the first experimental measurements of this quantity under high altitude conditions. More accurate values of  $C_3$  are needed to remove this unknown in the analysis of falling sphere experiments could then be designed to measure still other unknown quantities such as temperature. Dual falling sphere measurements of both temperature and density at high altitudes have been proposed and appear to be an experiment well worth performing.

### Acknowledgements

The author is grateful to Dr. R. E. Smith and G. Swenson of NASA/MSFC for their support and valuable discussions. The author is also grateful to K. D. McWatters of the University of Michigan High Altitude Engineering Laboratory for providing the computer output for the falling sphere tests used in this work.

### References

1. Committee on Extension to the Standard Atmosphere, U. S. Standard Atmosphere, 1962, Superintendent of Documents, U. S. Government Printing Office, Washington, D. C.
2. U. S. Standard Atmosphere Supplements, 1966, Superintendent of Documents, U. S. Government Printing Office, Washington, D. C.
3. Peterson, J. W., Hansen, W. H., McWatters, K. D., and Bonfanti, G., "Falling Sphere Measurements over Kwajalein," *Journal of Geophysical Research*, 70, 4477-4489, September 15, 1965.
4. Faire, A. C. and Champion, K. S. W., "Falling Sphere Measurements of Atmospheric Density, Temperature, and Pressure up to 115 Kilometers," *Space Research V*, Hilde Kallmann-Bijil, ed., p. 1039, 1965.
5. Pearson, P. H. O., "Basic Atmospheric Parameters as Measured by Four Falling Sphere Experiments at Woomera, December 1964 - March 1965," Australian Weapons Research Establishment, Tech. Note Pad 109, November 1965.
6. Bailey, A. B. and Hiatt, J., "Free-Flight Measurements of Sphere Drag at Subsonic, Transonic, Supersonic, and Hypersonic Speeds for Continuum, Transition and Near-Free-Molecular Flow Conditions," Arnold Engineering Development Center, Arnold Air Force Station, Tennessee, AEDC-TR-70-291, March 1971.
7. Peterson, J. W. and McWatters, K. D., "The Measurement of Upper-air Density and Temperature by two Radar-tracked Falling Spheres," NASA Contractor Report NASA CR-29, NASA, Washington, D. C., April 1964.
8. Bartman, F. L., Chaney, L. W., Jones, L. M., and Liu, V. C., "Upper Air Density and Temperature by the Falling Sphere Method," *Journal of Applied Physics*, 27, pp. 706-712, July 1956.
9. Matting, F. W., "Approximate Bridging Relations in the Transitional Regime between Continuum and Free-Molecule Flows," *Journal of Spacecraft* 8, pp. 35-40, January 1971.

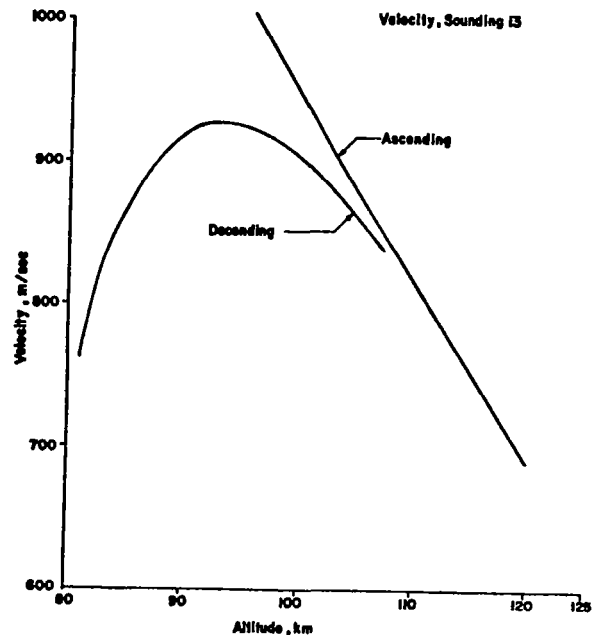


Figure 1. Velocity-altitude history for falling sphere sounding 13 in which ascent and descent trajectory overlap.

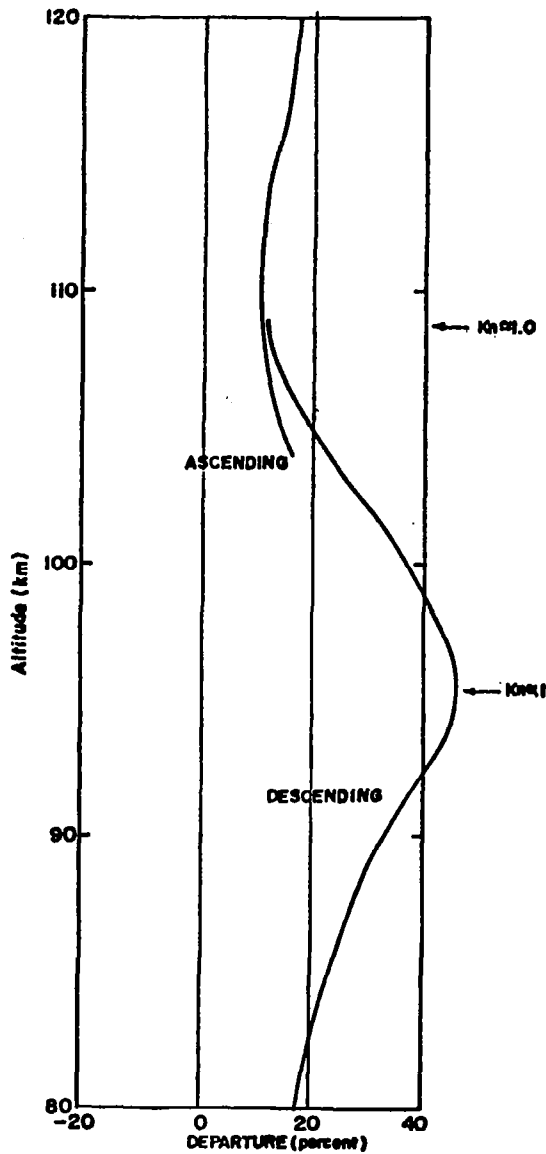


Figure 2. Average of ratio of density computed using equation (19) and density obtained in original experiment for soundings 8, 13, and 14 with  $C_3 = 4 \times 10^6 \text{ m}^2/\text{kg}$ .

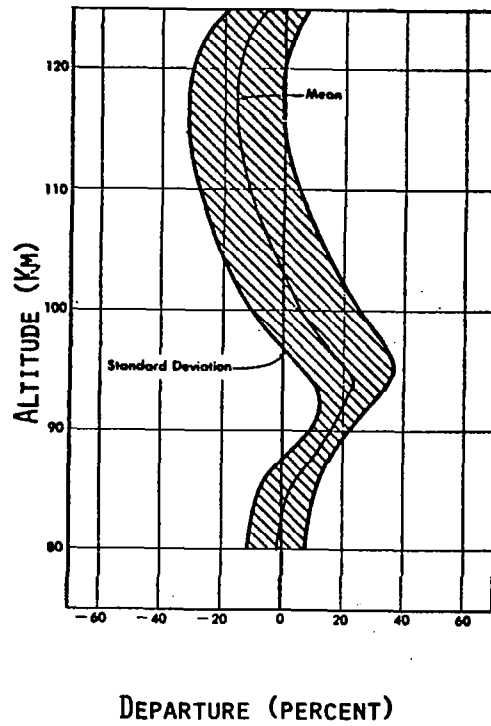


Figure 3. Departure from standard atmosphere of the mean and standard deviations of 13 density measurements deduced in the original experiments at Kwajalein Island (plot is copied from reference 2).

CHAPTER V

A SPHERE DRAG BRIDGING RELATIONSHIP IN THE LOW  
MACH NUMBER TRANSITION REGIME

A Sphere Drag Bridging Relationship in the Low  
Mach Number Transition Regime\*

by

Gerald R. Karr\*\*  
The University of Alabama in Huntsville  
Huntsville, Alabama 35807

Introduction

Transition flow is defined as the flow regime in which the mean free path of the gas molecules is of the same order as a typical dimension of the body under consideration.<sup>1</sup> At the boundaries of the transition regime are the free molecule regime (mean free path much larger than the characteristic dimension) and the continuum regime (mean free path much less than the characteristic dimension). The drag coefficient of a sphere is known to change markedly in the transition flow regime between the limits of free molecule and continuum flow and is a strong function of Mach Number. The drag coefficient in the free molecule regime approaches infinity at zero Mach Number and approaches a value near 2 at hypersonic Mach numbers. At the continuum limit, on the other hand, the sphere drag coefficient has a more complex nature which is known to depend on the Reynold's Number and the turbulence or lack of turbulence in the flow. In this work, however, the high density boundary of the transition regime will be assumed to be at  $Re_{\infty} \approx 10^4$  for which the drag coefficient has a value of near 0.4 at subsonic velocities, increases in the transonic regime to a value of near 1.0 and approaches 0.92 at hypersonic velocities.

---

\* Research supported under National Aeronautics and Space Administration Contract NAS8-28248, Marshall Space Flight Center, Huntsville, Ala.

\*\* Assistant Research Professor, Mechanical Engineering Dept., Member AIAA.

The continuum limit of the transition regime was taken as  $Re_{\infty} = 10^4$  for two reasons: (1) the sphere drag data employed in this work all corresponds to  $Re < 10^5$  and (2) sphere drag variations which occur above  $Re_{\infty} = 10^4$  are more clearly correlated with continuum parameters ( $Re$  and turbulence) rather than what is normally considered transition flow parameters ( $Kn$  and surface to gas temperature ratio).

Due to the lack of adequate theory of the aerodynamics in the transitional regime, analytic determination of the sphere drag coefficient is usually made through semi empirical relations which are based on near free molecule flow theory and experimental results. These formulas are called bridging relationships, a number of which are reviewed in references 2, 3 and 4. The accuracy of a bridging relationship may be determined by comparison with experiment and most formula have at least one free parameter in order to obtain a best fit with given data. As discussed in reference 4, it is found, however, that available bridging relationships are typically accurate only over a limited range in Mach Number and Knudsen Number. The purpose of this paper is to report on a bridging formula which, with three free parameters, was found to predict to about 6% accuracy the sphere drag results obtained by the ballistic range method by Bailey and Hiatt.<sup>5</sup> Although Bailey and Hiatt provide plots of curve fits of drag coefficient as a function of Reynold's Number to a claimed accuracy of  $\pm 2\%$ , the analytic results obtained here are provided as a function of Knudsen Number and have the advantage of allowing for ready interpolation as a function of Mach Number and Knudsen Number. Finally, it should be noted that the results obtained here are applicable only to fitting the Bailey and Hiatt measurements which are somewhat unique for sphere drag data in that the sphere surface temperature

was equal to the gas temperature ( $T_w/T_\infty = 1$ ). The results then have application, for example, to falling sphere data analysis where  $T_w/T_\infty \approx 1$  but would not be applicable to wind tunnel data where typically  $T_w/T_\infty \gg 1$ .

### The Bridging Relationship

The bridging relationship used in this work is a modification of that developed by Matting<sup>6</sup> and also given by Rott and Whittenburg.<sup>7</sup> Using a first collision, two fluid flow approximation, Matting obtained the result which can be written as

$$C_D = C_{D_c} + \left( C_{D_{FM}} - C_{D_c} \right) e^{-E/Kn} \quad (1)$$

where  $C_D$  is the drag coefficient,  $C_{D_c}$  is the continuum drag coefficient,  $C_{D_{FM}}$  is the free molecule drag coefficient,  $Kn$  is the Knudsen Number (defined as  $Kn = \text{mean free path/sphere diameter}$ ), and  $E$  is the free parameter. Equation 1 is seen to provide the correct limits as  $Kn$  is allowed to vary. At the free molecule flow limit,  $Kn \rightarrow \infty$ , which gives  $C_D = C_{D_{FM}}$ . At the continuum limit which in this work is taken as  $Re_\infty = 10^4$ ,  $Kn \rightarrow 0$ , which gives  $C_D = C_{D_c}$ . The limits are approached asymptotically which is what is observed experimentally. As will be shown, however, Equation 1 is not found to accurately predict the  $C_D$  variation in the low Mach Number transition regime for any value of the free parameter  $E$ . Equation 1 is found to predict a much steeper variation in  $C_D$  than what is observed in recent experimental results of Bailey and Hiatt.<sup>5</sup>

In order to correct the failure of Equation 1, a second free parameter was introduced which was found to improve the accuracy considerably. The new form of the bridging relation is given by

$$C_D = C_{D_c} + \left( C_{D_{FM}} - C_{D_c} \right) e^{-E/(Kn)^x} \quad (2)$$

where  $x$  is the new free parameter introduced here. By raising  $Kn$  to a power, the steepness of the variation of  $C_D$  with respect to  $Kn$  may be controlled, thereby better fitting the experimental results.

#### Method of Determination of Free Parameters

The values of free parameters are determined from a best fit to experimental data. The experimental data used here is that reported by Bailey and Hiatt<sup>5</sup> which are obtained by the ballistic range method for which  $T_w/T_\infty = 1$  and covers a range in Mach Numbers from 0.1 to 6.0 and a range in Reynold's Numbers from 15 to 50,000. Due to a lack of coverage in the transition regime at the lowest Mach Numbers, the data used in this work is limited to between  $M_\infty \approx .72$  and  $M_\infty \approx 6.0$ . Also, since only 6 of the 356 data points in the range have  $10^4 < Re_\infty < 10^5$ , a value of  $Re_\infty = 10^4$  has been used as the continuum limit. This range in flow parameters is of particular interest to falling sphere data analysis and also has application to satellite reentry and sounding rocket trajectories.

Bailey and Hiatt provide tables of the experimental results arranged in groups of approximately the same Mach Number. For example, 32 measurements of sphere drag coefficients were made for  $1.45 \leq M_\infty \leq 1.65$  and 36 measurements made for  $2.8 \leq M_\infty \leq 3.2$  (see Table I for complete list). For each measurement the values of  $M_\infty$ ,  $Re_\infty$ , and  $C_D$  are given from which a Knudsen Number can be derived using<sup>1</sup>

$$Kn = \frac{\ell}{d} = \left( .499 \sqrt{\frac{\pi}{8}} \right)^{-1} \frac{\sqrt{\gamma} M_\infty}{Re_\infty} \quad (3)$$

where  $\ell$  is the mean free path,  $d$  is the sphere diameter, and  $\gamma = 1.4$ .

The continuum and free molecule drag coefficients are assumed to be functions of Mach Number only. The free molecule drag coefficient<sup>8</sup> is given by

$$C_{D_{FM}} = 2 \left[ \left( 1 + \frac{1}{S^2} - \frac{1}{4S^4} \right) \operatorname{erf} S + \left( \frac{1}{S} + \frac{1}{2S^3} \right) \frac{e^{-S^2}}{\pi} \right] (1+K) \quad (4)$$

where  $\operatorname{erf}$  is the error function and where  $S$  is the speed ratio given by  $S = V / \sqrt{2 RT}$ , which can also be expressed in terms of Mach Number as  $S = M \sqrt{\gamma/2}$ . The quantity  $K$  in Equation 4 is a factor of order unity dependent on the gas surface interaction.

Since the evaluation of Equation 4 is complicated by the presence of the error function, a useful expansion of Equation 4 for low and high values of  $S$  was employed in the analysis. The results of the expansion are

$$C_{D_{FM}} (S \leq 1.25) = \frac{2}{\sqrt{\pi}} \left[ \frac{8}{3} \frac{1}{S} + \frac{8}{15} S - \frac{8}{210} S^3 \right] (1+K) \quad (5)$$

$$C_{D_{FM}} (S \geq 1.25) = 2 \left[ 1 + \frac{1}{S^2} - \frac{1}{4S^4} \right] (1+K) \quad (6)$$

which are accurate to better than .1% with respect to Equation 4.

The continuum values of drag coefficient were obtained also from Bailey and Hiatt using values of  $C_D$  versus  $M_\infty$  for  $Re = 10,000$  which, for the Mach numbers of interest here, correspond to  $Kn \approx 10^{-4}$ . The expression employed is given by

$$C_{D_c} (M \geq 1.0) = .92 + .166/M - .366/M^3 \quad (7)$$

which is found to give an accuracy of at least 5% with respect to the experimental results. For Mach Numbers below 1.0, the following values were used

$$C_{D_c} (.1 < M \leq 1.0) = .403 - .142 M^2 + .459 M^4 \quad (8)$$

Using the relations given above, the data in a given Mach Number group were used to find the best values of  $x$  and  $E$  in a least squares sense. The least squares equation was written and the partial derivatives with respect to  $x$  and  $E$  were found. A computer program was developed to find the values of  $x$  and  $E$  which made the derivatives zero and thereby made the error a minimum.

### Results and Discussion

For each Mach Number set tested, a root-mean-square (rms) value was computed and used as a measure of the accuracy of the fit for that set of data. The value of  $K$  required for the free molecule drag coefficient value was found to have influence on the results obtained. The RMS value for a given Mach Number was found to be improved if the value of  $K$  was taken to be a small negative number. Therefore,  $K$  becomes a third free parameter of the fitting process.

The least square results showed that  $x$  and  $K$  have a Mach Number dependence while  $E$  is nearly constant. The  $x$  and  $K$  values were found to be nearly linear in Mach Number and approximated by the following relationships,

$$x = .399 + .016 M \quad (9)$$

$$K = -.002438 - .01842697 M \quad (10)$$

and the average value of  $E$  was found

$$E = .212 \quad (11)$$

A set of  $x$ ,  $K$ ,  $E$  values are thus obtained over the full range of Mach Numbers under consideration. Equations 9, 10, and 11 were employed in Equation 2 and the results compared to the ARO drag data. The RMS values that resulted are given in Table I along with the number of data points and the values of  $x$ ,  $K$ , and  $E$ . The average RMS value of the 16 sets of data tested in Table I is .059.

Figure 1 shows a plot of  $C_D$  vs  $Kn$  for six of the seventeen sets of data employed in the analysis. The bridging relationship is shown as the solid lines which are calculated based on the midrange Mach number of a given set of data. The figure illustrates the success of the bridging relationship in the transition regime and shows that much of the 6% rms error can be traced to scatter in the data which is nearly  $\pm 10\%$  at some values of  $Kn$ . One failure worth noting, however, is the tendency of the bridging relationship to underestimate the  $C_D$  value in the  $10^{-3} < Kn < 10^{-2}$  range by about 5% in some cases. This is likely a slip flow influence which has not been taken into consideration in this work.

Table I  
RMS Values of Curve Fit to ARO Data Using Equations 9,  
10, and 11 in Equation 2

Midrange Mach Number	Mach Number Range	Number of Data Points	X	E	K	RMS
.72	.70 - .74	7	.4105	.212	-.016	.013
.81	.79 - .83	9	.4120	.212	-.017	.076
.915	.88 - .95	20	.4136	.212	-.019	.065
.965	.96 - .97	10	.4144	.212	-.020	.123
.989	.98 - .998	8	.4148	.212	-.021	.082
1.135	1.08 - 1.19	24	.4172	.212	-.023	.036
1.25	1.2 - 1.3	15	.4190	.212	-.025	.055
1.375	1.3 - 1.45	28	.4210	.212	-.028	.075
1.55	1.45 - 1.65	32	.4238	.212	-.031	.050
1.75	1.65 - 1.85	23	.4270	.212	-.035	.051
2.05	1.9 - 2.2	30	.4318	.212	-.040	.060
2.55	2.4 - 2.7	18	.4398	.212	-.049	.059
3.00	2.8 - 3.2	36	.4470	.212	-.058	.054
4.00	3.8 - 4.2	28	.4630	.212	-.076	.060
5.00	4.8 - 5.2	40	.4790	.212	-.095	.041
6.00	5.8 - 6.2	33	.4950	.212	-.113	.042

## Conclusions

A sphere drag bridging relationship has been developed for the low Mach Number transition flow regime which fits recent experimental results to an accuracy of about 6% rms. The experimental results used were exclusively those reported by Bailey and Hiatt in tests ran at ARO and reported in March 1971 in which the sphere surface temperature was equal to the gas temperature. The results of this work should have application, for example, to the analysis of falling sphere data in which  $T_w/T_\infty \approx 1$ .

Due to the unique nature of the Bailey and Hiatt data (i.e.,  $T_w/T_\infty = 1$ ), it is of interest to examine the conclusions these data indicate concerning the nature of the transition flow regime. Using the parameters found in fitting these data, Eq. 2 was plotted,  $C_D$  vs  $M$ , (Fig. 2) for  $0 < Kn < \infty$  and  $.1 < M < 6$  for constant values of  $Kn$ . Since the highest  $Kn$  tested by Bailey and Hiatt was  $10^{-1}$  and since there was little transition flow data below  $M = 1$ , the curves for  $Kn > 10^{-1}$  and all the curves for values of  $Kn$  for  $M < 1$  are extrapolations. The results obtained, however, point to two important conclusions: (1) the width of the transition regime in terms of Knudsen Number is wider than usually assumed and (2) the free molecule drag coefficient implied by the results is less than usually assumed.

Since the value of  $x$  (which is a measure of the slope of the  $C_D$  vs.  $Kn$  curve in the transition regime) was found to be about .45, the width of the transition regime is increased over that obtained using the Matting relation which has  $x = 1$  (Equation 1). This conclusion is illustrated by substituting into Equation 2 the value  $Kn = 5$  which is the usually assumed upper limit of the transition regime.<sup>1</sup> The results

at  $M = 6$ ,  $Kn = 5$  give  $C_D/C_{D_{fm}} = .956$  which shows that the free molecule limit has not been reached at this value of Knudsen Number. A value of  $C_D/C_{D_{fm}} = .99$  is found to be reached for  $M = 6$  at a value of  $Kn = 100$ .

The free molecule limit was found to be of importance in the development of the bridging relationship since  $K$  had to be adjusted to negative values in order to obtain an accurate fit. This implies a free molecule drag coefficient less than two for the high values of Mach Number tested. Results from other experimenters<sup>9</sup> show that the drag coefficient in the free molecule limit is greater than 2 at Mach Numbers from 4 to 6. This departure from the results of others is likely explained in that much of the sphere drag data at high Knudsen Numbers and high Mach Numbers used by others are obtained in low density windtunnels whereas the experimental data employed in this study was obtained exclusively from ballistic range data. The higher surface-to-gas-temperature ratios that occur in windtunnels cause higher free molecule drag due to the energetic reflection of molecules at the surface. This effect is clearly shown in recent sphere drag experiments<sup>9,10</sup> in which  $C_{D_{fm}}$  is found to decrease as  $T_w/T_\infty$  is decreased. In fact, an extrapolation of the data of reference 10 down to  $T_w/T_\infty = 1$  indicates a  $C_D$  of 2 or less. A free molecule sphere drag coefficient of less than 2 requires that the gas surface interaction be non uniform on the surface of the sphere. This possibility is discussed by Cook<sup>11</sup> in which he proposes that the lowest possible free molecule drag of a sphere is 1.5. The lowest value implied in this work is 1.844 at  $M = 6$  where  $K = -.113$ .

The above conclusions are tentative but point to a need for free molecule experimental data in the low Mach Number regime at surface

temperatures close to ambient. Although the Bailey and Hiatt data do not reach free molecule conditions, the extrapolation discussed above show that the data lead to different conclusions than obtained from  $T_w/T_\infty \neq 1$  experiments.

## References

1. Schaaf, S. A. and Chambre, P. L., Flow of Rarefied Gases, Number 8 Princeton Aeronautical Paperbacks, Princeton University Press, Princeton, New Jersey, 1961, pp. 3-8.
2. Baker, R. M., Jr. and Charwat, A. F., "Transitional Correction to the Drag of a Sphere in Free Molecular Flow," The Physics of Fluids, Vol. 1, No. 2, March-April 1958, pp. 73-81.
3. Hadjimichalis, K. S., Univ. of Oxford, Eng. Sc. Report 1073/73 (1973).
4. Kinslow, M. and Potter, J. L., "The Drag of Spheres in Rarefied Hypervelocity Flow," AEDC-TDR-62-205, December 1962, Arnold Engineering Development Center, Arnold Air Force Station, Tenn.
5. Bailey, A. B. and Hiatt, J., "Free-Flight Measurements of Sphere Drag at Subsonic, Transonic, Supersonic, and Hypersonic Speeds for Continuum, Transition, and Near Free-Molecular Flow Conditions," AEDC-TR-70-291, March 1971, Arnold Engineering Development Center, Arnold Air Force Station, Tenn.
6. Matting, F. W., "Approximate Bridging Relations in the Transitional Regime Between Continuum and Free-Molecule Flows," AIAA J. Spacecraft, Vol. 8, No. 1, January 1971, pp. 35-40.
7. Rott, N. and Whittenburg, C. G., "A Flow Model for Hypersonic Rarefied Gasdynamics with Applications to Shock Structure and Sphere Drag," Douglas Aircraft Col, Report SM-38524, May 12, 1961.
8. Karr, G. R., "Dual Falling Sphere Determination of Density and Transition Flow Parameter," AIAA Paper No. 74-216, AIAA 12th Aerospace Sciences Meeting, Washington, D. C., Jan. 30-Feb. 1, 1974.
9. Whitfield, D. L. and Smithson, H. K., "Low-Density Supersonic Sphere Drag with Variable Wall Temperature," AEDC-TR-71-83, July 1971, Arnold Engineering Development Center, Arnold Air Force Station, Tenn.
10. Hadjimichalis, K. S. and Brundin, C. L., "The Effect of Wall Temperature on Sphere Drag in Hypersonic Flow," Rarefied Gas Dynamics, Proceedings of Ninth International Symposium, M. Becker ed., Vol. III, pp. D.13-1 - D.13-9, 1974.
11. Cook, G. E., "Drag Coefficients of Spherical Satellites," Technical Report No. 65218, October 1965, Royal Aircraft Establishment, Farnborough, Hants, England.

#### FIGURE CAPTIONS

- Figure 1. Comparison with Equation 2 of Sphere Drag Coefficient Data (Ref. 5) as a Function of Free Stream Knudsen Number for Constant Values of Mach Number.
- Figure 2. Sphere Drag Coefficient as a Function of Free Stream Mach Number for Constant Values of Knudsen Number.

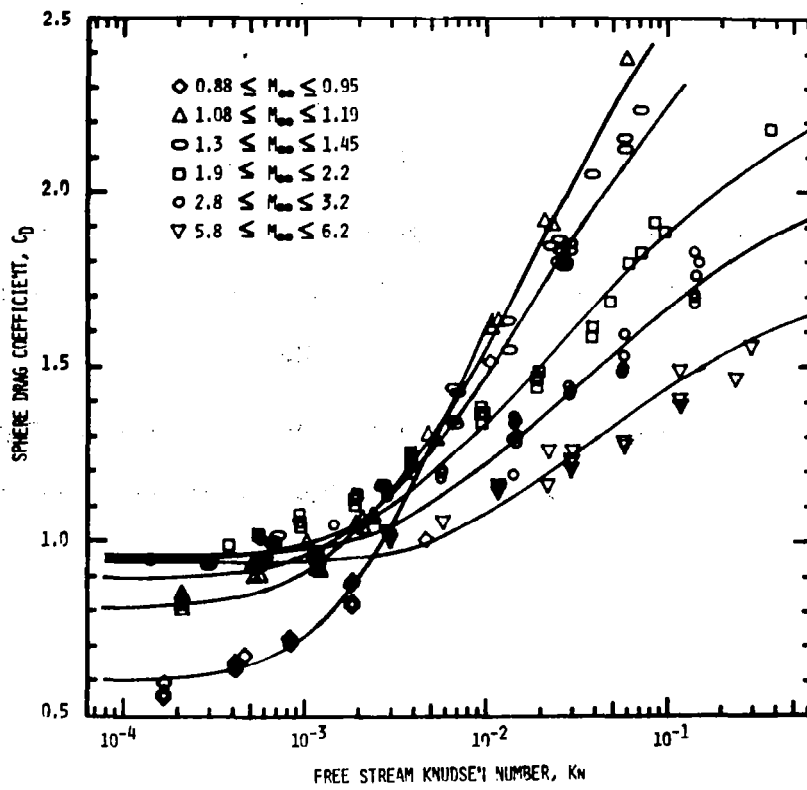


Figure 1

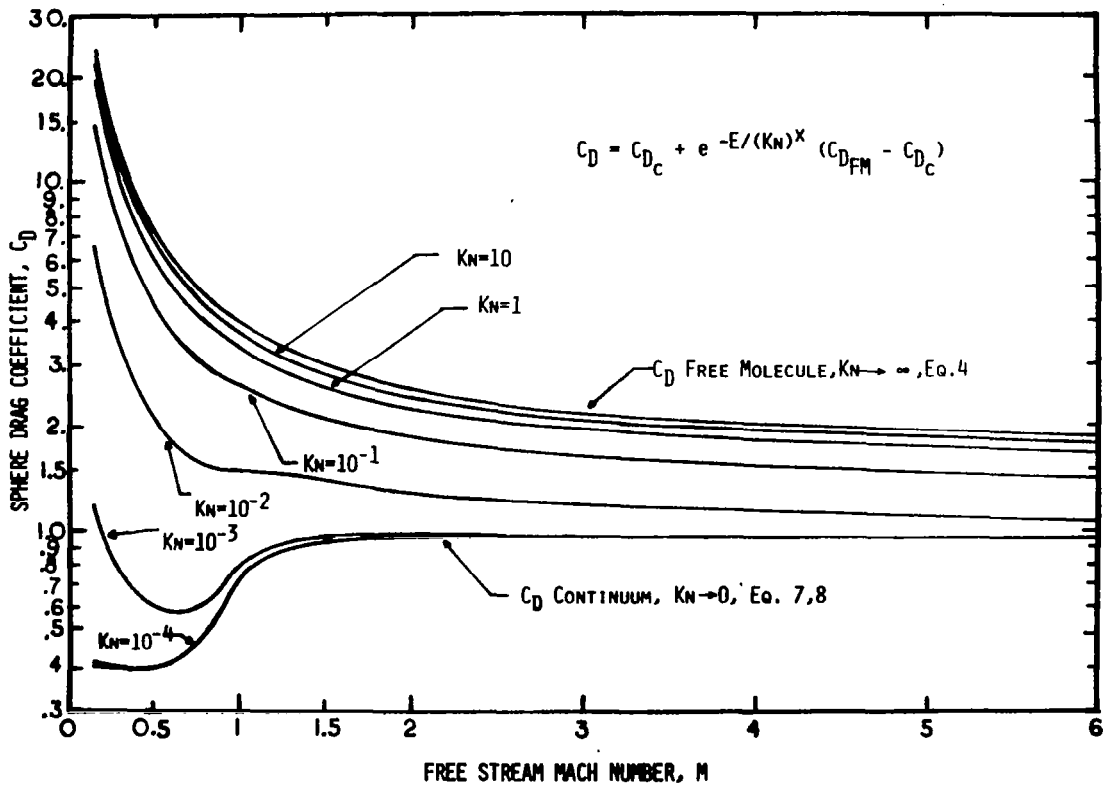


Figure 2

CHAPTER VI

IMPROVEMENTS IN FALLING SPHERE DATA ANALYSIS IN THE 80 TO 120 KM REGION

1111

12

# Improvements in Falling Sphere Data Analysis in the 80 to 120 Km Region

by

Gerald R. Karr and Robert E. Smith

The analysis of falling sphere drag data is a principle means of density and temperature determination in the 80 to 120 Km region of the earth's atmosphere. This important method of atmospheric probing was reported by Bartman, et al<sup>1</sup> in 1956 and has found wide use in upper atmospheric research. The method is particularly useful in the 80 to 120 Km region which is above the altitude capability of most aircraft and balloon probes but below normal satellite altitudes.

In a typical falling sphere experiment, a sphere is ejected from a sounding rocket and the trajectory of the sphere is measured as it falls through the atmosphere. The trajectory information is analyzed to determine the velocity and acceleration as a function of altitude. This information is then used in the drag equation

$$\text{Drag} = \frac{1}{2} \rho v^2 C_D A \quad (1)$$

where density,  $\rho$ , is obtained for a given value of drag coefficient,  $C_D$ , and sphere crosssection area  $A$ .

Temperature values are obtained from the density measurement using the hydrostatic equation

$$dp = - g \rho dz \quad (2)$$

where  $g$  is the acceleration of gravity,  $z$  is the altitude, and  $p$  is the pressure. Equation 2 may be integrated between any two limits in altitude to give the pressure at  $z$

$$p(z) = - \int_{z_0}^z g \rho dz + p(z_0) \quad (3)$$

The temperature at  $z$  is obtained by substituting the values of  $p$  and  $\rho$  into the equation of state,

$$p(z) = \rho(z) (R/W(z)) T(z) \quad (4)$$

where  $R$  is the universal gas constant,  $W$  is the molecular weight and  $T$  is the temperature.

The temperature determination is seen to require knowledge of the pressure or equivalent temperature at some reference altitude ( $p(z_0)$  in Equation 3). In practice, the integration of Equation 3 is taken in the negative direction, from the point of highest ascent down to the lower altitudes. The temperature at  $z_0$  is usually obtained from some atmospheric model. The error caused by possible incorrect temperature selection is minimized by the practice of downward integration since the term  $p(z_0)$  in Equation 3 becomes small in comparison to the first term as the integration proceeds to the lower altitudes. Thus, the effect of error in the initial temperature selection should become unimportant at one to two scale heights below the initial selection point. This was verified in the present study by selecting temperatures from  $0^\circ\text{K}$  to  $1000^\circ\text{K}$  at 120 Km. The effect on results below 100 Km due to such wide choices in temperature at 120 Km was found to be negligible ( $< 1\%$ ).

Another source of error in the falling sphere method is the value of  $C_D$  used in the drag equation, Equation 1. The typical trajectory of falling spheres in the 80 to 120 Km region is found to correspond to an aerodynamic flight regime for which sphere drag coefficients have been highly uncertain. Due to the low densities ( $10^{-5}$  to  $10^{-8}$   $\text{Kg/m}^3$ ) and the low Mach numbers

(1 to 5) experienced by falling spheres in this region, the aerodynamic flight regime is classified as the transition flow regime (Ref. 2). The mean free paths of gas molecules in this region of the atmosphere vary between  $10^{-3}$  m to 10m which means that the flow is too dense to be considered free molecule but too rarefied to be considered continuum. While the free molecule and continuum values of sphere drag coefficients have long been well known, the values of  $C_D$  in the transition flow region have only recently been measured to adequate accuracy.

The purpose of this paper is to report on improvements made in the falling sphere method of analysis. The most important of which is an improved relationship for the sphere drag coefficient which has estimated accuracy of at least 5% over the range applicable to falling sphere trajectories. The second improvement in the analysis is to employ both the ascent and descent trajectory data in the data reduction. These improvements are applied to published falling sphere data and comparison is made with the results of previous analysis.

### Drag Coefficient Relationship

Recent sphere drag experiments reported by Bailey and Hiatt<sup>3</sup> have provided and improved the drag coefficient information in the transition regime. The experiments were made in a Mach number and Reynold's number range of particular application to falling sphere data analysis ( $0.1 < M_\infty < 6.2$  and  $20 < R_e < 10^5$ ). These data were obtained in ballistic range in which the temperature of the gas and the sphere temperatures were approximately the same. The data are obtained in a consistent manner by one group of experimenters over the complete range of flow parameters applicable to the falling sphere flight regime. In view of the importance of this single source of drag data, a curve fitting relationship employing

this data exclusively has been prepared by Karr.<sup>4</sup> The sphere drag bridging relationship thus developed is given by

$$C_D = C_{D_c} + e^{-E/a (Kn)^x} (C_{D_{FM}} - C_{D_c}) \quad (5)$$

where  $a = .499 \frac{8}{\pi}$  and where  $C_{D_c}$  and  $C_{D_{FM}}$  are the continuum and free molecule drag coefficient, respectively. The quantities  $E$  and  $x$  are parameters of the curve fit and  $Kn$  is the free stream Knudsen number.

The free molecule and continuum drag coefficients may be written as functions of speed ratio,  $S$ , and Mach number,  $M$ , given by<sup>4</sup>

$$C_{D_{FM}} (S \leq 1.25) = \frac{16}{3 \pi} \left( \frac{1}{S} + \frac{S}{5} - \frac{S^3}{70} \right) (1 + K) \quad (6)$$

$$C_{D_{FM}} (S \geq 1.25) = 2 \left( 1 + \frac{1}{S^2} - \frac{1}{45^4} \right) (1 + K) \quad (7)$$

$$C_{D_c} (M \geq 1.0) = .92 + .166/M - .366/M^3 \quad (8)$$

$$C_{D_c} (.1 < M \leq 1.0) = .403 - .142M^2 + .459M^4 \quad (9)$$

where

$$S = V / \sqrt{2 \frac{RT}{W}} \quad \text{and} \quad M = V / \sqrt{\gamma \frac{RT}{W}} \quad (10)$$

where  $\gamma$  is the ratio of specific heats of the gas, and  $(1 + K)$  in Equations 6 and 7 is a factor or order unity which is related to the gas-surface interaction. The least squares curve fit of the above relations to the data of Bailey and Hiatt has revealed that Equation 5 will fit the

data to an accuracy of about 5% (based on RMS value) for the following values of the parameters

$$x = .399 + .016 M \quad (11)$$

$$K = -.002438 - .01842697 M \quad (12)$$

$$E = .212 \quad (13)$$

The use of Equations 6 through 13 in the sphere drag bridging relation given in Equation 5 provides values of drag coefficients which are based on the most accurate and applicable information now available. In order to use this relationship in the drag equation, values must be available for the velocity  $V$ , temperature  $T$ , molecular weight  $W$ , and the Knudsen number,  $Kn$ . The velocity is a measured quantity while values for the others are obtained as discussed in the following.

#### Knudsen Number

Knudsen number is defined as the ratio of near free path,  $\ell$ , to the characteristic length of the object. We take the characteristic length to be the sphere diameter,  $d$ . Therefore,

$$Kn = \ell / d \quad (14)$$

The mean free path is inversely proportional to number density,  $n$ , for a simple gas (c.f. Ref. 5) and given by

$$\ell = (2 \pi n \sigma^2)^{-1} \quad (15)$$

where  $\sigma$  is the diameter of the gas molecules. Using the average molecular weight, we write the mean free path as a function of density

$$\ell = \left( 2 \pi \frac{\rho}{W/N_A} \sigma^2 \right)^{-1} \quad (16)$$

where  $N_A$  is the Avogadro constant. Using a value of  $\sigma = 3.72 \times 10^{-10} \text{ m}$  which is representative of air<sup>5</sup>, we obtain

$$Kn = 2.7 \times 10^{-9} \frac{W}{\rho d} \quad (17)$$

for  $\rho$  in units of  $\text{Kg/m}^3$  and  $d$  in meters.

In developing Equation 17, we have neglected the small effect temperature has on the value of  $\sigma$  and we have assumed the gas molecules each have a mass corresponding to the average molecular weight of the gas.

### Molecular Weight

A value of molecular weight is required for the Mach number, speed ratio, and Knudsen number expressions. (We assume  $\gamma = 1.4$ , independent of the molecular weight). The mean molecular weight is known to be a constant of 28.964 up to about 90 Km altitude. At that altitude, the heavier molecules begin to settle out causing a drop in molecular weight. Models of this molecular weight with altitude are provided in Ref. 6. Representative values of the variation is given by the following equation

$$W = 24.68 + .1235 z - .000874 z^2 \quad (18)$$

where  $z$  is the altitude. Equation 18 gives values of molecular weight with an accuracy of better than 1% in comparison with a nominal spring/fall values given in Ref. 6.

### Temperature and Density Iteration

The temperature at a given altitude is determined as stated in the introduction, by downward integration of the density profile. However, since the drag coefficient is a function of temperature (i.e., Mach number and speed ratio are inversely proportional to the square root of temperature),

values of temperature must be available before determination of density is made using the drag equation. Thus, we are lead to an iterative procedure for finding both density and temperature. The procedure is begun by assuming some initial temperature profile from which, given the unusual velocities, the Mach number and speed ratio are found. Once a density profile is obtained (to be discussed in the next paragraph) using the assumed temperature profile, a new temperature profile may be constructed. This process is repeated until the values of both temperature and density no longer change beyond a specified error limit.

Since the drag coefficient has been written as a function of density, the drag equation becomes of the following form

$$\text{Drag} = \frac{1}{2} \rho V^2 A C_{D_c} + e^{-b\rho^x} (C_{D_{FM}} - C_{D_c}) \quad (19)$$

where b is defined through Equation 17 and 5.

$$b = E/(2.7 \times 10^{-9} W/d)^x \quad (20)$$

Equation 19 is a nonlinear equation in the unknown density and must be solved using numerical procedures.

Solving for density from the drag equation of the form given in Equation 19 has two advantages. First, as already pointed out, the relationship for  $C_D$  represents recent, accurate drag measurements. Second, by solving Equation 19 for density directly, we eliminate the uncertainty of choosing a drag coefficient from a set of values tabulated as a function of Mach number and Reynold's number. Falling sphere experimenters effectively solve an equation like Equation 19 by iterating between tabulated  $C_D$  values and using the simple drag equation. The solution of Equation 19 is obtained

much faster and the solution is likely more accurate than that obtained in such iterative procedures.

### Application of the Proposed Method

The procedure outlined above was applied to sets of falling sphere data reported by Peterson, et al.<sup>7</sup> for measurements made over Kwajalein during 1963 and 1964. One of the reasons for using this data to illustrate the application of the proposed method of analysis is the importance of the results which were obtained in the original experiment. This set of data is of particular interest since it forms the basis for the density and temperature model in the 80 to 120 Km region for what is labeled "15<sup>0</sup>N, Annual" in the U. S. Standard Atmosphere Supplements, 1966.<sup>6</sup> A summary of the density results obtained by Peterson, et al.<sup>7</sup> are given in Figure 1 which is a copy of Figure 2.20 of Reference 6.

A second reason for using this particular set of data was the availability of the information required in our analysis. Through one of the original experimenters, K. McWatters,<sup>8</sup> we obtained the detailed computer output (a sample of which for one flight is given in Reference 7) for the falling sphere measurements made by the group. The data of interest is the density,  $\rho_o$ , temperature  $T_o$ , drag coefficient  $C_{Do}$ , Reynold's number  $R_{eo}$ , Mach number  $M_o$ , and velocity  $V_n$ , as a function of altitude,  $z_n$ , which resulted from their analysis of the falling sphere trajectory. Of these quantities, only velocity and altitude were measured where the subscript n is used to indicate this. The remaining quantities were deduced and we use the subscript o to indicate this. The measured drag force, however, can be found by taking the deduced density and the drag coefficient employed in obtaining that density, and substitute these values into the drag equation. Therefore,

$$(\text{Drag})_n = \frac{1}{2} \rho_o V_n^2 C_{D_o} A_n$$

where the area is based on 0.66 m sphere diameter. Thus, in this manner, the values of altitude, velocity, and drag force are obtained as measured in the original experiments. The accuracy of these measurements is expected to be at least 5%.

In order to begin the iteration for density and temperature, the data analysis requires that an initial temperature profile be given. Of all the temperatures given in this initial profile, the only one of importance is the one given at the altitude at which the downward integration is begun. For the Kwajalein data, the highest altitude for which data are available is 120 Km since data above 120 was considered too inaccurate. In our analysis we have taken the temperature at 120 Km to be 460<sup>o</sup>K which is based on the 15<sup>o</sup>N Annual model given in Reference 6. For comparison, Peterson, et al.<sup>7</sup> used a temperature value of 361<sup>o</sup>K at 120 Km which is based on the 1962 U. S. Standard Atmosphere.<sup>9</sup> The higher temperature was chosen in this work in view of the fact that the results obtained in the original analysis revealed that the temperatures were generally higher than the USSA 1962 at the high altitudes. The effect the choice of a 100<sup>o</sup>K higher temperature has on the final results will be discussed more in the conclusions.

#### Temperature Interpolation for the Descent Trajectory

At this point in the discussion, we describe another improvement to the data analysis which is applicable to the Kwajalein falling sphere data. Much of the data obtained over Kwajalein consists of two trajectories; ascent and descent. Soon after ejection of the sphere, the radar tracks the sphere during its ascent to apogee. This tracking begins usually near 100 Km and data is then terminated at 120 Km for accuracy reasons as discussed above. During the passage through apogee, the radars "lose" the

sphere. Also because of smoothness requirements, data processing during descent generally does not start again until about 100 Km. In the original analysis of this data by Peterson, et al.<sup>7</sup>, the ascent and descent trajectories were analyzed separately. That is, the downward integration required for temperature determination was begun again at the top of the descent trajectory with a temperature choice based on USSA 1962. The temperature thus chosen at the top of the descent trajectory is potentially erroneous, the effect of which will propagate two scale height down into the descent trajectory. We have developed a more accurate procedure for choosing the temperature value at the top of the descent trajectory which employs the ascent temperature values and an isentropic relationship. The ascent temperature values in the 100 Km region are considered to be more accurate than the higher altitude values since this corresponds to two scale heights below the 120 Km altitude where the temperature is taken arbitrarily to be 460°K.

The temperature determination procedure employed in the present analysis is as follows:

Step 1. Density profiles are determined for both the ascent and descent trajectories,  $\rho_A(z)$  and  $\rho_D(z)$ , respectively. The 15° N Annual model is used to give an initial temperature profile.

Step 2. A new ascent temperature profile,  $T_A(z)$ , is determined for the ascent data using the downward integration method.

Step 3. For the region of altitude for which both ascent and descent data points are available, an isentropic relationship is employed to find the temperature for the descent trajectory points,  $T_D(z)$ , given by

$$T_D(z) = T_A(z) \left( \rho_D(z) / \rho_A(z) \right)^{\gamma - 1}$$

where  $\gamma$  is the ratio of specific heats. In using this relationship, we are assuming that the densities which have been measured at the same altitude by the drag method are different due to an isentropic process. The sphere trajectory is such that at about 100 Km altitude, the ascent and descent trajectories are about 80 Km apart. Wave motion in this region of the atmosphere could then account for the differences in density which are seen. Over the length and time scales of interest here, the assumption that such processes are isentropic is reasonable.

Step 4. For the remaining altitude points in the descent trajectory, the temperatures are determined using the downward integration method.

Step 5. Based on the new temperature values, calculate new values of Mach number and drag coefficient to be employed in the determination of new density profiles. That is, start again at Step 1 above and continue the iteration procedure until convergence is reached in both temperature and density results.

The above procedure requires at Step 3 that at least one data point of the descent trajectory be at the same, or nearly the same, altitude as a point on the ascent trajectory. This requirement is met for six of the thirteen flights made over Kwajalein and reported in reference 7. Table I gives some of the characteristics of the flights studied in this work including the range of overlap for the six flights. Two of the six flights had only one point in common while flight # 13 was found to have 12 data points in common (data is provided approximately every kilometer, on the kilometer).

## Results

Density and temperature profiles were obtained by the methods described above for the six falling sphere flights over Kwajalein which had overlap in altitude coverage of the ascent and descent trajectories. The density profiles were compared with that published in the U. S. Standard Atmosphere 1962.<sup>9</sup> The ratio of the density found in this work to the USSA 1962 densities is shown for each of the six flights in Figures 3 through 8. Also contained in these figures are the temperature profiles obtained in the analysis. Table 1 lists the sounding number which was designated by the experimenters, the time and date of the flight, and the altitude range covered on the ascent and descent trajectories for the six flights analyzed.

The mean and standard deviation of the density and temperature profile ratios (with respect to the models indicated) are plotted in Figures 9 and 10, respectively. For the altitudes outside the region of overlap, six values were used in construction of the mean and standard deviation. For some altitudes within the overlap region, as many as 12 values were used.

## Discussion of Results

The summary of density results given in Figure 9 show a significant departure from that obtained in the original analysis of Peterson, et al. 1966. This departure is found to be primarily because of the incomplete information on drag coefficients available to the original experimenter at that time. The drag coefficient values employed in the present analysis are considerably more accurate and reveal a point of maximum departure from the 1962 standard at 105 Km rather than at 92 Km.

The temperature results given in Figure 10 show better agreement with the original analysis than does density. The departure at 120 Km is artificial since the choice of a temperature value at 120 Km is completely arbitrary. The departure in temperature between the present and original analysis at high altitudes is not the cause for the departure in density at these altitudes. In fact, if the value of temperature at 120 Km used by Peterson, et al. were to be employed in the present analysis, the departure in density results would be even greater than given in Figure 9. The colder temperatures used by Peterson, et al. would result in lower drag coefficients and therefore even higher densities would be obtained from the drag equation. The results we have obtained seem to clearly point towards the higher values of temperature at altitudes near 120 Km.

Table 1

Figure Number	Sounding Number	Time & Date of Flight	(GMT)	Range of Ascent Altitude	Range of Descent Altitude	Overla Range
3	2	0257	March 29, 1963	100-120	102-80	100-10
4	3	0328	June 18, 1963	99-120	102-80	99-10
5	8	1458	Nov. 14, 1963	104-120	109-80	104-10
6	12	1820	March 13, 1964	99-120	104-80	99-10
7	13	1125	May 12, 1964	96-120	107-80	96-10
8	14	0101	June 17, 1964	102-120	102-80	120

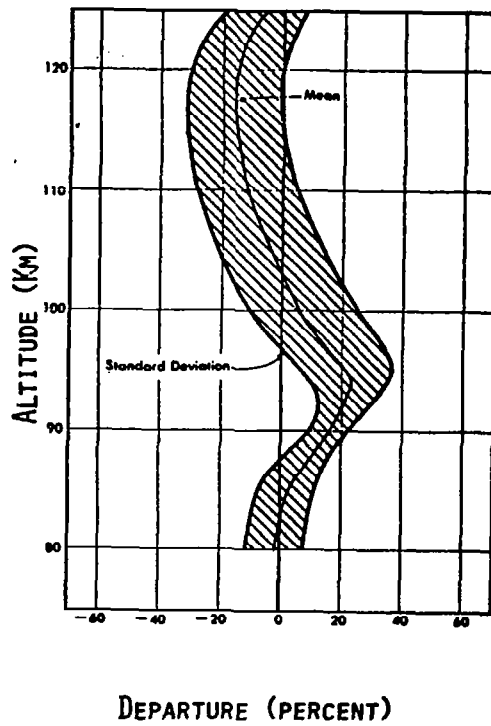


Fig. 1. Departure from standard atmosphere of the mean and standard deviations of 13 density measurements deduced in the original experiments at Kwajalein Island (plot is copied from Ref. 2).

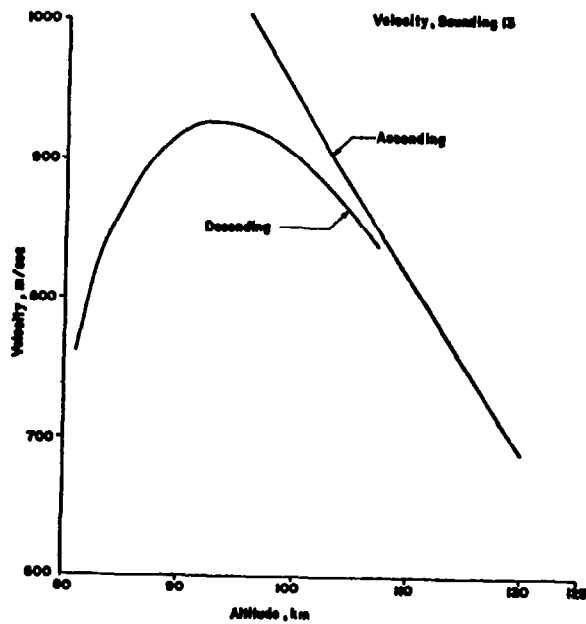


Fig. 2. Velocity-altitude history for falling sphere sounding 13 in which ascent and descent trajectory overlap.

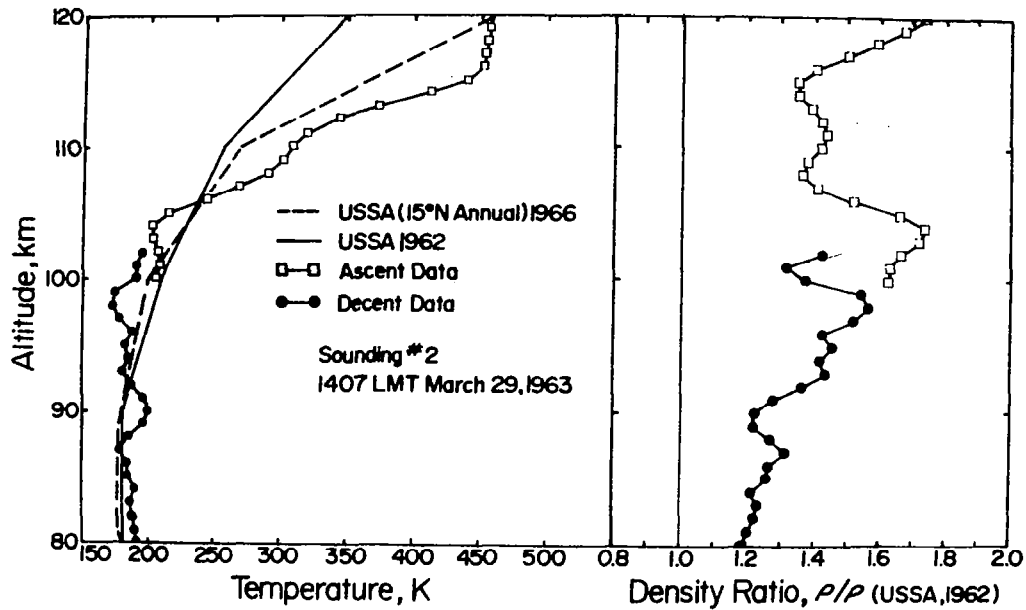


Figure 3. Temperature and Density Profiles Obtained from Sounding # 2.

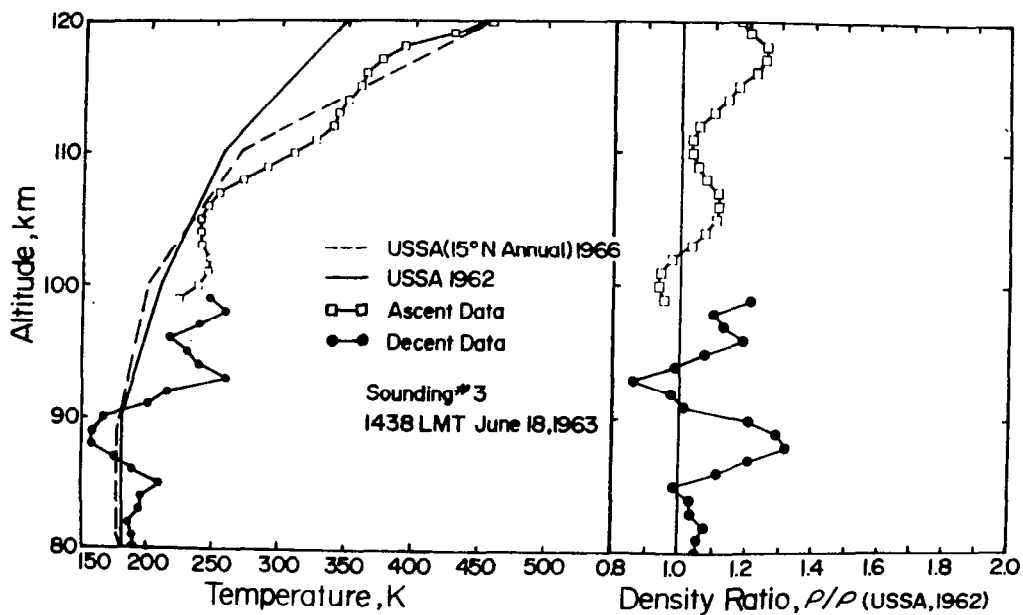


Figure 4. Temperature and Density Profiles Obtained from Sounding # 3.

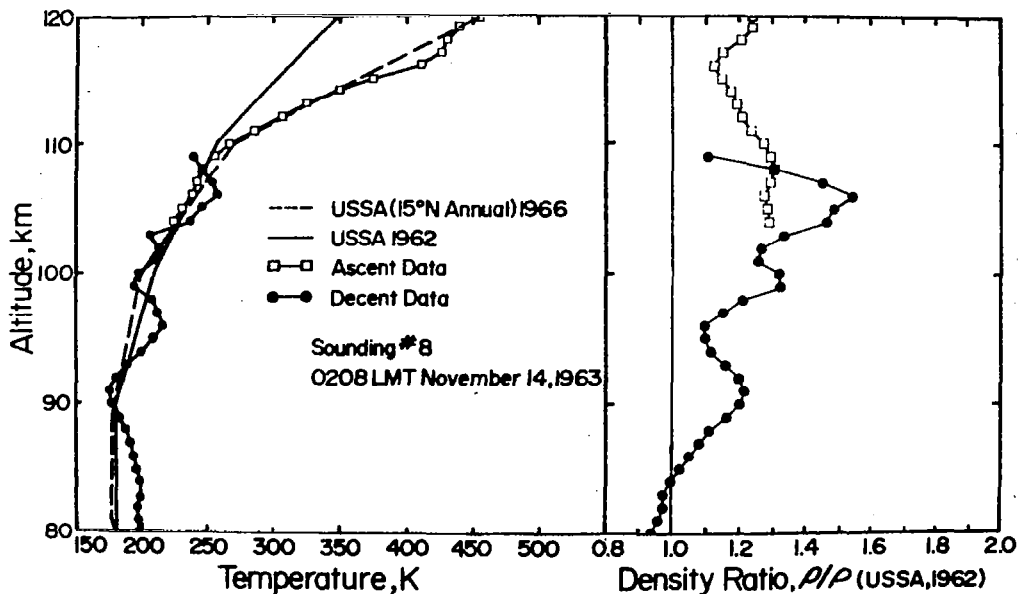


Figure 5. Temperature and Density Profiles Obtained from Sounding # 8.

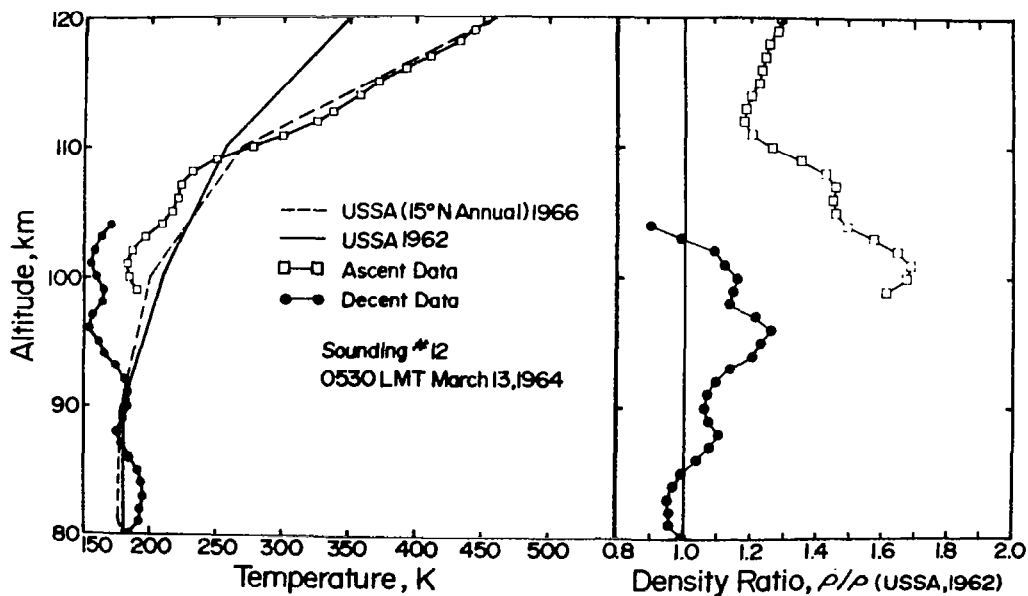


Figure 6. Temperature and Density Profiles Obtained from Sounding # 12.

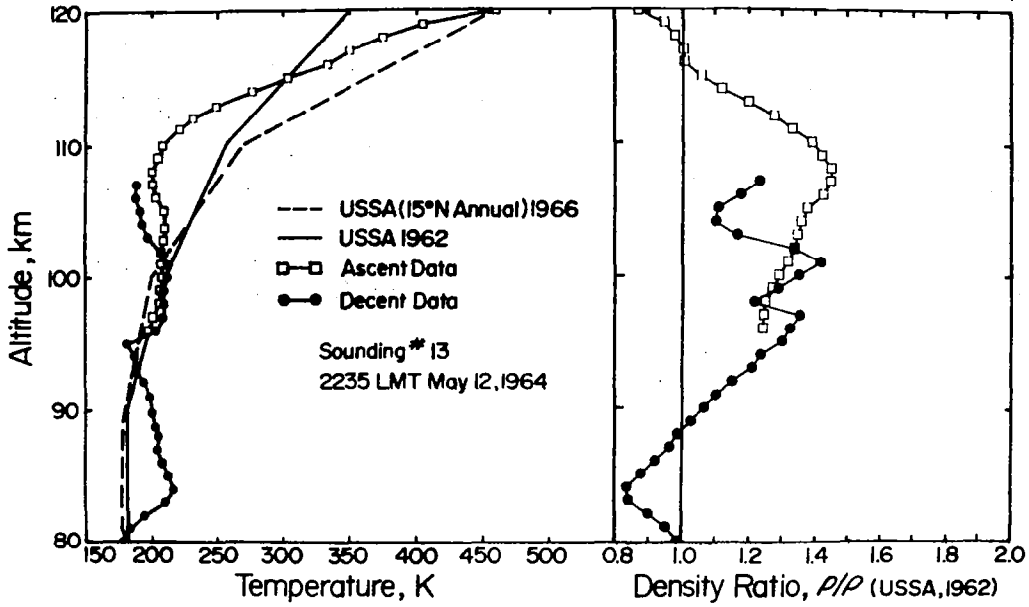


Figure 7. Temperature and Density Profiles Obtained from Sounding # 13.

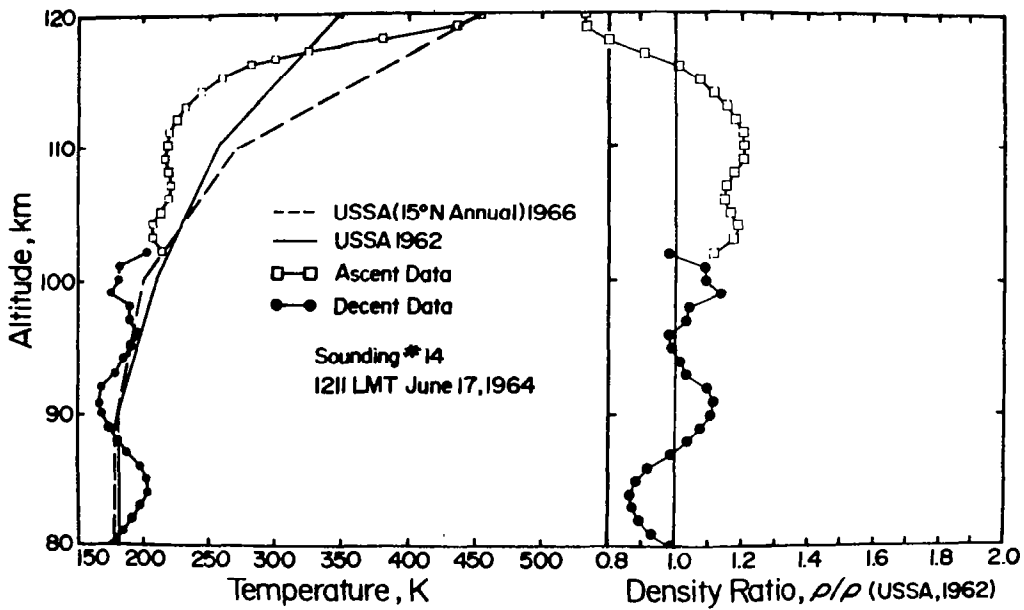


Figure 8. Temperature and Density Profiles Obtained from Sounding # 14.

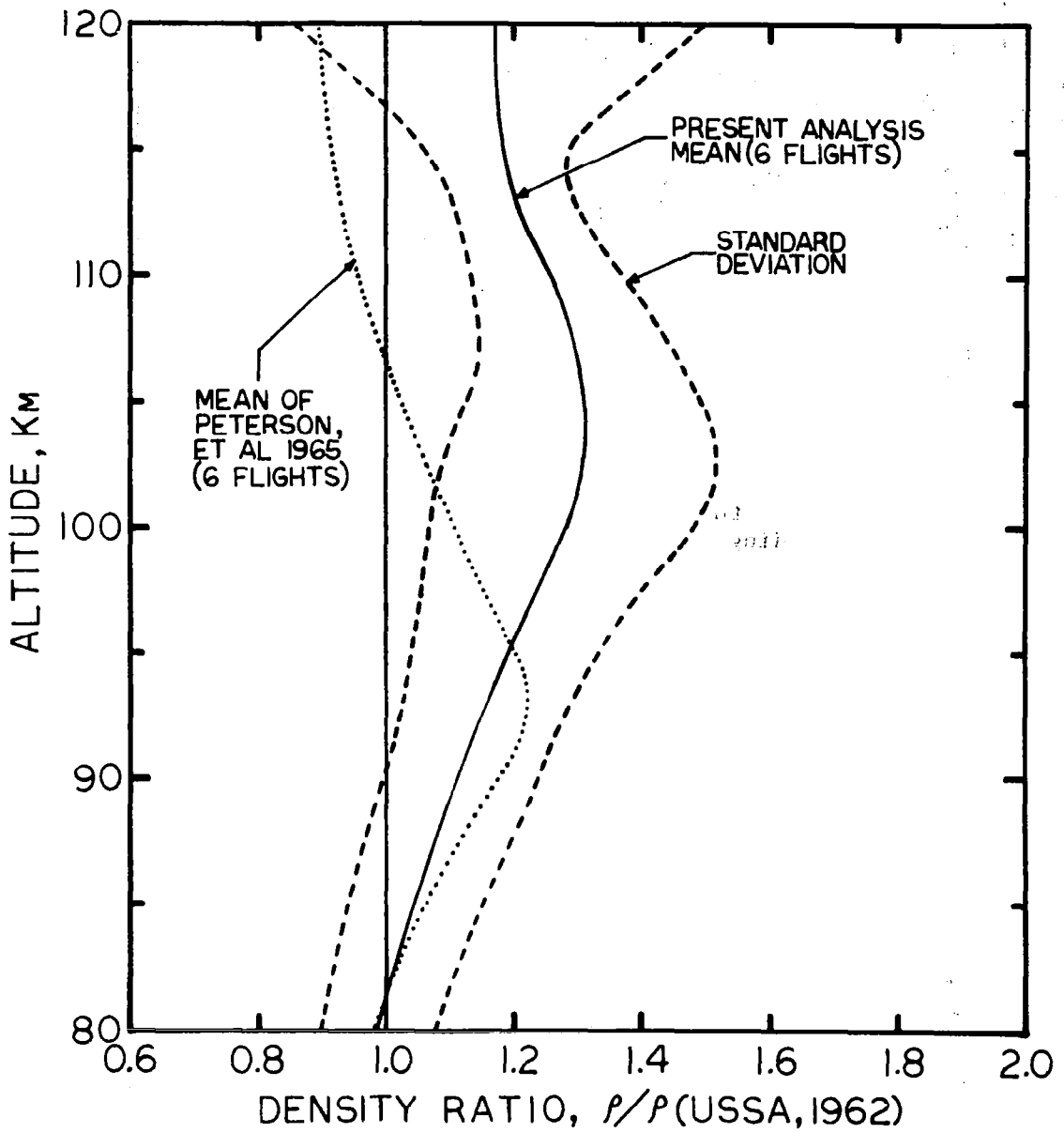


Figure 9. Mean and standard deviation of density results obtained in the present analysis for six falling sphere flights over Kwajalein. Mean of results from original analysis given for comparison.

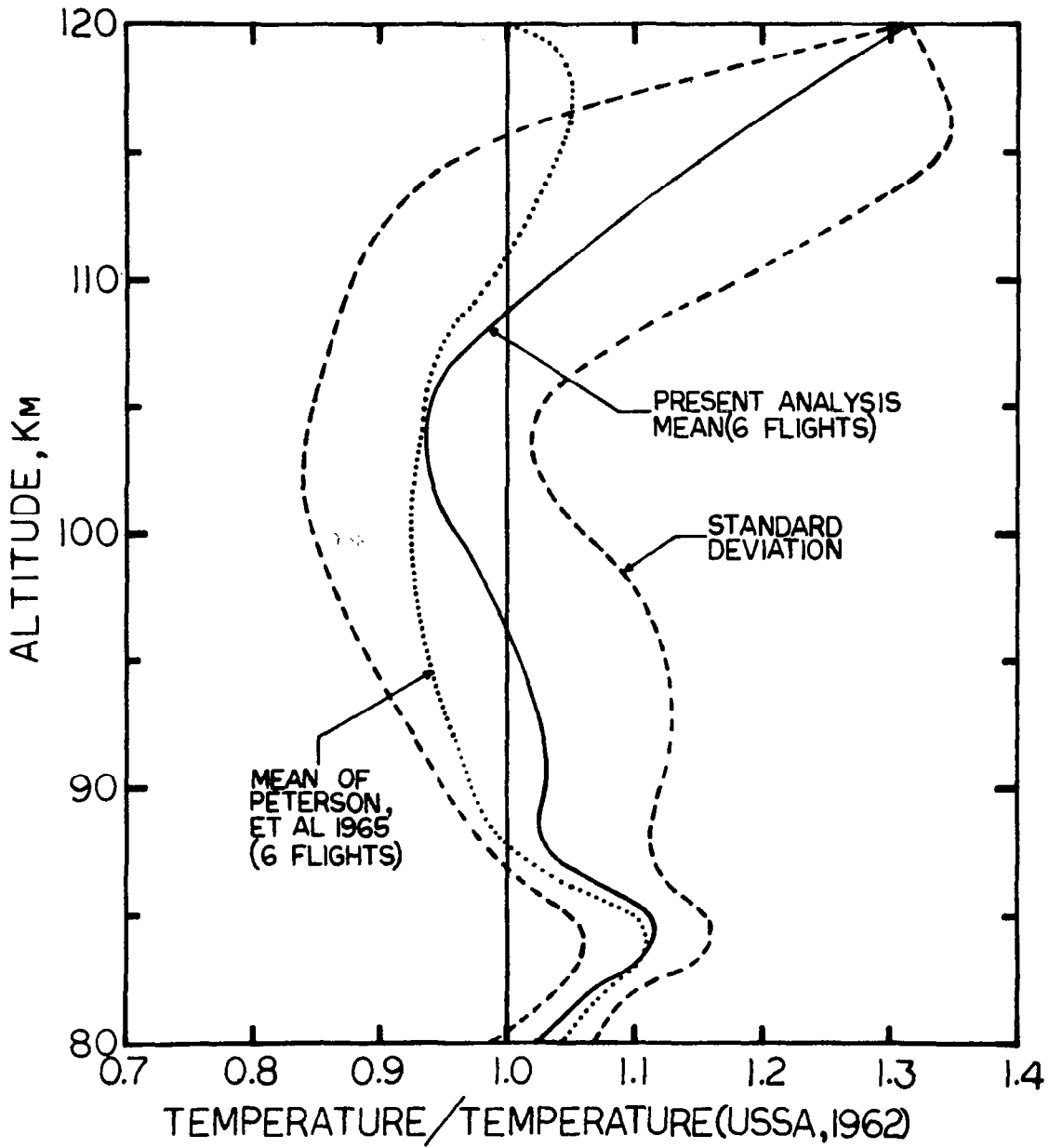


Figure 10. Mean and standard deviation of temperature results obtained in the present analysis for six falling sphere flights over Kwajalein. Mean of results from original analysis given for comparison.

## References

1. Bartman, Chaney, Jones, and Liu, "Upper Air Density and Temperature by the Falling Sphere Method," *Journal of Applied Physics*, 27, pp 706-712, July 1956.
2. Schaaf and Chambre, "Flow of Rarefied Gases," Section H of Princeton Series on High Speed Aerodynamics and Jet Propulsion, 1958, Princeton University Press.
3. Bailey, A. B. and Hiatt, J., "Free-Flight Measurements of Sphere Drag at Subsonic, Transonic, Supersonic and Hypersonic Speeds for Continuum Transition and Near-Free Molecular Flow Conditions," Arnold Engineering Development Center, Arnold Air Force Station, Tennessee, AEDC-TR-70-291, March 1971.
4. Karr, G. R., "A Sphere Drag Bridging Relationship in the Low Mach Number Transition Regime," Chapter 5 of this report.
5. Kennard, Earle H., Kinetic Theory of Gases, McGraw-Hill Book Co., 1938.
6. U. S. Standard Atmosphere Supplements, 1966, Superintendent of Documents, U. S. Government Printing Office, Washington, D. C.
7. Peterson, J. W., Hansen, W. H., McWatters, K.D., and Bonfanti, G., "Falling Sphere Measurements over Kwajalein," *Journal of Geophysical Research*, 70, 4477-4489, September 15, 1965.
8. McWatters, K. D., Private Communication.
9. Committee on Extension to the Standard Atmosphere, U. S. Standard Atmosphere, 1962, Superintendent of Documents, U. S. Government Printing Office, Washington, D. C.

## CHAPTER VII

### FREE MOLECULE DRAG AT SPEED RATIO LESS THAN UNITY

c. h.

v. p.

# Free Molecule Drag at Speed Ratio Less Than Unity

by

Gerald R. Karr  
Assistant Research Professor  
Mechanical Engineering Department  
The University of Alabama in Huntsville

This work concerns results obtained in the calculation of the drag force acting on objects which (1) have dimensions much less than the mean free path of the gas (Knudsen number much less than one) and (2) have velocity with respect to the gas which is much less than the thermal velocity of the gas (Speed ratio,  $S$ , much less than one). These conditions are characteristic of those experienced by certain aerosols and Brownian type particles which are suspended in a gas or which are forced to travel through a gas such as in separation processes.

The purpose of this work is to investigate the influence of two factors which enter the calculation of the free molecule drag force; (1) the shape of the object and (2) the gas surface interaction. Past investigations<sup>1,2,3</sup> have concentrated on the second of these factors while assuming the particles are perfectly spherical in shape. The gas surface interaction has generally been taken to be composed of a specular fraction and a second fraction which is purely diffusive (see, for example, Ref. 4) or a modified diffusive such as the elastic-diffusive reflection employed in Ref. 3. The form of the diffusive fraction of the reflected molecules has received considerable attention because comparison of sphere drag calculations with experiment lead to the conclusion that all the molecules must be diffusively reflected in order to explain the observed high drag coefficients at low speed ratios.

In the work reported in this paper, the drag coefficients for both specular and diffuse reflection were obtained for non-spherical objects in order to investigate the influence of shape at very low speed ratios.

The drag coefficients were obtained by employing the expression for force acting on an element of surface in a free molecule flow valid at any speed ratio and taking the component of that force which acts in the direction of the velocity vector. The drag component of force was divided into a part due to the momentum of impinging molecules,  $D_i$ , and a part produced by the reaction force of the molecules leaving the surface,  $D_r$ . Expressions for both specular  $D_r(\text{specular})$  and diffusive  $D_r(\text{diffusive})$  reflections were developed. The total drag force is then given by  $D = D_i + D_r$  for an element of surface at any angle with respect to the flow and any speed ratio. The expressions were then integrated over the surfaces of various shapes including oblate spheroids, cylinders with flat and spherical ends, and cones with flat ends. The drag force coefficients were obtained for these objects at low speed ratios for both specular and diffusive reflection. The total drag force acting on an object is written

$$D = D_i \left( 1 + \frac{D_r}{D_i} \right)$$

where the ratio  $D_r/D_i$  represents the effect of the reflection normalized with respect to the incident contribution. For a perfect sphere, for example, and for  $S \ll 1$

$$D_i(\text{sphere}) = \frac{8}{3} \rho \pi r^2 \sqrt{2\pi RT} V$$

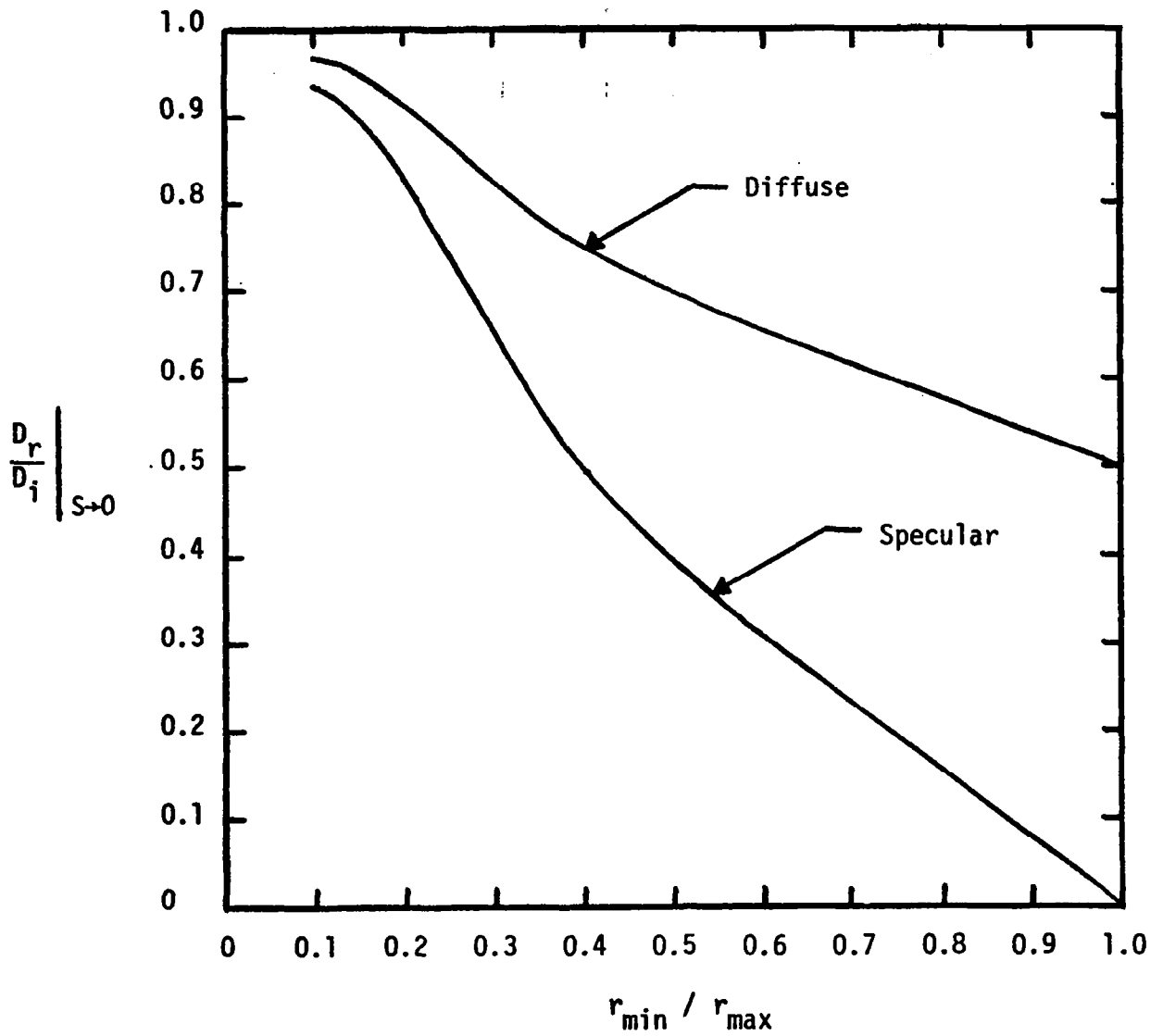
The attached figure presents examples of values of  $D_r/D_i$  for oblate spheroid shapes as a function of the minimum-to-maximum radius ratio.

The results show the sensitivity of the  $D_r/D_i$  to both the reflection characteristic and the object shape.

The results obtained in this work show that the magnitude of the force coefficient is strongly dependent upon the shape and orientation of the object for both specular and diffusive reflection. Since non-spherical aerosol or Brownian particles would present random orientation with respect to the velocity vector, the force coefficient for a given object would be an average value. The results obtained in this work provide the information needed to obtain the average force coefficient for various non-spherical shapes. One conclusion reached in this work is that both specular and diffuse reflections can produce high drag force coefficients at low speed ratios for non-spherical objects and neither should be excluded from consideration in such cases.

#### References

1. Epstein, P. S., Phys. Rev. 23, 710 (1924).
2. Millikan, R. A., Phys. Rev. 22, 1 (July 1923).
3. Mason, E. A. and Chapman, S. J., Chem. Phys., 36, 627 (1962).
4. Waldmann, Z., Naturforsch, 14a, 589 (1959).



$D_r/D_i$  ratio at low speed ratio for oblate spheroid shapes as a function of minimum-to-maximum radius for both specular and diffuse reflection models.

**CHAPTER VIII**

**RECOMMENDATIONS FOR FUTURE WORK**

## Proposal to Develop Zero-g Brownian Motion Experiments

by

G. R. Karr

Introduction

Robert Brown in 1828 is credited with establishing as an important phenomenon the observed irregular and perpetual motion of macroscopic particles suspended in gases or liquids. The theory of this motion, which has become known as Brownian motion, has received the attention of Einstein, van Smoluchowski, Langevin, Uhlenbeck and Ornstein, Chandrasekhar, and many others. The motion received much early interest because it has been established through the theory that Brownian motion is direct observation evidence of the molecular state of matter. For example, from observation of Brownian motion, one can measure Avogadro's number and this method was in fact considered to provide the most accurate measurement of this quantity in the early 1900's. The theory of Brownian motion establishes that the motion is described as a random process which is found to be a major step in the development of the field of study now called stochastic processes.

Experimental investigations of Brownian motion has not received the interest of physicists recently and modern interest in Brownian motion is primarily in the theory and its application. However, with the unique environment which will be provided by the Space Shuttle, the possibility now exists for performing experiments involving Brownian motion that could not be done in a one-g environment. It is proposed here to study possible experiments that may be performed in a zero-g environment which involve the observation of Brownian motion. It is proposed to assess the feasibility and importance of such experiments.

## The Theory of Brownian Motion

The currently accepted theory of Brownian motion was presented by Ornstein and Uhlenbeck in 1930. Beginning with the equation of motion of a Brownian particle (called the Langevin equation) we have

$$m \frac{d^2 x}{dt^2} = -m \beta v + F(t) \quad (1)$$

where  $\beta$  is a drag coefficient and where  $F(t)$  is a random forcing term characteristic of the Brownian motion. Ornstein and Uhlenbeck obtain the solution for the mean square displacement of the particle given by

$$\overline{s^2} = \frac{2 k T}{m \beta^2} (\beta t - 1 + e^{-\beta t}) \quad (2)$$

which has the limits for  $t$  large compared to  $\beta^{-1}$

$$\overline{s^2} = \frac{2 k T}{m \beta} t \quad (3)$$

which is the result obtained by Einstein and for  $t$  small compared to  $\beta^{-1}$  the result is

$$\overline{s^2} = \overline{u_0^2} t^2 \quad (4)$$

where  $u_0$  is the initial velocity of the particle.

Other quantities may also be calculated. For example, the mean square velocity of Brownian particles all starting at velocity  $u_0$  is

$$\overline{u^2} u_0 = \frac{k T}{m} + \left( u_0^2 - \frac{k T}{m} \right) e^{-2 \beta t} \quad (5)$$

and the velocity distribution function of the particles is given by

$$G(u_0, u, t) = \left( \frac{m}{2 \pi k T (1 - e^{-2 \beta t})} \right)^{1/2} \exp \left\{ \frac{m}{2kT} \frac{(u - u_0 e^{-\beta t})^2}{1 - e^{-\beta t}} \right\} \quad (6)$$

which shows that the particles eventually reach a Maxwell-Boltzmann distribution.

The above results are all for what is called a free particle. That is, the only forces acting on the Brownian particle are the drag term  $m\beta v$  and the random forcing term  $F(t)$ . For the case of Brownian motion in an external force field, such as gravity, theory is not so clear nor as complete as for the free Brownian motion. Uhlenbeck and Ornstein, for example, consider the Brownian motion of a particle which is bound in a harmonic force field at frequency  $\omega_0$ . Three cases result and the solutions for the mean square displacement under these conditions are provided.

Overdamped case;  $\beta \gg 2 \omega$

$$\overline{x^2} = \frac{kT}{m\omega^2} + \left( x_0^2 - \frac{kT}{m\omega^2} \right) e^{-\beta t} \left( \cosh \omega' t + \frac{\beta}{2\omega'} \sinh \omega' t \right)^2 \quad (7)$$

$$\text{where } \omega' = \frac{\beta^2}{4} - \omega^2$$

Critically damped case;  $\beta = 2 \omega$

$$\overline{x^2} = \frac{kT}{m\omega^2} + \left( x_0^2 - \frac{kT}{m\omega^2} \right) \left( 1 + \frac{\beta t}{2} \right)^2 e^{-\beta t} \quad (8)$$

Underdamped case;  $\beta < 2 \omega$

$$\overline{x^2} = \frac{kT}{m\omega^2} + \left( x_0^2 - \frac{kT}{m\omega^2} \right) e^{-\beta t} \left( \cos \omega_1 t + \frac{\beta}{2\omega_1} \sin \omega_1 t \right)^2 \quad (9)$$

$$\text{where } \omega_1^2 = \omega^2 - \frac{\beta^2}{4}$$

While Uhlenbeck and Ornstein obtained solutions for the harmonic forcing cases, the case for constant forcing has not been solved as completely.

For example, Wang and Uhlenbeck state in their 1945 paper that they have been unable to find the general solution for the constant force case. Solutions do exist, however, for the special case when the friction force is high and the observation time is large (i.e., for  $t \gg \beta^{-1}$ ). Chandrasekhar, for example, obtains the time varying distribution of Brownian particles in a gravity field and is able to show that the particles arrange themselves in a barometric distribution with respect to the gravity vector.

Solutions for other observables of Brownian motion in a constant force field are apparently not available. For example, the mean square displacement or the velocity distribution function in a gravity field were not found in the references cited. Part of this study will be directed toward a thorough investigation of the recent literature on this subject. From the literature that has been searched, however, it is apparent that Brownian motion in a gravity field will be much more complex than the free motion and that sensitive experiments in one-g would be strongly influenced by gravity.

### Zero-g Experiments

The zero-g environment offers at least three advantages in the performance of Brownian motion studies.

1. The theory of Brownian motion in zero-g is well established while the motion under gravity is difficult at best to interpret.
2. Convection currents can be minimized or eliminated in zero-g.
3. In zero-g, particles of larger sizes and masses can be employed in Brownian motion studies.

The purpose of the proposed work is to study possible Brownian motion experiments and to assess the value and feasibility of such experiments. While it is expected that other experiments will be proposed

and studied during this work, the following set of experiments have already received preliminary consideration and will be described briefly.

#### A. Particulate drag in the transition regime

As is well known, Brownian motion is observed in both liquids and gases. The drag or friction coefficient,  $\beta$ , in these media is, however, considerably different. The friction factor in a liquid for example is in the fluid dynamic flow regime called "Stokes flow" and is described as a highly-viscous flow. For a Brownian motion in a gas, however, the flow is free molecule if the mean free path of the molecules is large compared with the size of the particle. It is therefore proposed that a possible zero-g experiment is to vary the properties of the suspension medium or the particles, so as to obtain friction factor information in the transition flow regime between the Stokes regime and the free molecule regime. The proposed work would consist of determining the range of particle and medium properties that would be required to probe the transition regime. Also to be studied is the limits imposed on such an experiment by the one-g environment. The transition flow regime has proved very difficult to probe in ground-based experiments and becomes progressively more difficult as the speed is reduced. The experiments proposed here would provide data at the very low end of the velocity spectrum, a region for which little or no data now exists. This possibility of increasing the range of understanding of fluid dynamic drag appears to be of great value.

#### B. Gas surface interaction

Brownian motion observations provide an excellent basis for studying the interaction of molecules with surfaces. The motion is a direct consequence of the bombardment of the particle surface with

molecules of the surrounding medium. The free molecule regime is best for such observations since the motion is isolated from the effects of viscosity that occur in the Stokes flow regime. The proposed experiments would consist of (1) the preparation of particles of known composition and surface properties, (2) the preparations of gases of known composition and temperature, and (3) collection of data on the resultant mean displacement and velocity distribution to determine the friction factor  $\beta$ . The value of  $\beta$  determined in such an experiment can be directly related to the effect of the gas surface interaction. The data can then be correlated with respect to the gas and surface properties.

The physics of the gas surface interaction is not well understood at present and experimental data of the type proposed here would be valuable in identifying the important characteristics of the interaction. A factor of two variations in the friction coefficient,  $\beta$ , is theoretically possible due to the effect of the gas surface interaction. Ground based experiments such as the oil drop experiment do not have the sensitivity needed to determine these effects.

### C. Verification of Brownian Motion Theory

The Brownian motion theory proposed by Uhlenbeck and Ornstein is the currently accepted theory of the motion. The theory of Einstein and Smoluchowski is found to be the limiting case of the Uhlenbeck and Ornstein theory for large times ( $t \gg \beta^{-1}$ ) for the free particle case. Edward Nelson further proposes that the Einstein-Smoluchowski theory is also limited to the case of large friction ( $\beta$  large) and points to experimental results of Kappler and of Barnes and Silverman to show that, for the harmonic forcing case, the Einstein-Smoluchowski approximation is invalid for the underdamped case even for  $t \gg \beta^{-1}$ . For the same reasons as mentioned above, the presence of the one-g field requires

that particles be small and light. For such cases then, it is difficult to probe the Brownian motion for short times ( $t \lesssim \beta^{-1}$ ). The motion for short times can be used to verify the Uhlenbeck-Ornstein theory. The results for  $t \gg \beta^{-1}$  are the same for both the Uhlenbeck-Ornstein and the Einstein-Smoluchowski theories and thus such results can not be used to distinguish the theories. Due to the difficulty in making measurements in the short time on earth, there appears to be little, if any, experimental verification of the Uhlenbeck-Ornstein theory. It is, therefore, proposed that since the zero-g environment offers the opportunity to adjust the size of  $\beta$  over a wide range, a properly designed Brownian motion experiment in space would allow for the verification of theory of Brownian motion. The proposed work will seek to establish the conditions required to perform such an experiment.

#### Proposed Work

The three experiments proposed above are clearly of great value and preliminary study indicates that they are also feasible. During the proposed study, these experiments and others will be considered in detail to determine the value of the experiment, the reasons that zero-g are required, and the feasibility of performing the experiment. Extensive literature searches and personal contacts will be made to ascertain the state-of-the-art knowledge of Brownian motion theory, motion experiments, friction coefficients, gas-surface interaction, etc. Experimental techniques will be surveyed and recommendations made for space experiments. It is also expected that preliminary experimental development will be undertaken to test observation methods, data collection methods, and data analysis techniques.

## References

Edward Nelson, Dynamical Theories of Brownian Motion, Mathematical Notes, Princeton University Press, 1967.

Nelson Wax, Editor, Selected Papers on Noise and Stochastic Processes, Dover Publication, 1954. This book contains copies of the following papers:

Chandrasekhar, S., "Stochastic Problems in Physics and Astronomy," Rev. of Mod. Physics, Vol. 15, No. 1, 1943.

Uhlenbeck, G. E. and Ornstein, L. S., "On the Theory of the Brownian Motion," Physical Review, Vol. 36, No. 3, 1930.

Ming Chen Wang and Uhlenbeck, G. G., "On the Theory of the Brownian Motion II," Rev. of Mod. Physics, Vol. 17, No. 2 and 3, 1945.

Benjamin G. Levich, Theoretical Physics, Vol. 2, John Wiley & Sons, 1971.

Albert Einstein, Investigations on the Theory of the Brownian Movement, Dover, 1956. This book contains 5 papers by Einstein between 1905 and 1908, translated by Cowper and edited by Fürth.

## An Experiment Using the Molecular Beam Apparatus Proposed for Space Shuttle

Title: Aerodynamic Force Measurements in Space

Principal Investigator: Dr. Gerald R. Karr, The University of Alabama in Huntsville, Huntsville, Alabama.

### Summary of Proposed Work

The feasibility is to be determined of employing the satellite orbit environment in the measurement of forces resulting from the interaction of atmospheric gas with solid surfaces at satellite velocities. To be considered is an experiment designed to measure the aerodynamic forces acting on surfaces exposed to the high-velocity, low-density gas flow which is generated as a satellite travels through the upper atmosphere. In particular, the use of the proposed Molecular Beam Laboratory will be considered for providing the required beam definition and orientation. Engineering and scientific gains would be generated by the results of this experiment which utilizes an aspect of the orbital flight environment not easily reproduced in ground based facilities. The study would evaluate means for measuring the aerodynamic forces on a selection of surfaces having a broad range of material and physical properties. The study would determine the desirable number of surface materials, the range of surface temperatures, the range in degree of surface contamination, the number of surface coatings, and the angles of attack to be tested in the proposed experiment. Finally, the feasibility would be determined of correlating the force measurements with changes in gas properties.

### Justification

The determination of the feasibility of the proposed experiment is desirable in view of the potential benefits the experiment would provide.

At present, satellite aerodynamic properties cannot be predicted accurately because of the lack of information the proposed experiment could provide. Analytic studies reveal that satellite aerodynamic properties are a strong function of the character of the force caused by the gas surface interaction. The gas surface interaction, in turn, is expected to be a strong function of surface properties and surface orientation. The design of satellites to take advantage of (or to reduce) the aerodynamic forces and torques has not been possible because of the lack of information on the forces caused by the gas surface interaction. Knowledge of the character of the surface forces and the major influences on these forces is necessary to the design of satellites to have specified aerodynamic drag, lift, and torque characteristics. Such knowledge is also needed in order to interpret the dynamic response of satellites in the atmosphere as is done in the determination of atmospheric density from satellite drag measurements.

In addition to the engineering information provided by the proposed experiment, the results would also contribute to the scientific knowledge of the gas surface interaction at satellite velocities. The expected results would compliment both orbital and ground-based molecular beam studies which provide force information indirectly. The proposed experiment would then serve to guide future investigations into the more subtle details of the interaction.

Finally, the study of the feasibility of the proposed experiment is justified on the basis that the experiment may be a relatively inexpensive method of obtaining valuable information. Consequently, the experiment could require few equipment components with low development cost and short development time. The information gained would be of immediate engineering value and would be a valuable complement for future gas-surface experiments.

## Method

The objective of this study is to determine the feasibility of performing a space experiment to measure the aerodynamic forces on surfaces as a function of gas and surface properties and surface orientation. The study is divided into three areas: (a) Methods of making measurements, (b) Selection of surfaces and surface conditions, and (c) Correlation of results with gas properties.

### (a) Measurement Techniques

The feasibility of making the measurements required will be investigated taking into consideration the expected low level of force and the perturbing influences of environmental factors. To be considered is the feasibility of the aerodynamic forces acting on flat or shaped surface samples exposed to the gas flow generated by the motion of the satellite through the atmosphere. The perturbing influence of molecules reflected from the satellite may require that the surface samples be extended on a boom ahead of the vehicle. Methods will be evaluated for measuring the forces, orienting the surface samples, and changing the surface properties.

The accuracy of the proposed measurements is to be evaluated considering perturbing environmental influences such as upper atmospheric wind and density fluctuations. Methods of calibration and monitoring of the environment will be considered as means of increasing the accuracy of the proposed experiment.

### (b) Selection of Surfaces

The selection of surfaces to be tested in the proposed experiment will consider the need to reduce satellite payload weight and volume while yielding results of the widest possible interest. The selection of surfaces will be on the basis of providing information of the

many factors thought to influence the forces caused by the gas surface interaction. Among the factors of interest are the influence of surface material, surface temperature, surface roughness, surface coatings, surface contaminants, and surface angle-of-attack to the flow. The feasibility study would establish a series of experiments which best isolate the influence of the individual factors. The surfaces selected will span those used in satellite construction so as to provide engineering information for future design.

(c) Measurement of the Influence of Gas Properties

Since the gas surface interaction is influenced by both the surface properties and the gas properties, the feasibility is considered of determining the influence of the gas properties on the surface forces. The upper atmospheric gas composition, temperature, and degree of ionization are a strong function of altitude, geocentric latitude and longitude, and time. To be investigated is the possible correlation of the measured forces with the changes in gas properties that occur naturally over the orbit. The feasibility will be studied of identifying the gas-property influences on the forces caused by the gas surface interaction. Study will be made of the orbital parameters which provide the best conditions for the experiment.

Personnel

The principal investigator of the proposed study is Dr. G. R. Karr (resume attached) who has done considerable work on the theory of the gas surface interaction and satellite aerodynamics. Since Dr. Karr has primarily theoretical experience and capability, there is a recognized need for cooperation with personnel who have experimental capability and experience. In view of the good working relationship which exists between Dr. Karr, The University of Alabama in Huntsville, and NASA Marshall Space Flight

Center, Huntsville, it is proposed that the theoretical expertise of Dr. Karr be complemented with the experimental expertise of MSFC personnel such as Dr. P. Peters (a surface physicist) and/or Dr. R. Smith (an atmospheric physicist) both of the Space Science Laboratory at MSFC.

APPENDIX

Listing of computer programs developed and employed under NASA Contract  
Number NAS8-28248.

<u>Program Name</u>	<u>Page</u>
LESQA	106
RHORAT	111
AFILIP-HIGH CM	119
AFILIP-LOW CM	123
CDCLEV	127
CFEVAL	130
RUFSPH	133
CLELAN	137

## PROGRAM LESQA

This is a computer program which analyzes density, temperature, velocity and altitude measurements from falling sphere experiments. Also in the input data are the densities and drag coefficients employed by the original experimenters so that acceleration data can also be deduced. Both ascent and descent data are employed. The data are employed in an orthogonal curve fitting routine so that ascent and descent data can be correlated at equivalent altitudes. Speed ratio effects, molecular weight changes and drag coefficient variations are all taken into consideration. A density is determined which best represents the data based on the measured properties and those predicted by theory. A density profile is thus determined using both ascent and descent information.

```

XXF(S)= .399+.016*S
GSIF(S) = .9975617977-.018426966*S
DIMENSION C3D(900),C3A(900),RHO(900),CDCD(900),DACHD(900),CDFMD(90
10),SRD(900),CDCA(900),DACHA(900),CDFMA(900),SRA(900),VRATIO(900)
DIMENSION VAOR(900),VDOR(900)
DIMENSION WVA(900),WVD(900),CVA(900),CVD(900),ALPHVA(900),BETVA(90
10),BETVD(900),ALPHVD(900)
DIMENSION AT(900),TEMP(900),WT(900),CT(900),ALPHAT(900),BETAT(900)
1,TOR(900)
DIMENSION WD(900)
DIMENSION ALT(900),YAOK(900),YDOR(900)
DIMENSION WA(900),CA(900),ALPHAA(900),BETAA(900),T1(900),T2(900),
1T3(900),YA(900),YD(900),CD(900),ALPHAD(900),BETAD(900),BD(900),BA
1(900)
DIMENSION AA(900),RHOA(900),CDA(900),RHOD(900),CDD(900),AD(900),
1TEMPA(900),TEMPO(900),VA(900),VD(900)
10 READ (5,302) (SA)
302 FORMAT (I3)
READ(5,250)(C3,E)
READ(5,301)(MA,MD,N,ALTM)
READ(5,300)(AA(I),RHOA(I),TEMPA(I),CDA(I),VA(I),I=1,MA)
READ(5,300)(AD(I),RHOD(I),TEMPO(I),CDD(I),VD(I),I=1,MD)
WRITE(6,251)(C3,E)
WRITE(6,304)MA,MD,N,ALTM
WRITE(6,303)(AA(I),RHOA(I),TEMPA(I),CDA(I),VA(I),I=1,MA)
WRITE(6,303)(AD(I),RHOD(I),TEMPO(I),CDD(I),VD(I),I=1,MD)
304 FORMAT (//3HMA=,I4,3HMD=,I4,3HN=,I4,5HALTM=,E10.5)
303 FORMAT (4X,F8.4,2X,E8.4,2X,F8.4,2X,F8.4,2X,F9.4/)
GAMMA=1.4
PI=3.141592653
CONVSM=(GAMMA*.5)**.5
DO 80 I=1,MA
AT(I)=AA(I)
80 TEMP(I)=TEMPA(I)
DO 81 I=1,MD
AT(MA+I)=AD(I)
81 TEMP(MA+I)=TEMPO(I)
MT=MA+MD
300 FORMAT (F7.3,E6.3,F8.4,F5.3,F8.2)
301 FORMAT(3I3,F6.2)
DO 70 I=1,MA
70 WA(I)=1.0
DO 71 I=1,MD
71 WD(I)=1.0
WRITE (6,305) SA
305 FORMAT (4X, 17HSOUNDING NUMBER =,I3/)
WRITE(6,201)
DO 2 I=1,MD
YID=RHOD(I)*CDD(I)
SXD=SXD+AD(I)
WRITE(6,100)AD(I),YID
Y=ALOG(RHOD(I)*CDD(I))
YD(I)=Y

```

```

2  CONTINUE
  WRITE(6,200)
  DO 1 I=1,MA
  YIA=RHOA(I)*CDA(I)
  Y=ALOG(RHOA(I)*CDA(I))
  YA(I)=Y
  WRITE(6,100)AA(I),YIA
1  CONTINUE
  WRITE(6,200)
  DO 60 I=1,MA
60  WRITE(6,100)AA(I),YA(I)
  WRITE(6,201)
  DO 61 I=1,MD
61  WRITE(6,100)AD(I),YD(I)
  N=61
  DO 30 K=1,N
30  ALT(K)=ALTM+.5*(K-1)+10.0
  LT=0
  JT=0
  KFT=3
  KT=3
  KD=2
  KA=2
  KFA=2
  KFU=2
  KCA=2
  KCU=2
  LA=0
  LD=0
  JA=0
  JD=0
  KVA=3
  LVA=0
  LVD=0
  KVD=3
  JVA=0
  JVD=0
  KFVA=3
  KFVD=3
  CALL ORTHLS(AT,TEMP,WT,MT,LT,JT,CT,ALPHAT,BETAT,KT,T1,T2,T3,IND1T
1)
  CALL ORTHLS(AA,YA,WA,MA,LA,JA,CA,ALPHAA,BETAA,KA,T1,T2,T3,IND1A)
  CALL ORTHLS(AD,YD,WD,MD,LD,JD,CD,ALPHAD,BETAD,KD,T1,T2,T3,IND1D)
  CALL ORTHLS(AA,VA,WVA,MA,LVA,JVA,CVA,ALPHVA,BETVA,KVA,T1,T2,T3,IN
1D1VA)
  CALL ORTHLS(AD,VD,WVD,MD,LVD,JVD,CVD,ALPHVD,BETVD,KVD,T1,T2,T3,IND
11VD)
  II=0
  WRITE(6,103)IND1VA,II,CVA(1),(II,CVA(II+1),ALPHVA(II),BETVA(II),
1II=1,KVA)
  II=0
  WRITE(6,103)IND1VD,II,CVD(1),(II,CVD(II+1),ALPHVD(II),BETVD(II),
1II=1,KVD)
  II=0
  WRITE(6,103)IND1A,II,CA(1),(II,CA(II+1),ALPHAA(II),BETAA(II),II=1,
1KA)
  II=0

```

```

WRITE(6,103)IND1D,II,CD(1),(II,CD(II+1),ALPHAD(II),BETAD(II),II=1,
1KD)
II=0
WRITE(6,103)IND1T,II,CT(1),(II,CT(II+1),ALPHAT(II),BETAT(II),II=1
1,KT)
103 FORMAT(//I3//2X,I4,2X,E20.7/(2X,I4,2X,3E20.7))
CALL COEFS (JA,CA,ALPHAA,BETAA,KCA,BA,T1,T2,T3,IND2A)
CALL COEFS (JD,CD,ALPHAD,BETAD,KCD,BD,T1,T2,T3,IND2D)
CALL FITY(ALT,N,JA,CA,ALPHAA,BETAA,KFA,YAOR,T1,T2,IND3A)
CALL FITY(ALT,N,JD,CD,ALPHAD,BETAD,KFD,YDOR,T1,T2,IND3D)
CALL FITY(ALT,N,JT,CT,ALPHAT,BETAT,KFT,TOR,T1,T2,IND3T)
CALL FITY(ALT,N,JVA,CVA,ALPHVA,RETVA,KFVA,VAOR,T1,T2,IND3VA)
CALL FITY(ALT,N,JVD,CVD,ALPHVD,BETVD,KFVD,VDOR,T1,T2,IND3VD)
WRITE(6,500)(K,ALT(K),TOR(K),VAOR(K),VDOR(K),K=1,N)
500 FORMAT(//3X,1HK,5X,6HALT(K),8X,6HTOR(K),8X,7HVAOR(K)8X,7HVDOR(K),/
1(2X,I3,F10.4,3E15.6))
WRITE(6,450)(I,BA(I),I=1,KCA)
WRITE(6,451)(I,BD(I),I=1,KCD)
450 FORMAT(//4X,1H1,15X,5HBA(I),/(2X,I5,3X,E20.7))
451 FORMAT(//4X,1H1,15X,5HBD(I),/(2X,I5,3X,E20.7))
WRITE(6,202)
DO 3 I=1,N
EANM=24.68+.1235*ALT(I)-.000875*ALT(I)*ALT(I)
RG=8314.34/EANM
SRD(I)=VDOR(I)/(2.*RG*TOR(I))**.5
IF (SRD(I)-1.25)195,195,196
195 S=SRD(I)
CMD = S/CONVSM
GSI = GSIF(CMD)
CDFMD(I) =(2./(PI**.5))*(8./(3.*S)+8.*S/15.-8.*S*S*S/210.)*GSI
GO TO 197
196 S=SRD(I)
CMD = S/CONVSM
GSI = GSIF(CMD)
SI2=1./(S*S)
SI4=SI2*SI2
CDFMD(I)=2.*(1.+SI2-.25*SI4)*GSI
197 DACHD(I)=SRD(I)/CONVSM
DM=DACHD(I)
CDCA(I)=.92+.1660714/DM-.3660714/(DM*DM*DM)
VRATIO(I)=VAOR(I)/VDOR(I)
SRA(I)=VAOR(I)/(2.*RG*TOR(I))**.5
IF (SRA(I)-1.25) 95,95,96
95 S=SRA(I)
CMA = S/CONVSM
GSI = GSIF(CMA)
CDFMA(I) =(2./(PI**.5))*(8./(3.*S)+8.*S/15.-8.*S*S*S/210.)*GSI
GO TO 97
96 S=SRA(I)
CMA = S/CONVSM
GSI = GSIF(CMA)
SI2=1./(S*S)
SI4=SI2*SI2
CDFMA(I)=2.*(1.+SI2-.25*SI4)*GSI
97 DACHA(I)=SRA(I)/CONVSM
DM=DACHA(I)
CDCA(I)=.92+.1660714/DM-.3660714/(DM*DM*DM)

```

```

RHOCDA=EXP(YAOR(I))
RHOCDD=EXP(YDOR(I))
DENOM=CDCA(I)*CDFMD(I)-CDCD(I)*CDFMA(I)
RHO(I)=(RHOCDA*(CDFMD(I)-CDCD(I))-RHOCDD*(CDFMA(I)-CDCA(I)))/DENOM
RHOIN=1./RHO(I)
XX=(RHOCDA*RHOIN-CDCA(I))/(CDFMA(I)-CDCA(I))
IF(XX)77,79,79
77 C3A(I)=-1.
GO TO 78
79 X = XXF(CMA)
C3A(I)=- (RHOIN**X )*ALOG(XX)
78 XY=(RHOCDD*RHOIN-CDCD(I))/(CDFMD(I)-CDCD(I))
IF(XY) 87,89,89
87 C3D(I)=-1.
GO TO 88
89 X = XXF(CMD)
C3D(I)=- (RHOIN**X )*ALOG(XY)
88 AOV RD=RHOCDA/RHOCDD
FMRA=CDFMA(I)/CDFMD(I)
CONRA=CDCA(I)/CDCD(I)
TMIN=((1.-AOV RD)/(AOV RD/(VDOR(I)**2.)-1./(VAOR(I)**2.)))/(2.*PG)
WRITE(6,102)ALT(I),YAOR(I),RHOCDA,YDOR(I),RHOCDD,FMRA,AOV RD,CONRA,
1TMIN
3 CONTINUE
WRITE(6,333)(ALT(I),SRA(I),CDCA(I),CDFMA(I),DACHA(I),I=1,N)
WRITE(6,334)(ALT(I),SRD(I),CDCD(I),CDFMD(I),DACHD(I),I=1,N)
WRITE(6,335)(ALT(I),C3A(I),C3D(I),VRATIO(I),RHO(I),I=1,N)
333 FORMAT(//4X,3HALT,9X,3HSRA,9X,4HCDC A,9X,5HCDFMA,8X,5HDACHA,/(2X,F1
10.4,4E13.5))
334 FORMAT(//4X,3HALT,10X,3HSRD,10X,4HCDCD,9X,5HCDFMD,8X,5HDACHD,/(2X,
1F10.4,4E13.5))
335 FORMAT(//4X,3HALT,10X,3HC3A,10X,3HC3D,8X,6HVRATIO,8X,3HRHO,/(2X,F1
10.6,4E13.5))
GO TO 10
100 FORMAT(2X,F10.4,2X,E12.6)
102 FORMAT (2X,F10.4,8E14.6)
200 FORMAT(///5X,5HAA(I),10X,3HYIA//)
201 FORMAT(///5X,5HAD(I),10X,3HYID//)
202 FOKMAT(///6X,3HALT,12X,2HYA,8X,6HRHOCDA,10X,2HYD,10X,6HRHOCDD,8X,4
1HFMR A,10X,5HAOVRD,9X,5HCONRA)
250 FORMAT(2E20.10)
251 FORMAT(//,4X,3HC3=,E20.10,4X,2HF=,E20.10)
END

```

## PROGRAM RHORAT

This program takes falling sphere data and performs the usual analysis to determine the temperature and density profiles. The data in the region of overlap of the ascent and descent trajectories is treated as if the atmosphere were influenced by isentropic waves. Thus, differences in density at the same altitude will result in differences in temperature at that altitude according to the isentropic relations.

The program also inputs various standard atmospheres so that ratios of the measured density and temperature can be readily compared to the standard values.

```

XXF(S) = .399+.016*S
GSIF(S) = .9975617977-.018426966*S
EANMF(G)=24.68+.1235*G-.000874*G*G
PARAMETER NPP=200
DIMENSION M(500),NAD(500),NAA(500),TU(500),TU2(500),TME(500),
ISIG(500),PU(500),PU2(500),PME(500),SIP(500),TMSR(500),SISR(500)
DIMENSION RHDD(100),RAISO(100),TRA(100),CISO(100)
DIMENSION TTA(NPP),WTA(NPP),CTA(NPP),APTTA(NPP),BETTA(NPP)
DIMENSION GR(100),GRA(100),ALPHG(100),BETAG(100),GRD(100),CG(100)
DIMENSION TINA(NPP),TIND(NPP),THA(NPP),THD(NPP)
DIMENSION SRA(NPP),CDFMA(NPP),DACHA(NPP),CDCA(NPP),SRD(NPP),CDFMD
1(NPP),DACHD(NPP),CDCD(NPP)
DIMENSION AA(NPP),RHOA(NPP),CDA(NPP),RHOD(NPP),CDD(NPP),AD(NPP),
ITEMPA(NPP),TEMPO(NPP),VA(NPP),VD(NPP),
IRHOGA(100),NAN(100),RHORA(100), CDGA(100),CDRA(100),RHOGD(100),NDN
1(100),RHORD(100),CDGD(100),CDRD(100)
DIMENSION RHLS(NPP),RHLSA(NPP),RHLSD(NPP)
DIMENSION RHOSA(NPP),RHOSD(NPP)
DIMENSION ALS(NPP),RHOS(NPP),TES(NPP),T1(NPP),T2(NPP),T3(NPP),FPS(
1NPP),SMOL(NPP),W(NPP),CS(NPP),ALPS(NPP),BETS(NPP)
DIMENSION AT(NPP)
1,XA(NPP),XD(NPP),C3A(NPP),C3D(NPP)
1,RHA(NPP),CRA(NPP),APA(NPP),BEA(NPP),RHD(NPP),TEMAD(100)
1,TTA(NPP),TTD(NPP)
CC = 307072000.**.64
KTA = 8
JTA = 0
LTA = 0
READ (5,801) (MS)
READ (5,800) (ALS(I),RHOS(I),TES(I),FPS(I),SMOL(I),I=1,MS)
READ (5,600) (GR(I),I=1,MS)
WRITE(6,599)
599 FORMAT(1H0 ,8X,'ALT',8X,'GRAVITY')
WRITE (6,601) (ALS(I),GR(I),I=1,MS)
600 FORMAT (10X,F10.5)
WRITE (6,803) (MS)
WRITE (6,802)(ALS(I),RHOS(I),TES(I),FPS(I),SMOL(I),I=1,MS)
801 FORMAT (110)
800 FORMAT (F15.5,E15.5,F15.5,E15.5,F15.5)
803 FORMAT (///,2X,3HMS=,110,2X,13HU.S. STANDARD,/,9X,3HALS,12X,4HRHO
1S,12X,3HTES,12X,3HFPS,12X,4HSMOL,/)
802 FORMAT (2X,F15.5,E15.5,F15.5,E15.5,F15.5)
ER=.0001
DO 60 I=1,MS
60 RHLS(I)=ALOG(RHOS(I))
KKK=6
CALL ORTHLS (ALS,RHLS,W,MS,0,0,CS,ALPS,BETS,KKK,T1,T2,T3,IND1)
GAMMA=1.4
CONVSM=(GAMMA*.5)**.5
PI=3.141592653
DO 84 I=80,120
M(I)=0
TU(I)=0.
TU2(I)=0.0

```

```

TME(I)=0.0
SIG(I)=0.
PU(I)=0.
PU2(I)=0.
PME(I)=0.
84 SIP(I)=0.
10 READ (5,302) (SA)
   READ(5,310)(MAD)
   READ (5,200) (C3,E)
   READ(5,301)(MA,MD,N,ALTM)
   READ(5,300)(AA(I),RHOA(I),TEMPA(I),CDA(I),VA(I),I=1,MA)
   READ(5,300)(AD(I),RHOD(I),TEMPD(I),CDD(I),VD(I),I=1,MD)
   TEA = TEMPA(I)
   TED = TEMPD(I)
   DO 48 I = 1,MA
   NAA(I)=AA(I)+.2
48 AT(I) = AA(I)
   DO 85 I=1,MD
   TEMAD(I)=0.0
   RHDD(I)=0.0
85 NAD(I)=AD(I)+.2
   DO 49 I = 1,5
49 WTA(I) = .5
   DO 47 I = 6,MA
47 WTA(I) = 1.0
   CALL ORTHLS (ALS,GR,W,MS,0,0,CG,ALPHG,BETAG,4,T1,T2,T3,IND1)
   CALL FITY (AA,MA,0,CG,ALPHG,BETAG,4,GRA,T1,T2,IND3)
   CALL FITY (AD,MD,0,CG,ALPHG,BETAG,4,GRD,T1,T2,IND3)
601 FORMAT (4X,2F10.5)
   WRITE (6,601) (AA(I),GRA(I),I=1,MA)
   WRITE (6,601) (AD(I),GRD(I),I=1,MD)
   DO 5 I=1,100
5 CDKA(I)=0.0
   CDRD(I)=0.0
   WRITE (6,305) SA
   WRITE(6,311)(MAD)
   WRITE (6,201) (C3,E)
   WRITE(6,304)MA,MD,N,ALTM
   WRITE(6,303)(AA(I),RHOA(I),TEMPA(I),CDA(I),VA(I),I=1,MA)
   WRITE(6,303)(AD(I),RHOD(I),TEMPD(I),CDD(I),VD(I),I=1,MD)
305 FORMAT (4X, 17HSOUNDING NUMBER =,13/)
301 FORMAT(3I3,F6.2)
300 FORMAT (F7.3,E8.4,F8.4,F5.3,F8.2)
311 FORMAT (4X,4HMAD=,14/)
310 FORMAT (I2)
304 FORMAT (///3HMA=,14,3HMD=,14,3H N=,14,5HALTM=,E10.5)
303 FORMAT (4X,F6.2,2X,E7.2,2X,F4.0,2X,F5.3,2X,F6.1/)
302 FORMAT (I3)
200 FURMAT (2E20.10)
201 FORMAT (//,4X,3HC3=,E20.10,4X,2HE=,E20.10)
   CALL FITY (AA,MA,0,CS,ALPS,BETS,KKK,RHLSA,T1,T2,IND3)
   CALL FITY (AD,MD,0,CS,ALPS,BETS,KKK,RHLSA,T1,T2,IND4)
   MNU=0
   DO 55 I=1,MD
55 RHUGD(I)=RHOD(I)
76 DO 12 I=1,MA
   ALTA=AA(I)

```

```

RG=8314.34/EANMF(ALTA)
SRA(I)=VA(I)/(2.*RG*TEMPA(I))*0.5
IF (SRA(I)-1.25) 95,95,96
95 S=SRA(I)
CMA = S/CONVSM
GSI = GSIF(CMA)
CDFMA(I) = (2./(PI**5))*(8./(3.*S)+8.*S/15.-8.*S*S/210.)*GSI
GO TO 97
96 S=SRA(I)
CMA = S/CONVSM
GSI = GSIF(CMA)
SI2=1./(S*S)
SI4=SI2*SI2
CDFMA(I)=2.*(1.+SI2-.25*SI4)*GSI
97 DACHA(I)=SRA(I)/CONVSM
DM=DACHA(I)
CDCA(I)=.92+.1660714/DM-.3660714/(DM*DM*DM)
DC=CDFMA(I)-CDCA(I)
NN=20
RHO0=RHOA(I)
K=-1
XA(I) = XXF(CMA)
X = XXF(CMA)
C3A(I) = .212*(CC/EANMF(ALTA))*XA(I)
C3 = C3A(I)
30 FX=RHOA(I)*CDA(I)/(CDCA(I)+DC*EXP(-C3*(RHO0**X)))
CALL WEGIT(RHO0,FX,E,K,NN)
GO TO (30,31,32,33),K
31 RHOGA(I)=RHO0
GO TO 34
32 RHOGA(I)=0.0
GO TO 34
33 RHOGA(I)=-1.0
34 NAN(I)=NN
RHORA(I)=RHOGA(I)/RHOA(I)
CDGA(I)=CDCA(I)+DC*EXP(-C3*(RHOGA(I)**X))
RHOSA(I)=EXP(RHLSA(I))
CDRA(I)=RHOGA(I)/RHOSA(I)
12 CONTINUE
IF(MAD=50) 20,21,21
20 DO 58 JK=1,MAD
TEMAD(JK)=TEMPA(MA-MAD+JK)
RHDD(JK)=RHOGA(MA-MAD+JK)
58 TEMPD(JK)=TEMAD(JK)*(RHOGD(JK)/RHDD(JK))*0.4
GO TO 22
21 TEMPD(I) = TED
22 DO 11 I=1,MD
ALTD=AD(I)
RG=8314.34/EANMF(ALTD)
SRD(I)=VD(I)/(2.*RG*TEMPD(I))*0.5
IF (SRD(I)-1.25)195,195,196
195 S=SRD(I)
CMD = S/CONVSM
GSI = GSIF(CMD)
CDFMD(I) = (2./(PI**5))*(8./(3.*S)+8.*S/15.-8.*S*S/210.)*GSI
GO TO 197
196 S=SRD(I)

```

```

CMD = S/CONVSM
GSI = GSIF(CMD)
SI2=1./ (S*S)
SI4=SI2*SI2
CDFMD(I)=2.*(1.+SI2-.25*SI4)*GSI
197 DACHD(I)=SRD(I)/CONVSM
DM=DACHD(I)
CDCD(I)=.92+.1660714/DM-.3660714/(DM*DM*DM)
DC=CDFMD(I)-CDCD(I)
NN=20
K=-1
RHOG=RHOD(I)
XD(I) = XXF(CMD)
X = XXF(CMD)
C3D(I) = .212*(CC/EANMF(ALT D))*XD(I)
C3 = C3D(I)
40 FX=RHOD(I)*CDD(I)/(CDCD(I)+DC*EXP(-C3*(RHOO**X)))
CALL WEGIT(RHOO,FX,E,K,NN)
GO TO (40,41,42,43),K
41 RHOGD(I)=RHOO
GO TO 44
42 RHOGD(I)=0.0
GO TO 44
43 RHOGD(I)=-1.0
44 NDN(I)=NN
RHORD(I)=RHOGD(I)/RHOD(I)
CDGD(I)=CDCD(I)+DC*EXP(-C3*(RHOGD(I)**X))
RHOSD(I)=EXP(RHLS D(I))
CDRD(I)=RHOGD(I)/RHOSD(I)
RAISO(I)=(RHDD(I)/RHOGD(I))**.4
11 CONTINUE
WRITE (6,902)
WRITE (6,900) (AA(I),RHOGA(I),RHORA(I), CDGA(I),CDRA(I),NAN(I),
1 XA(I),C3A(I),I=1,MA)
WRITE (6,901)
WRITE (6,900) (AD(I),RHOGD(I),RHDD(I), CDGD(I),CDRD(I),NDN(I),
1 XD(I),C3D(I),I=1,MD)
BB=0.0
DO 61 K=2,MA
BB=BB-(AA(K)-AA(K-1))*(RHOGA(K)*GRA(K)-RHOGA(K-1)*GRA(K-1))/ALOG
1 (RHOGA(K)*GRA(K)/(RHOGA(K-1)*GRA(K-1)))
61 TINA(K)=BB
BB=0.0
DO 63 K=2,MD
BB=BB-(AD(K)-AD(K-1))*(RHOGD(K)*GRD(K)-RHOGD(K-1)*GRD(K-1))/ALOG
2 (RHOGD(K)*GRD(K)/(RHOGD(K-1)*GRD(K-1)))
63 TIND(K)=BB
THA(1)=TEMPA(1)
DO 64 KK=2,MA
ALTA=AA(KK)
RG=8314.34/EANMF(ALTA)
64 THA(KK)=TINA(KK)*1000./(RHOGA(KK)*RG)+RHOGA(1)*THA(1)/RHOGA(KK)
THD(1)=TEMPD(1)
DO 65 KK=2,MD
ALTD=AD(KK)
RG=8314.34/EANMF(ALTD)
65 THD(KK)=TIND(KK)*1000./(RHOGD(KK)*RG)+RHOGD(1)*THD(1)/RHOGD(KK)

```

```

DO 57 I=1,MD
TRA(I)=TEMAD(I)/TEMPD(I)
57 CISO(I)=RAISO(I)/TRA(I)
WRITE (6,610) (AA(I),TEMPA(I),THA(I),I=1,MA)
WRITE(6,611)(AD(I),TEMPD(I),THD(I),RAISO(I),TEMAD(I),CISO(I),I=1,MD)
DO 71 I=1,MA
DIFA=ABS((TEMPA(I)-THA(I))/THA(I))+DIFA
71 TEMPA(I)=ABS(THA(I))
IF (MAD-50) 23,24,24
23 MA1=MAD+1
GO TO 25
24 MA1 = 1
25 DO 72 I=MA1,MD
DIFD=ABS((TEMPD(I)-THD(I))/THD(I))+DIFD
72 TEMPD(I)=ABS(THD(I))
SUMD=DIFA+DIFD
TEMPA(I) = TEA
IF (SUMD-ER) 74,74,75
75 MNO=MNO+1
IF (MNO-5) 78,78,74
78 GO TO 76
74 CONTINUE
DO 81 I=1,MD
JC=NAD(I)
M(JC)=M(JC)+1
TU2(JC)=TU2(JC)+TEMPD(I)**2
PU2(JC)=PU2(JC)+CDRD(I)**2
TU(JC)=TU(JC)+TEMPD(I)
PU(JC)=PU(JC)+CDRD(I)
81 CONTINUE
DO 82 I=1,MA
JC=NAA(I)
M(JC)=M(JC)+1
PU2(JC)=PU2(JC)+CDRA(I)**2
TU(JC)=TU(JC)+TEMPA(I)
PU(JC)=PU(JC)+CDRA(I)
TU2(JC)=TU2(JC)+TEMPA(I)**2
82 CONTINUE
DO 83 I=80,120
TME(I)=TU(I)/M(I)
SIG(I)=((TU2(I)/M(I))-TME(I)**2)**.5
PME(I)=PU(I)/M(I)
J = I-79
TMSR(I) = TME(I)/TES(J)
SISR(I) = SIG(I)/TES(J)
83 SIP(I)=((PU2(I)/M(I))-PME(I)**2)**.5
WRITE(6,650)(I,M(I),TME(I),SIG(I),PME(I),SIP(I),TMSR(I),SISR(I),
1 I =80,120)
650 FORMAT(6X,1H1,6X,4HM(I),7X,6HTME(I),9X,6HSIG(I),9X,6HPME(I),
1 9X,6HSIP(I),9X,7HTMSR(I),9X,7HSISR(I)//(5X,13,5X,13,6E15.7))
610 FORMAT (6X,5HAA(I),10X,8HTEMPA(I),14X,6HTHA(I)//(4X,F10.5,2E20.10)
3)
611 FORMAT(6X,5HAD(I),10X,8HTEMPD(I),13X,8HTEMAD(I),9X,8HRAISO(I),
112X,6HTRA(I),10X,7HCISO(I)//(4X,F10.5,5E20.10))
900 FORMAT (2X,F10.4,4E14.6,110,2E14.6)
901 FORMAT (///,6X,3HALT,9X,5HRHOGD,9X,5HRHDD ,10X, 4HCDGD,10X,4HCDRD,

```

111X,3HADN,9X,'XA',13X,'C3A')  
 902 FORMAT (///,6X,3HALT,9X,5HRHOGA,9X,5HRHORA,10X,4HCDGA,10X,4HCDRA,  
 111X,3HAAN,9X,'XD',13X,'C3D')  
 GO TO 10  
 END

0XQT

41

80.	1.999	-E5180.65	4.065	-E328.964
81.	1.662	-E5180.65	4.888	-E328.964
82.	1.382	-E5180.65	5.877	-E328.964
83.	1.150	-E5180.65	7.067	-E328.964
84.	9.563	-E6180.65	8.496	-E328.964
85.	7.955	-E6180.65	1.021	-E228.964
86.	6.617	-E6180.65	1.228	-E228.964
87.	5.504	-E6180.65	1.476	-E228.964
88.	4.579	-E6180.65	1.774	-E228.964
89.	3.819	-E6180.65	2.133	-E228.964
90.	3.170	-E6180.65	2.563	-E228.96
91.	2.598	-E6183.63	3.127	-E228.96
92.	2.137	-E6186.62	3.802	-E228.96
93.	1.763	-E6189.59	4.607	-E228.96
94.	1.459	-E6192.56	5.566	-E828.95
95.	1.211	-E6195.51	6.702	-E228.94
96.	1.008	-E6198.45	8.052	-E828.94
97.	8.415	-E7201.37	9.643	-E828.92
98.	7.044	-E7204.28	1.151	-E128.91
99.	5.911	-E7207.16	1.371	-E128.90
100.	4.974	-E7210.02	1.629	-E128.88
101.	4.159	-E7214.86	1.946	-E128.86
102.	3.493	-E7219.66	2.316	-E128.83
103.	2.945	-E7224.43	2.744	-E128.81
104.	2.492	-E7229.18	3.240	-E128.78
105.	2.117	-E7233.90	3.810	-E128.75
106.	1.804	-E7238.58	4.465	-E128.72
107.	1.543	-E7243.23	5.215	-E128.68
108.	1.323	-E7247.85	6.071	-E128.664
109.	1.139	-E7252.44	7.045	-E128.60
110.	9.829	-E8257.00	8.150	-E128.56
111.	8.360	-E8266.44	9.568	-E128.51
112.	7.153	-E8275.85	1.117	28.47
113.	6.153	-E8285.20	1.296	28.42
114.	5.321	-E8294.92	1.496	28.37
115.	4.623	-E8303.78	1.719	28.32
116.	4.035	-E8313.01	1.966	28.27
117.	3.536	-E8322.19	2.239	28.22
118.	3.112	-E8331.33	2.540	28.17
119.	2.748	-E8340.43	2.870	28.12
120.	2.436	-E8349.49	3.233	28.07

80.	9.564
81.	9.561
82.	9.558
83.	9.555
84.	9.552
85.	9.550
86.	9.547
87.	9.544
88.	9.541

000341	000	89.	9.538
000342	000	90.	9.535
000343	000	91.	9.532
000344	000	92.	9.529
000345	000	93.	9.526
000346	000	94.	9.523
000347	000	95.	9.520
000348	000	96.	9.517
000349	000	97.	9.514
000350	000	98.	9.511
000351	000	99.	9.508
000352	000	100.	9.505
000353	000	101.	9.502
000354	000	102.	9.499
000355	000	103.	9.496
000356	000	104.	9.493
000357	000	105.	9.490
000358	000	106.	9.488
000359	000	107.	9.485
000360	000	108.	9.482
000361	000	109.	9.479
000362	000	110.	9.476
000363	000	111.	9.473
000364	000	112.	9.470
000365	000	113.	9.467
000366	000	114.	9.464
000367	000	115.	9.461
000368	000	116.	9.458
000369	000	117.	9.455
000370	000	118.	9.452
000371	000	119.	9.449
000372	<del>000</del>	120.	9.447

**PROGRAM AFILIP-HIGH CM**

**This program computes values of drag coefficient for various values of Knudsen number and Reynolds numbers for Mach numbers above 1.**

```

HIGH CM
@FOR,15 MAIN,MAIN
  GSIF(S) = .9975617977-.018426966*S
  XF(S) = .399+.016*S
  CDFMLF(S)=(2./(PI**.5))*(8./(3.*S)+8.*S/15.-8.*S*S*S/210.)*GSI
  CDFMHF(S) = 2.*(1.+1./(S*S)-.25/(S*S*S*S))*GSI
  CUCF(S)=.92+.1660714 /S-.3660714 /(S*S*S)
  DIMENSION XM(100),RE(100),CD(100),BKN(100),
  1      CDLS(100),CR(100)
  PI = 3.14159265
  GAMMA = 1.4
  CONVSM = (GAMMA*.5)**.5
10 READ(5,1,END=100)CM,NI
  1 FORMAT(F10.0,15)
  READ(5,33) XL,EL,GSI
33 FORMAT(3F15.0)
  READ(5,2)      (XM(I),RE(I),CD(I),I=1,NI)
  2 FORMAT(3F20.0)
  GSI = GSIF(CM)
  SELK = 0.0
  SELK2 = 0.0
  SY = 0.0
  SYKN = 0.0
  WRITE(6,11)
11 FORMAT(1H1,13X,'PRESENT EXPERIMENTAL SPHERE DATA')
  WRITE(6,5)CM
  5 FORMAT(1H0,/,/,25X,'CM = ',F6.4,/,/,11X,'XM',17X,'RE',19X,'CD',/)
  WRITE(6,6)(XM(I),RE(I),CD(I),I=1,NI)
  6 FORMAT(5X,F10.4,10X,F10.4,10X,F10.4)
  AG=GAMMA**(-.5)
  7 DO 20 I=1,NI
  A = .499*(8./PI)**.5
  A = 1./A
  BKN(I) = XM(I)/(RE(I)*AG)
  BKN(I) = A*BKN(I)
  SR = XM(I)*CONVSM
  IF(SR=1.25) 95,95,96
95 CDFM = CDFMLF(SR)
  GO TO 97
96 CDFM = CDFMHF(SR)
97 GM = XM(I)
  CDCN = CDCF(GM)
  DC = CDFM-CDCN
  UC = CD(I)-CDCN
  CR(I) = UC/DC
  WRITE(6,4)DC,UC,CR(I)
  4 FORMAT(/,/,1H , 'DC = ',E20.10,5X,'UC = ',E20.10,5X,'CR(I) = ',E20.10)
20 CONTINUE
  E = .212
  DO 41 J=1,101
  X=.005*(J-1) +0.35
  FX=DSUX(CR,BKN,E,NI,X)

```

```

FX=FX-X
41 WRITE(6,12)X,FX,NI
   X = XF(CM)
   DO 42 J=1,101
   E=.005*(J-1)+.1
   FE=DSUE(CR,BKN,E,NI,X)
   FE=FE-E
42 WRITE(6,13)E,FE,NI
   X = XF(CM)
   E = .212
12 FORMAT(/,1H , 'X = ',E20.10,5X, 'FX = ',E20.10,5X, 'N = ',I3)
13 FORMAT(/,1H , 'E = ',E20.10,5X, 'FE = ',E20.10,5X, 'N = ',I3)
   SQD=0.0
   DO 75 I=1,NI
   SR=CM*CONVSM
   GM=CM
   IF(SR-1.25)85,85,86
85 CDLS(I) = CDCF(GM)+((CDFMLF(SR)-CDCF(GM))*EXP(-E/(BKN(I))*X))
   GO TO 70
86 CDLS(I) = CDCF(GM)+(CDFMHF(SR)-CDCF(GM))*EXP(-E/(BKN(I))*X)
70 SQD=SQD+(CDLS(I)-CD(I))*2.
75 CONTINUE
   RMS=(SQD/NI)**.5
   WRITE(6,74)
74 FORMAT(/,/,/,9X, 'CDLS',18X, 'CD',17X, 'BKN',/)
   WRITE(6,73)(CDLS(N),CD(N),BKN(N),N=1,NI)
73 FORMAT(1H ,3E20.10)
   WRITE(6,3)CM,NI,X,E,GS1
   3 FORMAT(/,/,/,/,/,/,1H ,9X, 'CM',18X, 'NI',/,/,1H ,7X,F6.4,16X,12,/,/,/
1,1H ,9X, 'X',19X, 'E',18X, 'GS1',/,/,1H ,3E20.10)
   WRITE(6,71)RMS
71 FORMAT(/,/,/, ' RMS=',E20.10)
   S1 = CM
   S2 = CM*CONVSM
   DCF = CDCF(S1)
   DFML = CDFMLF(S2)
   DFMH = CDFMHF(S2)
   WRITE(6,76) DCF, DFML, DFMH, S1, S2
76 FORMAT(/,/,/,1H , ' CDCF=',E20.10,/,/,1H , ' CDFMLF=',E20.10,
1 /,/,1H , ' CDFMHF=',E20.10,/,/,1H , ' S1=',E20.10,/,/,1H ,
1 . ' S2=',E20.10)
   DO 53 L=1,5
   DO 50 K=1,9
   BKN(K) = (0.01+0.01*(K-1))*(10.**L)
   BKN(K) = BKN(K)*(10.**(-3))
   SR = CM*CONVSM
   GM = CM
   IF(SR-1.25)55,55,56
55 CDLS(K) = CDCF(GM)+((CDFMLF(SR)-CDCF(GM))*EXP(-E/( BKN(K))*X))
   GO TO 51
56 CDLS(K) = CDCF(GM)+(CDFMHF(SR)-CDCF(GM))*EXP(-E/( BKN(K))*X)
51 WRITE(6,52)CM,SR,BKN(K),CDLS(K)
52 FORMAT(1H0,16X, 'CM',14X, 'SR',/,/,1H ,12X,F8.4,8X,F10.5,/,/,/,1H ,
1 9X, 'BKN',17X, 'CDLS',/,/,1H ,3X,E15.8,5X,E15.8)
50 CONTINUE
53 CONTINUE
   GO TO 10

```

```

100 STOP
    FUNCTION DSUX(CR,BKN,E,NI,X)
    DIMENSION CR(100),BKN(100)
    SX = 0.0
    DO 65 I=1,NI
    BKNX = BKN(I)**X
    SX = SX+(CR(I)-EXP(-E/BKNX))*(EXP(-E/BKNX))*(ALOG( BKN(I)))/BKNX
65 CONTINUE
    DSUX = X+SX
    RETURN
    FUNCTION DSUE(CR,BKN,E,NI,X)
    DIMENSION CR(100),BKN(100)
    SE = 0.0
    DO 66 I=1,NI
    BKNX = BKN(I)**X
    SE = SE+(CR(I)-EXP(-E/BKNX))*(EXP(-E/BKNX))/BKNX
66 CONTINUE
    DSUE = E+SE
    RETURN
    END

```



LOW CM

WFOR,IS MAIN,MAIN

```

XF(S) = .399+.016*S
GSIF(S) = .9975617977+.018426966*S
CDFMLF(S)=(2./(PI**.5))*(8./(3.*S)+A.*S/15.-8.*S*S/210.)*GS1
CDFMHF(S) = 2.*(1.+1./(S*S)-.25/(S*S*S))*GS1
CDCF(S) = 0.40297-0.1424799*S*S+0.45950669*(S**4.)
DIMENSION XM(100),RE(100),CD(100),BKN(100),
1      CDLS(100),CR(100)
PI = 3.14159265
GAMMA = 1.4
CONVSM = (GAMMA*.5)**.5
10 READ(5,1,END=100)CM,NI
1  FORMAT(F10.0,15)
  READ(5,33) XL,EL,GS1
33  FORMAT(3F15.0)
  READ(5,2)      (XM(I),RE(I),CD(I),I=1,NI)
2  FORMAT(3F20.0)
  GS1 = GSIF(CM)
  SELK = 0.0
  SELK2 = 0.0
  SY = 0.0
  SYKN = 0.0
  WRITE(6,11)
11  FORMAT(1H1,13X,'PRESENT EXPERIMENTAL SPHERE DATA')
  WRITE(6,5)CM
5  FORMAT(1H0,/,/,25X,'CM = ',F6.4,/,/,11X,'XM',17X,'RE',19X,'CD',/)
  WRITE(6,6)(XM(I),RE(I),CD(I),I=1,NI)
6  FORMAT(5X,F10.4,10X,F10.4,10X,F10.4)
  AG=GAMMA**(-.5)
7  DO 20 I=1,NI
  A = .499*(8./PI)**.5
  A = 1./A
  BKN(I) = XM(I)/(RE(I)*AG)
  BKN(I) = A*BKN(I)
  SR = XM(I)*CONVSM
  IF(SR-1.25) 95,95,96
95  CDFM = CDFMLF(SR)
  GU TO 97
96  CDFM = CDFMHF(SR)
97  GM = XM(I)
  CDCN = CDCF(GM)
  DC = CDFM-CDCN
  UC = CD(I)-CDCN
  CR(I) = UC/DC
  WRITE(6,4)DC,UC,CR(I)
4  FORMAT(/,/,1H ,*DC =',E20.10,5X,'UC =',E20.10,5X,'CR(I) =',E20.10:
20  CONTINUE
  E = .212
  DO 41 J=1,101
  X=.005*(J-1) +0.35
  FX=DSUX(CR,BKN,E,NI,X)

```

```

FX=FX-X
41 WRITE(6,12)X,FX,NI
   X = XF(CM)
   DO 42 J=1,101
   E=.005*(J-1)*.1
   FE=DSUE(CR,BKN,E,NI,X)
   FE=FE-E
42 WRITE(6,13)E,FE,NI
   X = XF(CM)
   E = .212
12 FORMAT(/,1H , 'X = ',E20.10,5X, 'FX = ',E20.10,5X, 'N = ',13)
13 FORMAT(/,1H , 'E = ',E20.10,5X, 'FE = ',E20.10,5X, 'N = ',13)
   SQD=0.0
   DO 75 I=1,NI
   SR=CM*CONVSM
   GM=CM
   IF(SR-1.25)85,85,86
85 CDLS(I) = CDCF(GM)+((CDFMLF(SR)-CDCF(GM))*EXP(-E/(BKN(I))*X))
   GO TO 70
86 CDLS(I) = CDCF(GM)+((CDFMHF(SR)-CDCF(GM))*EXP(-E/(BKN(I))*X))
70 SQD=SQD+(CDLS(I)-CD(I))*2.
75 CONTINUE
   RMS=(SQD/NI)**.5
   WRITE(6,74)
74 FORMAT(/,/,/,/,9X, 'CDLS',18X, 'CD',17X, 'BKN',/)
   WRITE(6,73)(CDLS(N),CD(N),BKN(N),N=1,NI)
73 FORMAT(1H ,3E20.10)
   WRITE(6,3)CM,NI,X,E,GS1
3 FORMAT(/,/,/,/,/,/,1H ,9X, 'CM',18X, 'NI',/,/,1H ,7X,F6.4,16X,12,/,/,/
1,1H ,9X, 'X',19X, 'E',18X, 'GS1',/,/,1H ,3E20.10)
   WRITE(6,71)RMS
71 FORMAT(/,/,/,/,' RMS=',E20.10)
   S1 = CM
   S2 = CM*CONVSM
   DCF = CDCF(S1)
   DFML = CDFMLF(S2)
   DFMH = CDFMHF(S2)
   WRITE(6,76) DCF, DFML, DFMH, S1, S2
76 FORMAT(/,/,/,1H , ' CDCF=',E20.10,/,/,1H , ' CDFMLF=',E20.10;
1 /,/,1H , ' CDFMHF=',E20.10,/,/,1H , ' S1=',E20.10,/,/,1H ,
1 ' S2=',E20.10)
   DO 53 L=1,5
   DO 50 K=1,9
   BKN(K) = (0.01+0.01*(K-1))*(10.**L)
   BKN(K) = BKN(K)*(10.**(-3))
   SR = CM*CONVSM
   GM = CM
   IF(SR-1.25)55,55,56
55 CDLS(K) = CDCF(GM)+((CDFMLF(SR)-CDCF(GM))*EXP(-E/( BKN(K))*X))
   GO TO 51
56 CDLS(K) = CDCF(GM)+((CDFMHF(SR)-CDCF(GM))*EXP(-E/( BKN(K))*X))
51 WRITE(6,52)CM,SR,BKN(K),CDLS(K)
52 FORMAT(1H0,16X, 'CM',14X, 'SR',/,/,1H ,12X,F8.4,8X,F10.5,/,/,/,1H ,
1 9X, 'BKN',17X, 'CDLS',/,/,1H ,3X,E15.8,5X,E15.8)
50 CONTINUE
53 CONTINUE
   GO TO 10

```

```

100 STOP
  FUNCTION DSUX(CR,BKN,E,NI,X)
  DIMENSION CR(100),BKN(100)
  SX = 0.0
  DO 65 I=1,NI
  BKNX = BKN(I)**X
  SX = SX+(CR(I)-EXP(-E/BKNX))*(EXP(-E/BKNX))*(ALOG( BKN(I)))/BKNX
65 CONTINUE
  DSUX = X+SX
  RETURN
  FUNCTION DSUE(CR,BKN,E,NI,X)
  DIMENSION CR(100),BKN(100)
  SE = 0.0
  DO 66 I=1,NI
  BKNX = BKN(I)**X
  SE = SE+(CR(I)-EXP(-E/BKNX))*(EXP(-E/BKNX))/BKNX
66 CONTINUE
  DSUE = E+SE
  RETURN
  END

```

**PROGRAM CDCLEV**

**This program computes free molecular drag and lift coefficients for flat surfaces at various angles of attacks and for a specified range of speed ratios.**

```

IMPLICIT REAL*8(A-H,O-Z)
DIMENSION ANG(20),CL(25,20),CD(25,20)
READ(5,100) PJ,ALJ,X
SQ2=1.41421356237
PI=3.141592653
SQPI=1.7724538509
SQ2=1.41421356237
E=2.718281828459
XR=X*PI/180.
P=0.3275911
A1=0.254829592
A2=-0.284496736
A3=1.421413741
A4=-1.453152047
A5=1.061405429
LOD=4.*3./PI
DO22I=1,25
S=I
DO 22 J=1,10
ANG=XR*(J-1)
ANGD(J)=ANG*180./PI
SA=SIN(ANG)
CA=COS(ANG)
Z=S*S*.5*SA*SA
EZ=E**(-Z)
T=Z/3.75
ES=E**(-5*S)
R=1.0/(1.0+P*S)
ERFS=1.0-(A1*R+A2*R*R+A3*(R**3.)+A4*(R**4.)+A5*(R**5.))*ES
F=SQPI*(S*S+1.0-(0.25/(S*S)))*ERFS+(S+(0.5/S))*ES
CDO=2.*F/(S*S*SQPI)
IF(Z-3.75)10,10,11
BU=(Z**5)*EZ*(1.0+3.5156229*T*T +3.0899424*(T**4.)
1+1.2067492*(T**6.) +.2659732*(T**8.) +.0360768*(T**10.)
2+.0045813*(T**12.))
B1=(Z**1.5)*EZ*(.5+.87890594*T*T +.51498869*(T**4.)
2+.15084934*(T**6.) +.02658733*(T**8.) +.00301532*(T**10.)
3+.00032411*(T**12.))
GO TO 12
BU=.39894228+.01328592/T+.00225319/(T*T)
1-.00157565/(T*T*T)+.00916281/(T**4.)
2-.02057706/(T**5.)+.02635537/(T**6.)
3-.01647633/(T**7.)+.00392377/(T**8.)
B1=.39894228-.03988024/T-.00362018/(T*T)
1+.00163801/(T*T*T)-.01031555/(T**4.)+.02282967/(T**5.)
2-.02895312/(T**6.)+.01787654/(T**7.)-.00420059/(T**8.)
AL=8.*SA*SA/3.
BL=-4.*SA*SA+PI*SA
C=-PI*.5*SA+(6.*SA*SA/6.)
AJ=ALJ
CL(I,J)=SQ2*SQPI*.5*CA*((BU+B1)*AJ*(AL+BL*PJ+C*PJ*PJ)
1+BU*(1.+(3.-PJ)*AJ)/(S*S)+B1*(1.+(1./3.+PJ/3.)*AJ)/(S*S))
CL(I,J)=(LOD/(1.+LOD))*CL(I,J)
AD=-1.+4.*SA*SA/3.

```

```

BU=PI-8.*SA*SA/3;
CDD=3./2.-PI+5.*SA*SA/3.
DD=-.5+PI/4.-SA*SA/3.
KD=AD+BD*PJ+CDD*PJ*PJ+DD*PJ*PJ*PJ
IF(J-1)20,21,20
CD(I,J)=SQ2*SA*((BO+B1)*(1.+AJ*KD)+BO*(1.+AJ*(3.-2.*PJ+.5*PJ*PJ))
1/(2.*S*S)+B1*(1.+ALJ*(1./3.+2.*PJ/3.-PJ*PJ/6.)))/(2.*S*S)
2+SQ2*(BO+B1)*(1.+ALJ*(-1.+1.5*PJ*PJ-.5*PJ*PJ*PJ))/(SA*S*S)
CD(I,J)=CD(I,J)*SQPI
CD(I,J)=(LOD/(1.+LOD))*CD(I,J)+CDO/(1.+LOD)
GO TO 22
CD(I,J)=SQPI*(1.+AJ*(-1.+1.5*PJ*PJ-.5*PJ*PJ*PJ))/S
CD(I,J)=(LOD/(1.+LOD))*CD(I,J)+CDO/(1.+LOD)
CONTINUE
WRITE(6,200)PJ,ALJ
WRITE(6,201)(ANGD(J),J=1,10)
DO 2 I=1,25
WRITE(6,202)I,(CD(I,J),J=1,10)
WRITE(6,203)PJ,ALJ
WRITE(6,201)(ANGD(J),J=1,10)
DO 3 I=1,25
WRITE(6,202)I,(CL(I,J),J=1,10)
GO TO 50
FORMAT(30I0,5)
FORMAT(1H1,25X,9HCD(S,ANG),8X,3HPJ=,E15.5,4X,4HALJ=,E15.5/)
FORMAT(4X,7HS..ANG=,10E12.5/)
FORMAT(3X,12,6X,10E12.5)
FORMAT(1H1,25X,9HCL(S,ANG),8X,3HPJ=,E15.5,4X,4HALJ=,E15.5/)
END

```

## PROGRAM CFEVAL

This program computes values of force coefficient for a specified speed ratio as a function of gas surface interaction parameters and angles of attack.

```

IMPLICIT REAL*8(A-H,O-Z)
DIMENSION A(50,2),G(50,2),H(50,2),Q(50,2),P(50,2)
DIMENSION E(50,2)
DIMENSION GAM(20),ALJ(15),PJ(15),CF(20,20,20)
DIMENSION AS(50,2),GS(50,2),HS(50,2),QS(50,2),PS(50,2)
DIMENSION FF(50,2)
READ(5,100)SRA1
SRA2=SRA1*SRA1
AR=1.5780
A1=.44325141463
A2=.06260601220
A3=.04757383546
A4=.01736506451
B1=.24998368310
B2=.09200180037
B3=.04069697526
B4=.00526449639
AA0=1.38629436112
AA1=0.09666344259
AA2=0.03590092383
AA3=0.03742563713
AA4=0.01451196212
BB0=0.5
BB1=0.12498593597
BB2=0.06880248576
BB3=0.03328355346
BB4=0.00441787012
PI=3.14159265359
DO51 I=1,19
GAM(I)=5.0*(I-1)
GAMR=5.0*(I-1)*PI/180.0
SING=SIN(GAMR)
COSA=COS(GAMR)
SINA=SING
FM1=1.0-SING*SING
FM2=FM1*FM1
FM3=FM1*FM2
FM4=FM1*FM3
J=1
IF(FM1)21,31,21
E(I,J)=1.+A1*FM1+A2*FM2+A3*FM3+A4*FM4+(B1*FM1+B2*FM2+B3*FM3+B4*FM4
1)*ALOG(1./FM1)
FF(I,J)=AA0+AA1*FM1+AA2*FM2+AA3*FM3+AA4*FM4+(BB0+BB1*FM1+BB2*FM2
1+BB3*FM3+BB4*FM4)*LOG(1./FM1)
GO TO 41
E(I,J)=1.
FF(I,J)=1000.
A(I,J)=2.+4.*AR*E(I,J)/PI
AS(I,J)=2.+5.*AR*FF(I,J)/PI
G(I,J)=AR*4.*E(I,J)/(3.*PI)+AR*16.*COSA*COSA*FF(I,J)/(9.*PI)
GS(I,J)=-AR*FF(I,J)/PI
H(I,J)=4./3.+AR*(E(I,J)*(-88./(9.*PI)+4.-16.*COSA*COSA/(9.*PI))
1+PI*SINA*SINA+.5-8.*FF(I,J)*COSA*COSA/(3.*PI))
HS(I,J)=4./3.+AR*2.*E(I,J)/(3.*PI)+AR*FF(I,J)*(-1.+2./(3.*PI))

```

```

1+AR*(-PI*SINA*SINA/4.-PI*3.*(SINA**4.)/16.)
Q(I,J)=1./6.+AR*E(I,J)*(16./(3.*PI)-4.+8.*COSA*COSA/(3.*PI))
1+AR*(6.*E(I,J)/PI-.25*PI*SINA*SINA+8.*COSA*COSA*FF(I,J)/(9.*PI))
QS(I,J)=1./6.-AR*E(I,J)*2./(3.*PI)+AR*FF(I,J)*(1.+16./(3.*PI))
1-AR=1.5*FF(I,J)/PI+AR*PI*(SINA*SINA*(1./8.+3.*SINA*SINA/32.))
P(I,J)=-1./6.+AR*E(I,J)*(-8./(9.*PI)+1.-8.*COSA*COSA/(9.*PI))
1-AR=2.*E(I,J)/PI
PS(I,J)=-1./6.+AR*E(I,J)/(3.*PI)-AR*FF(I,J)*(.25+2./PI)
1+.5*FF(I,J)*AR/PI
DO 51 J=1,11
DO 51 K=1,11
ALJ(J)=.2*(J-1)
PJ(K)=.2*(K-1)
PJ1=PJ(K)
PJ2=PJ1*PJ1
PJ3=PJ1*PJ2
CF(K,J,I)=A(I,1)+AS(I,1)/SRA2+ALJ(J)*(G(I,1)+PJ1*H(I,1)+PJ2*Q(I,1)
1+PJ3*P(I,1))+ALJ(J)*(GS(I,1)+PJ1*HS(I,1)+PJ2*QS(I,1)+PJ3*PS(I,1))
2/SRA2
CF(K,J,I)=CF(K,J,I)/(1.+AR)
51 CONTINUE
DO 15 J=1,11
WRITE(6,211) J,ALJ(J)
211 FORMAT(1X,4HALJ(,I2,4H) = F8.2)
WRITE(6,9797)
WRITE(6,9997)
WRITE(6,9899)
DO 1115 K=1,11
WRITE(6,2111)(CF(K,J,I),I=1,7)
WRITE(6,2111)(CF(K,J,I),I=8,14)
WRITE(6,2111)(CF(K,J,I),I=15,19)
1115 WRITE(6,162)
15 WRITE(6,163)
GO TO 99
162 FORMAT(//)
163 FORMAT(////)
2111 FORMAT(1XE15.9,2XE15.9,2XE15.9,2XE15.9,2XE15.9,2XE15.9,2XE15.9)
9797 FORMAT(7X,1HD,16X,1HS,16X,2HD,15X,2H15,15X,2H20,15X,2H25,15X,2H30
1)
9997 FORMAT(7X,2H35,15X,2H40,15X,2H45,15X,2H50,15X,2H55,15X,2H60,15X,2H
165)
9899 FORMAT(7X,2H70,15X,2H75,15X,2H80,15X,2H85,15X,2H90)
100 FORMAT(D10.5)
END

```

## PROGRAM RUFSPH

This program was used to compute drag coefficients for a number of non-spherically shaped objects. The copy shown here was used to compute the drag coefficient of ellipsoids of various eccentricities and gas surface interaction parameters.

```

IMPLICIT REAL*8(A-H,O-Z)
DIMENSION FB(21),FF(21),THB(21),THF(21),TXB(21),TXF(21)
DIMENSION DI(21),DR(21,21),X(21),W(21),PJ(21),COF(21,21),GAM(21),
1 THI(21),WW(21)
DIMENSION THX(40)
DIMENSION GA(10),GA2(10)
DIMENSION GR(20)
DIMENSION FI(21),SS(21)
DIMENSION RR(21)
X(1)=0.07652652113350
X(2)=0.22778585114165
X(3)=0.37370608871542
X(4)=0.51086700195083
X(5)=0.63605368072652
X(6)=0.74633190646015
X(7)=0.83911697182222
X(8)=0.91223442825133
X(9)=0.96397192727791
X(10)=0.9931285991851
W(1)=0.1527533871307
W(2)=0.1491729864726
W(3)=0.1420961093183
W(4)=0.1316886384492
W(5)=0.1181945319615
W(6)=0.1019301198172
W(7)=0.0832767415767
W(8)=0.0626720483341
W(9)=0.0406014298004
W(10)=0.017614007132
P=0.3275911
A1=0.254829592
A2=-0.284496736
A3=1.421413741
A4=-1.453152027
A5=1.061405429
PI=3.14159265358976
DO 2 I=1,10
J=11-I
GAM(I)=PI*.5*(1.-X(J))
2 WW(I)=W(J)
DO3 I=1,10
J=I+10
GAM(J)=PI*.5*(1.+X(I))
3 WW(J)=W(I)
DO 40 M=1,5
ECC = 0.0001*M
GA2(M)=.5*(10.***(M-1))*PI/(360.**3600.)
GA(M)=ECC
AS=1.0
BS=(1.-ECC*ECC)**.5
DO4 I=1,21
DO4 J=1,21
4 DR(I,J)=0.0
DO 29 I=1,10

```

```

SGA=SIN(GAM(I))
CGA=COS(GAM(I))
C2=CGA*CGA
S2=SGA*SGA
RR(I)=(C2/(BS*BS)+S2/(AS*AS))**.5)
DRDTH=((RR(I))**.3.)*(BS**(-2.)-AS**(-2.))*CGA*SGA
GR(I)=ATAN(DRDTH)
29 CONTINUE
DO 27 I=1,20
GR(I)=0.0
RR(I)=1.0
27 CONTINUE
DO5I=1,10
SS(I)=10.**(-I)
T=1./(1.+P*SS(I))
S=SS(I)
ERFS=2.*(S-S*S*S/3.+(S**5.)/10.+(S**7.)/42.
I+(S**9.)/216.)/(PI**.5)
DI(I)=0.0
DO6J=1,20
Y=ABS(S*COS(GAM(J)))
T=1./(1.+P*Y)
ERFY=2.*(Y-Y*Y*Y/3.+(Y**5.)/10.-(Y**7.)/42.
I+(Y**9.)/216.)/(PI**.5)
CGA=COS(GAM(J))
IF(CGA)31,33,33
31 Y=-Y
ERFY=-ERFY
33 PQ=.5+.5*ERFY
Q=S*Y*(1.+ERFY)+S*EXP(-Y*Y)/(PI**.5)
FI(J)=(Q*Q+2.*PQ*Q*CGA+PQ*PQ)**.5
THI(J)=PI*.5-ACOS((Q*CGA+PQ)/FI(J))
THX(J)=PI*.5-THI(J)
6 CONTINUE
DO 70 J=1,20
ANB=GAM(J)-GR(J)
ANF=GAM(J)-GR(J)
YB=ABS(S*COS(ANB))
YF=ABS(S*COS(ANF))
TB=1./(1.+P*YB)
TF=1./(1.+P*YF)
ERFYB=2.*(YB-YB*YB*YB/3.+(YB**5.)/10.-(YB**7.)/42.+(YB**9.)/216.)/
I(PI**.5)
ERFYF=2.*(YF-YF*YF*YF/3.+(YF**5.)/10.-(YF**7.)/42.+(YF**9.)/216.)/
I(PI**.5)
CANB=COS(ANB)
CANF=COS(ANF)
IF(CANB)51,53,53
51 YB=-YB
ERFYB=-ERFYB
53 PQB=.5+.5*ERFYB
QB=S*YB*(1.+ERFYB)+S*EXP(-YB*YB)/(PI**.5)
FB(J)=(QB*QB+2.*PQB*QB*CANB+PQB*PQB)**.5
THB(J)=PI*.5-ACOS((QB*CANB+PQB)/FB(J))
IF(CANF)61,63,63
61 YF=-YF
ERFYF=-ERFYF

```

```

63 PQF=.5+.5*ERFYF
   QF=S*YF*(1.+ERFYF)+S*EXP(-YF*YF)/(PI**.5)
   FF(J)=(QF*QF+2.*PQF*QF*CANF+PQF*PQF)**.5
   THF(J)=PI*.5-ACOS((QF*CANF+PQF)/FF(J))
   TXB(J)=PI*.5-THB(J)
   TXF(J)=PI*.5-THF(J)
70 CONTINUE
   DO 85 L=1,20
   DIB=FB(L)*COS(GAM(L)-PI*.5+THB(L)-GR(L))
   DR(L)=RR(L)*RR(L)*WW(L)*SIN(GAM(L))/COS(GR(L))
   DI(I)=DIB+DI(I)
85 CONTINUE
   DI(I)=DI(I)*PI*.5
   DO 7K=1,21
   PJ(K)=.1*(K-1)
   DO 8 L=1,20
   THRF=PJ(K)*PI*.5+(1.-PJ(K))*THF(L)
   DRF=FF(L)*COS(THRF+PI*.5-GAM(L)+GR(L))*WW(L)*SIN
   (GAM(L))*RR(L)*RR(L)/COS(GR(L))
   DR(I,K)=DR(I,K)-DRF
8 CONTINUE
   DR(I,K)=PI*.5*DR(I,K)
   COF(I,K)=DR(I,K)/DI(I)
7 CONTINUE
5 CONTINUE
   DO 9 I=1,10
   WRITE(6,101) SS(I),DI(I)
   WRITE(6,103) GAM(I)
   DO 10K=1,21
   WRITE(6,102) PJ(K),COF(I,K),DR(I,K)
10 CONTINUE
9 CONTINUE
40 CONTINUE
   WRITE(6,105)
   DO 28 I=1,20
   AI=I
   GR(I)=GR(I)*180./PI
   GAM(I)=GAM(I)*180./PI
   WRITE(6,104)AI,GAM(I),RR(I),GR(I)
28 CONTINUE
105 FORMAT(//4X,1HI,6X,6HGAM(I),6X,5HRR(I),6X,5HGR(I)/)
104 FORMAT(2X,F10.5,2X,E10.5,2X,E10.5,2X,E10.5)
103 FORMAT(4X,3HGA=,E10.5/)
101 FORMAT(////4X,2HS=,E10.5,2X,6HDI(S)=,E13.5//8X,2HPJ,6X,7HK(PJ,S);
15X,8HDR(PJ,S)/)
102 FORMAT(4X,F10.5,2X,E10.5,4X,E10.5)
200 FORMAT(////4X,2HS=,E10.5,2X,6HDI(S)=,E10.5,//8X,1HK,10X,6HGAM(K),
16X,6HTHI(K),6X,5HFI(K)/)
201 FORMAT(4X,F10.5,2X,E10.5,2X,E10.5,2X,E10.5)
END

```

**PROGRAM CLELAN**

**This program was employed to calculate orbit perturbations  
due to lifting satellite shapes.**

```

C   CALCULATION OF SATELLITE ORBIT CHANGE CAUSED BY LIFT AND DRAG
C   PERTURBATIONS..... NUMERICAL INTEGRATION USING A MODIFIED RUNGA-
C   KUTTA TECHNIQUE
C
C   IMPLICIT DOUBLE PRECISION (A-H,O-Z)
C   DIMENSION Y(7),W(7),Q(7),PHINT(10),PHIW(10),AA(5),YY(7,60),DEN(60
1) ,HT(60)
C   DOUBLE PRECISION MU
C   REAL ESTEP,DIFPER,W,Q
C   EXTERNAL DIFPER
C   COMMON TA,MU,P,FF,ACT,M,R,ACN,ACK,VMEAN
C
C   INPUT OF INITIAL VALUES
C
C   L = NUMBER OF ECCENTRICITIES TIMES NUMBER OF PERIGEE HEIGHTS
C   M = NUMBER OF DIFFERENT SATELLITE ATTITUDES
C   N = NUMBER OF AREA/MASS RATIOS
C   NO = UPPER LIMIT ON THE NUMBER OF ORBITS FOR A SINGLE LAUNCH
C   READ (5,3) N,M,L,NO
3  FORMAT (4I5)
   READ (5,4)(AA(I),I= 1,N )
4  FORMAT(E15.9)
   READ (5,14)(PHINT(K),PHIW(K), K = 1,M)
14 FORMAT (2F15.10)
   READ(5,10)VE,RE,MU
10  FORMAT(3E15.9)
   READ (5,13) GA,PJ
13  FORMAT (2F10.8)
   READ (5,15) ((YY(MM,NN),MM = 1,7) ,DEN(NN),HT(NN), NN = 1,L)
15  FORMAT (5E15.9/2E15.9/2E15.6)
   PI = 3.14159265359
   PSTEP=.2
   STEPEX=.3010299956
C
C   DO 1010 I = 1,N
C   AM = AA(I)
C   DO 1020 K = 1,M
C   P1 = (PI/180.) * PHINT(K)
C   P2 = (PI/180.) * PHIW (K)
C   WRITE (6,12) N,M,L,NO
12  FORMAT(1H1, 'FLAT PLATE IN AN ELLIPTIC ORBIT ABOUT THE EARTH',15X,
1416,///)
   WRITE(6;16) AM,PHIW(K),PHINT(K),GA,PJ,VE,RE, MU,ESTEP
16  FORMAT (1X,'PARAMETERS',///, ' SATELLITE AREA/MASS = ',15X,F7.3,9X
1,'M2/KG',//,' ATTITUDE ANGLE PHIW = ',15X,F7.3,9X,'DEG',//,' ATTIT
2UDE ANGLE PHINT = ',14X,F7.3,9X,'DEG',//,' GA (GAS SURFACE PARAMET
3ER) = ',8X,FB.4,20X,' (GAMMA) X SQRT(1-ALPHA) ----- REF. 1',//,
4' PJ (GAS SURFACE PARAMETER) = ',8X,FB.4,//,' EARTH ANGULAR VELOC1
5TY = ',11X,E14.8, 1X,'RAD/SEC',//,' EARTH RADIUS = ',23X,E10.6
6,3X,'M',//,' EARTH GRAVITATIONAL CONSTANT = ',7X,E11.7,2X,'M3/SE
7C2',//,' ECCENTRIC ANOMALY STEP SIZE = ',7X,F11.7,5X,'RAD',//,1H1)
   AT=COS(P2)*COS(P1)
   AN=AT*TAN(P1)

```

AK=SIN(P2)

\*\*\*\*\*  
MAIN ORBITAL ELEMENTS

Y1=ECCENTRIC ANOMALY  
Y2=SEMI MAJOR AXIS  
Y3=ECCENTRICITY  
Y4=ORBITAL INCLINATION  
Y5=ARGUMENT OF PERIGEE (WITH RESPECT TO ASCENDING NODE)  
Y6=LONGITUDE OF ASCENDING NODE (WITH RESPECT TO VERNAL EQUINOX)  
Y7=TIME OF PERIGEE PASSAGE  
TIME=TIME INTO ORBIT(S)

\*\*\*\*\*

DO 1000 II = 1,L  
DO 20 MM = 1,7  
20 Y(MM) = YY(MM,II)  
RHOO = DEN(II)  
HH = HT(II)  
HPI = Y(2)\*(1.-Y(3))-RE  
VP=SQRT((MU/Y(2))\*(1.+Y(3))/(1.-Y(3)))  
DYNAPP=RHOO\*VP\*\*2  
OLDY=0.0  
OLDT=0.0  
NORBIT=1  
ITER=0  
J = 1  
NULL = 0

CALCULATION OF VARIABLES

24 NEXT=0  
NDIP = 0  
25 ITER=ITER+1  
R = Y(2)\*(1.-Y(3)\*COS(Y(1)))  
H=R-RE  
RP=Y(2)\*(1.-Y(3))  
HP = RP - RE  
IF (HP.LT.0.0.OR.Y(3).LT.0.0) GO TO 999  
RHO=RHOO\*EXP(-(H-HP)/HH)  
FF = SQRT((1.-Y(3)\*\*2)\*(1.+Y(3)\*COS(Y(1)))/(1.-Y(3)\*COS(Y(1))))  
P = Y(2)\*(1.-Y(3)\*\*2)  
TA = ACOS((COS(Y(1))-Y(3))/(1.-Y(3)\*COS(Y(1))))  
TASIN = (SIN(Y(1))\*SQRT(1.-Y(3)\*\*2))/(1.-Y(3)\*COS(Y(1)))  
IF (TASIN) 40,50,50  
40 TA=(2.\*P1)-TA  
50 U=TA+Y(5)  
AR=(1./FF)\*(AT\*Y(3)\*SIN(TA)+AN\*(1.+Y(3)\*COS(TA)))  
AS=(1./FF)\*(AT\*(1.+Y(3)\*COS(TA))-AN\*Y(3)\*SIN(TA))  
A=SQRT(AR\*\*2+AS\*\*2+AK\*\*2)  
VR= SQRT(MU/Y(2))\*(Y(3)\*SIN(Y(1)))/(1.-Y(3)\*COS(Y(1)))  
VS=SQRT(MU\*(1.+Y(3)\*COS(TA))/R)-(VE\*R\*COS(Y(4)))  
VK=VE\*R\*COS(U)\*COS(Y(4))  
V=SQRT(VR\*\*2+VS\*\*2+VK\*\*2)

```

VMEAN=SQRT(MU/Y(2)**3)
DOT=(AR*VR+AS*VS+AK*VK)/(A*V)
IF (ABS(DOT),LT,1.0) GO TO 51
DOT=1.
51 ANGATK=ACOS(DOT)
TAS=ANGATK
IF (TAS) 55,54,55
54 COTAS = 0.0
GO TO 56
55 COTAS = COTAN (TAS)
56 TAJ = (PI/2.-TAS)
CDV=2.*SIN(TAJ)-2.*GA*SIN(TAJ)*COS((PI/2.)*PJ+(2.-PJ)*TAJ)
CDR=(VR/V)*CDV
CDS=(VS/V)*CDV
CDK=(VK/V)*CDV
CLZ=-2.*GA*SIN(TAJ)*SIN(PI/2.*PJ+(2.-PJ)*TAJ)
CLR=(AR-(VR/V)*SIN(TAJ))*CLZ/SIN(TAS)
CLS=(AS-(VS/V)*SIN(TAJ))*CLZ/SIN(TAS)
CLK=(AK-(VK/V)*SIN(TAJ))*CLZ/SIN(TAS)
CDV = CDV*1.486792117
CLZ = CDV*(PI/SIN(P2))
AMM = AM/2.00
BL = CLZ*AMM
BD = CDV*AMM
ACR=(RHO*V**2)*((BL *AR/(VMEAN*SIN(TAS)))*((1.-Y(3)*COS(Y(1)))-Y(2)
1)*Y(3)*SIN(Y(1)))+(BL * COTAS +BD )/V)
ACS=(RHO*V**2)*((BL *AS/(VMEAN*SIN(TAS)))*((1.-Y(3)*COS(Y(1)))-
1(SQRT(1.-Y(3)**2)-(VE*COS(Y(4)))/VMEAN)*((1.-Y(3)*COS(Y(1)))*
1(Y(2)/V)*(BL * COTAS +BD ))
ACK=(RHO*V)*((VE*Y(2)/VMEAN)*SIN(Y(4))*COS(U)*((1.-Y(3)*COS(Y(
1)))*2)*((BL *COTAS +BD ))+(BL *V/VMEAN)*AK*((1.-Y(3)*COS(Y(1)))))
ACN=(1./FF)*((1.+Y(3)*COS(TA))*ACR+Y(3)*SIN(TA)*ACS)
ACT=(1./FF)*(Y(3)*SIN(TA)*ACR+(1.+Y(3)*COS(TA))*ACS)
TIME=(Y(1)-Y(3)*SIN(Y(1)))/VMEAN +Y(7)
RA=Y(2)*(1.+Y(3))
DYNA = RHO*V**2
IF((DYNA/DYNAPP),LT,1.00*5) GO TO 58
ESTEP = (PSTEP*(DYNA/DYNAPP)**(+STEPX))*0.01745329251
GO TO 59
58 ESTEP=.1396263401
59 ORBIT=NORBIT

IF (NDIP.EQ.1.OR.NEXT.EQ.1) GO TO 81
IF (NORBIT.EQ.1.AND.ITER.EQ.1) GO TO 60
GO TO 70
60 OLDRA = RA
OLDT = TIME
TAJ=TA
Y2=Y(2)
Y3=Y(3)
Y4=Y(4)
Y5=Y(5)
Y6=Y(6)
HP1=HP
OLDHP=HP1
OLDY3=Y3
V1=V

```

```

ACTI=ACT
WRITE (6,18) (Y(MN),MN=1,7),TA,HP,RHO
18  FORMAT(35X,'***** INITIAL MAIN ORBITAL ELEMENTS *****',///
1,IX,'ECCENTRIC SEMIMAJOR ECCENTRICITY ORBITAL ARGUMENT
20F LONGITUDE OF',8X,'TIME OF',8X,'TRUE',5X,'PERIGEE PERIGEE',/,
3' ANOMALY',6X,'AXIS',20X,'INCLINATION PERIGEE ASCENDING NOD
4E PERIGEE PASSAGE ANOMALY HEIGHT DENSITY',/,4X,'Y1',10X,
5'Y2',11X,'Y3',12X,'Y4',12X,'Y5',12X,'Y6',15X,'Y7',12X,'TA',8X,'HP',
6,7X,'RHO',//,F9.6,E14.7, F9.4,F16.7,2F14.7,F17.7,F14.5,2E10.4,/,/
7,52X,'(M-K-5-RADIANS)',/// )
70 IF (Y(1)-(2.*PI) ) 90,80,80
80 NORBIT=NORBIT+1
81 DELRA=OLDRA-RA
DELTA=TIME-OLDT
DELTA=2.*PI+(TA-TA1)
DELA=Y2-Y(2)
DELACT=ACTI-ACT
DELV=V1-V
DELHP=HP-HP1
DELE=Y(3)-Y3
DELI=Y(4)-Y4
DELW=Y(5)-Y5
DELWW=Y(6)-Y6
ADECAY = DELRA/TIME
THETA=180.*TA/PI
EE=180.*Y(1)/PI
IF ( NDIP.EQ.1.OR.NEXT.EQ.1) GO TO 620
OLDRA = RA
OLDT = TIME
TA1=TA
Y2=Y(2)
Y3=Y(3)
Y4=Y(4)
Y5=Y(5)
Y6=Y(6)
HP1=HP
OLDHP=HP1
OLDY3=Y3
V1=V
ACTI=ACT
IF (NULL.EQ.1) GO TO 82
Y(1)=Y(1)-2.*PI
82 DYNAP=(RHO*V**2)*.00001
DYNAPP=(RHO*V**2)

OUTPUT

IF(HP.GT.0.0.AND.Y(3).GT.0.0 ) GO TO 610
WRITE (6,700)
700 FORMAT (//,10X,' SATELLITE HAS CRASHED ON THIS ORBIT OR THE ORBIT
1 HAS BEEN REDUCED TO CIRCULAR',///)
610 WRITE (6,800)
IF (NULL.EQ.1) GO TO 620
WRITE (6,801)
620 WRITE (6,810) NORBIT,THETA,EE,Y(2),Y(3),Y(4)
WRITE (6,820)
WRITE (6,830) Y(5),Y(6),Y(7),TIME

```



```

999  NULL = 1
      GO TO 81
1000 CONTINUE
1020 CONTINUE
1010 CONTINUE
      END
@FOR, IS DIFFEQ, DIFFEQ
      REAL FUNCTION DIFFEQ(Y, I)
      DIMENSION Y(1)
      DOUBLE PRECISION Y, TA, MU, P, FF, ACT, U, R, ACN, ACK, VMEAN
      COMMON TA, MU, P, FF, ACT, U, R, ACN, ACK, VMEAN
      *****
C
C      DIFFERENTIAL EQUATIONS FOR ORBITAL PARAMETERS, Y2-Y7, WITH RESPECT
C      TO THE INDEPENDENT PARAMETER, Y1
C
C      *****
C      GO TO (310,320,330,340,350,360), I
310  DIFFEQ=(2.*(Y(2)**2)/SQRT(MU*P))*FF*ACT
      GO TO 400
320  DIFFEQ=(SQRT(P/MU)/FF)*(2.*(COS(TA)+Y(3))*ACT+R*(1.-Y(3)**2)*SIN(
      TA)*ACN/P)
      GO TO 400
330  DIFFEQ=R*COS(U)*ACK/SQRT(MU*P)
      GO TO 400
340  DIFFEQ=(SQRT(P/MU)/Y(3))* ((2.*SIN(TA)*ACT-(R/P)*(2.*Y(3)+COS(TA)+
      1*(Y(3)**2)*COS(TA))*ACN)/FF-R*Y(3)*SIN(U)*ACT/(P*TAN(Y(4))))
      IF (Y(4)) 400,399,400
350  DIFFEQ=(R*SIN(U)*ACK)/(SQRT(P*MU)*SIN(Y(4)))
      IF (Y(4)) 400,399,400
360  DIFFEQ=(Y(2)/MU)*(2.*(P/Y(3)+R*Y(3))*SIN(TA)/FF-3.*SQRT(MU/P)*FF*(
      1*(Y(1)-Y(3)*SIN(Y(1)))/VMEAN)*ACT+((R*P*COS(TA))/(MU*Y(3)*FF))*ACN
      GO TO 400
399  DIFFEQ=0.0
400  RETURN
      END
@FOR, IS GILL, GILL
      SUBROUTINE GILL (DY, Y, Z, H, W, Q, N)
      DIMENSION Y(N), W(N), Q(N), A(4), C(4), B(4)
      DOUBLE PRECISION Y
      DATA(A(1),C(1),B(1),I=1,4)/2*.5,2.,2*.292893283,1.,2*1.70710671,
      11.,.1666666666,.5,2./
C
C      THIS ROUTINE IS A MODIFIED RUNGA-KUTTA NUMERICAL INTEGRATION
C      TECHNIQUE
C
C      -----
C      DX= IS THE INTERVAL SIZE.
C      W= IS THE ARRAY USED TO STORE THE
C      VALUE OF Y'(X), W(1)=FD(X)=1
C      -----
C
C      DX=H
C      W(1)=1.
C
C      -----
C      FOR THE FIRST INTERVAL THE Q'S ARE SET TO ZERO, FOR
C      SUBSEQUENT INTERVALS THE PREVIOUSLY COMPUTED Q'S
C      ARE USED.

```

```

C -----
5 DO 5 J=1,N
6 Q(J)=0.
10 DO 20 J=1,4
15 DO 15 K=2,N
15 W(K)=DY(Y,K-1)
DO 20 K=1,N
Y(K)=Y(K)+DX*A(J)*(W(K)-B(J)*Q(K))
20 Q(K)=Q(K)+3.*A(J)*(W(K)-B(J)*Q(K))-C(J)*W(K)
C -----
C TEST IF VALUE OF INDEPENDENT VARIABLE
C HAS BEEN REACHED.
C -----
IF(Y(1)+DX.GT.Z) DX=Z-Y(1)
IF(DX.LT.ABS(Y(1))*2.*E-8) GO TO 25
IF(Y(1)-Z) 10,25,25
25 RETURN
END

```